ARTICLE IN PRESS

Acta Biomaterialia xxx (xxxx) xxx

Contents lists available at ScienceDirect

Acta Biomaterialia

journal homepage: www.elsevier.com/locate/actbio

Review article

Calcium-Deficient hydroxyapatite as a bone graft material: From hydrated-layer chemistry to clinical performance

Marc Bohner [a,*,1], Nicola Döbelin [a], Christophe Drouet [b], Maria-Pau Ginebra [c], Yassine Maazouz [a], David Marchat [d]

[a] RMS Foundation, Robert Mathys Strasse 1, CH-2544 Bettlach, Switzerland
[b] Université de Toulouse, Toulouse INP, CNRS, CIRIMAT, Toulouse, France
[c] Biomaterials, Biomechanics and Tissue Engineering Group, Department of Materials Science and Engineering and Barcelona Research Center in Multiscale Science and Engineering, Universitat Politècnica de Catalunya - BarcelonaTech, Av. Eduard Maristany 16, 08019 Barcelona, Spain
[d] Mines Saint-Étienne, Université Jean Monnet, INSERM U1059 Sainbiose, Saint-Étienne, France

ARTICLE INFO

Keywords:
Calcium phosphate
Calcium-deficient hydroxyapatite
Hydrated layer
Biomimetic apatite
Bone
Osteoconduction
Osteoinduction

ABSTRACT

Calcium-deficient hydroxyapatite (CDHA) is a widely studied calcium phosphate biomaterial due to its chemical similarity to bone mineral and its relevance as a bone graft substitute. This review presents a comprehensive analysis of CDHA's structure, composition, physico-chemical properties, synthesis methods, and biological performance. Attention is given to the material's multiphasic nature, consisting of a crystalline core and an amorphous hydrated surface layer, and to how this structural-chemical duality governs CDHA's thermal stability, mechanical behavior, solubility, and ion exchange capacity. Various synthesis routes, including aqueous precipitation, hydrolysis, and cementitious reactions, are examined with respect to their impact on particle morphology and clinical applicability. Biological performance is assessed through *in vitro* and *in vivo* studies, highlighting CDHA's biocompatibility, osteoconductivity, osteoinductivity, and resorption mechanisms. Challenges such as precise compositional characterization and the dynamic behavior of the hydrated surface layer are addressed, underscoring the need for further research. Overall, CDHA stands out as a promising and versatile material for bone substitution, with significant potential for future developments in regenerative medicine and beyond.

Statement of Significance: Calcium-deficient hydroxyapatite (CDHA) is widely used as a bone graft substitute, yet its structure, composition, and biological behavior are often misunderstood or inconsistently described. This review provides a focused and chemically rigorous analysis of CDHA as a distinct material class within the Ca–P–O–H system, separating it from ion-substituted or loosely defined "biomimetic" apatites. By critically examining its crystalline core, hydrated surface layer, synthesis pathways, ion-exchange properties, and *in vivo* performance, we try to clarify long-standing ambiguities regarding its solubility, resorption, and osteoinductive potential. The review highlights the central role of the hydrated layer in governing reactivity and biological response, offering guidance for improved characterization, terminology harmonization, and rational design of next-generation bone graft substitutes.

1. Introduction

Bone defects resulting from trauma, disease, or surgery represent a significant clinical challenge, often necessitating the use of bone graft materials to support regeneration [1–5]. Among synthetic substitutes, calcium phosphate-based biomaterials have gained widespread attention due to their biocompatibility and chemical resemblance to natural bone mineral [6,7]. Within this family, calcium-deficient hydroxyapatite (CDHA), generally represented in first approximation as $Ca_{(10-x)}(HPO_4)_x(PO_4)_{(6-x)}(OH)_{(2-x)}$ occupies a unique position. Unlike stoichiometric hydroxyapatite (HA; $Ca_{10}(PO_4)_6(OH)_2$), CDHA exhibits a lower calcium-to-phosphorus molar ratio, which reduces its

* Corresponding author.
E-mail address: marc.bohner@rms-foundation.ch (M. Bohner).
[1] Dr. Marc Bohner was an editor of the journal during the review period of the article. To avoid a conflict of interest, Prof. William R. Wagner acted as editor for this manuscript.

https://doi.org/10.1016/j.actbio.2026.06.010
Received 23 February 2026; Accepted 4 June 2026
Available online 5 June 2026
1742-7061/© 2026 The Authors. Published by Elsevier Inc. on behalf of Acta Materialia Inc. This is an open access article under the CC BY-NC-ND license (http://creativecommons.org/licenses/by-nc-nd/4.0/).

thermodynamic stability and enhances its biological activity and resorption potential [8]. This superior resorption behavior stems from its higher solubility product and susceptibility to active osteoclastic resorption — collectively positioning CDHA as a substantially more resorbable alternative to HA.

Although several reviews have addressed biomimetic or nanocrystalline apatites [9–12], these studies sometimes included also ion-substituted and compositionally variable materials. Furthermore, all non-stoichiometric HA do not systematically share the bone-like structure involving a non-apatitic amorphous surface layer. To our knowledge, no review has specifically analyzed CDHA, defined in the strict chemical sense (Ca–P–O–H system without foreign ionic substitutions), as a distinct bone-graft material class. This narrower focus is essential because CDHA exhibits structural and functional properties that differ from more heterogeneous biomimetic apatites. By isolating CDHA as a chemically constrained sub-family of materials, this review offers a focused analysis of the structural complexity, fabrication routes, and biological performance of this material family. It further highlights the challenges that remain in fully understanding and optimizing CDHA for targeted clinical use. Table 1 summarises the position of CDHA within the broader family of calcium phosphate materials used for bone repair and highlights how it differs from sintered HA, the tricalcium phosphates, biphasic calcium phosphates, octacalcium phosphate, and the dicalcium phosphates. Table 2 lists the abbreviations and formulae of all calcium phosphate phases discussed in this review.

One of the major challenges in writing a review article on CDHA is the insufficient and often inconsistent characterization of the materials described in the literature, a difficulty rooted in the inherently complex structure and composition of CDHA. This lack of rigorous characterization in some studies leaves considerable room for assumptions and limits the reliability of reported findings. For example, the Ca/P molar ratio of CDHA is frequently not measured at all, or not determined according to international standards, leaving uncertainty about the actual phase obtained. The same issue arises in studies that claim to investigate "HA" although the synthesis conditions used almost certainly yield CDHA instead. Moreover, key compositional features such as carbonate or sodium content, both of which strongly influence the structure of the crystalline core, are seldomly quantified. Furthermore, there is a discrepancy between the resolution of analytical techniques and the (nanocrystalline) size of CDHA particles which only allow the determination of average properties. As a result, conclusions about CDHA composition and validity are often inferred solely from synthesis routes rather than validated by experimental data and a strong characterization analysis. Consequently, a significant portion of literature cannot be regarded as strictly focused on CDHA. In this review, we carefully selected and examined only those references that provide the most relevant and reliable information for a meaningful assessment of CDHA.

This review is organized as follows. Section 2 establishes the

Table 1
Positioning of CDHA within the family of calcium phosphate materials used for bone repair. Entries describe general trends reported in the literature for the nominal material rather than intrinsic material constants, and several rows are strongly modulated by the factors listed in footnote (a). CDHA (highlighted) is the subject of the present review. Details about the abreviations and compositions are given in Table 2.

Material	Ca/P molar ratio	Thermodynamic stability at pH 7.4	Typical processing route	Resorbability	Osteoclastic resorption	Comparative osteoconductivity (vs sintered HA)	Main clinical formats
CDHA (this review)	1.33–1.67	Intermediate	Low-temperature: aqueous precipitation, hydrolysis, CPC setting	Intermediate–high	Yes	High	Granules, injectable pastes, CPC-derived scaffolds (see Table 9)
Sintered HA	1.67	High	High-temperature sintering	Low	Limited	Intermediate (reference)	Granules, dense/porous ceramics, coatings
Carbonated apatite	Variable (B-type substitution)	Intermediate	Low-temperature precipitation or conversion	Intermediate–high	Yes	High	Granules
Sintered arbonated apatite	Variable (AB-type substitution)	Low to intermediate	High-temperature sintering	Low to intermediate	Yes	High	Granules, porous scaffolds
β-TCP	1.50	Intermediate	High-temperature sintering (e.g. from CDHA precursor) Low-temperature: non-aqueous precipitation	Intermediate–high	Yes	Intermediate	Granules, porous scaffolds
α-TCP	1.50	Low	High-temperature synthesis	High	— (converts to CDHA)	— (converts to CDHA)	CPC precursor, granules
BCP (HA + β-TCP)	1.50–1.67	Intermediate (tunable by composition)	High-temperature sintering; composition-tunable	Composition-dependent	Yes	Intermediate–high	Granules, porous scaffolds
OCP	1.33	Low	Low-temperature precipitation	High; converts to CDHA *in vivo*	Yes	High	Granules, emerging products
DCPA	1.00	Low	Low-temperature precipitation; Thermal conversion of DCPD	High	Partially	Low to intermediate	Granules, porous scaffolds and blocks (emerging products)
DCPD	1.00	Low	Low-temperature precipitation; CPC setting	Very high; converts to CDHA *in vivo*	Passive dissolution	Low	CPC-derived scaffolds

(a) The entries above reflect trends in the literature for the nominal material; the clinical performance of any specific product is strongly modulated by macroporosity, pore-entry size, crystallite size, SSA, surface impurities (carbonate, sodium, magnesium, silicate, fluoride), residual precursor phases, and processing history. Two products labelled with the same material can differ more from one another than from a well-defined CDHA. A small chemical modification of α- and β-TCP granules, undetectable by XRD and barely detectable even by XPS, has been shown to produce quantitatively significant differences in the multinucleated giant-cell response, vascularisation, degradation, and new bone formation *in vivo* [346]. The table should therefore be read as a map of typical positions rather than as a ranking of products.

Table 2
Abbreviations of calcium minerals.

Abbreviation	Denomination	Formula	Ca/P Molar Ratio
ACP	Amorphous calcium phosphate ("Posner's clusters")	$Ca_3(PO_4)_2{\cdot}nH_2O$	1.50
CC	Calcium carbonate	$CaCO_3$	∞
CDHA	Calcium-deficient hydroxyapatite	Simplified composition: $Ca_{(10-x)}(HPO_4)_x(PO_4)_{(6-x)}(OH)_{(2-x)}$	1.33-1.67
β-CPP	β-Calcium pyrophosphate	β-$Ca_2P_2O_7$	1.00
CSA	Calcium sulfate anhydrous	$CaSO_4$	∞
CSH	Calcium sulfate hemihydrate Plaster of Paris	$CaSO_4{\cdot}½H_2O$	∞
CSD	Calcium sulfate dihydrate Gypsum	$CaSO_4{\cdot}2H_2O$	∞
DCPA	Dicalcium phosphate (anhydrous) Monetite	$CaHPO_4$	1.00
DCPD	Dicalcium phosphate dihydrate Brushite	$CaHPO_4{\cdot}2H_2O$	1.00
HA	Hydroxyapatite	$Ca_{10}(PO_4)_6(OH)_2$	1.67
MCPA	Monocalcium phosphate anhydrous	$Ca(H_2PO_4)_2$	0.50
MCPM	Monocalcium phosphate monohydrate	$Ca(H_2PO_4)_2{\cdot}H_2O$	0.50
OCP	Octacalcium phosphate (triclinic form)	$Ca_8(HPO_4)_2(PO_4)_4{\cdot}5H_2O$	1.33
α-TCP	α-Tricalcium phosphate	α-$Ca_3(PO_4)_2$	1.50
β-TCP	β-Tricalcium phosphate	β-$Ca_3(PO_4)_2$	1.50
TTCP	Tetracalcium phosphate Hilgenstockite	$Ca_4(PO_4)_2O$	2.00

structural and compositional foundations of CDHA, examining the models proposed to describe its non-stoichiometry, the crystallographic structure and composition of the apatitic core, the nature and organisation of the hydrated surface layer, and the broader question of compositional heterogeneity and phase assignement. Section 3 examines the intrinsic physicochemical properties that follow directly from this structure: thermal stability, mechanical behaviour, solubility, dissolution, and ion exchange. Section 4 reviews the analytical methods required to characterise CDHA reliably, with particular attention to their mutual inconsistencies and the risk of misinterpretation. Section 5 describes the synthesis routes through which CDHA powders, granules, and scaffolds are produced. Section 6 examines CDHA's behaviour as a bone substitute, first *in vitro* — covering the physicochemical interactions with cell culture media and the cellular responses relevant to bone regeneration — and then *in vivo*, covering biocompatibility, osteoconductivity, osteoinduction, and resorption, before turning to clinical use and CDHA's potential as a drug delivery platform. Section 7 discusses the principal remaining challenges and future directions, and Section 8 presents the conclusions and outlook.

2. Structure and composition of CDHA

A meaningful discussion of CDHA as a bone-graft material must begin with its chemistry, since every property examined in the subsequent sections is ultimately governed by the compositional and structural features established here. This section therefore focuses exclusively on structure and composition, leaving the physicochemical properties that follows from this structure — thermal stability, mechanical behavior, solubility, dissolution, and ion exchange — to Section 3. The section examines, in turn, the structural and compositional models proposed in the literature, the crystallographic structure and composition of the apatitic core, the nature and organisation of the hydrated layer in five dedicated subsections, and the broader question of compositional heterogeneity and phase assignement.

The composition of CDHA is generally approximated by $Ca_{(10-x)}(HPO_4)_x(PO_4)_{(6-x)}(OH)_{(2-x)}$ where x can vary between 0 and 2. The two extreme compositions correspond to a Ca/P molar ratio of 1.33 ($Ca_8(HPO_4)_2(PO_4)_4$) which is a composition very similar to that of octacalcium phosphate (OCP; $Ca_8(HPO_4)_2(PO_4)_4{\cdot}5H_2O$) and of 1.67 which is HA. This formula captures the basic concept of non-stoichiometry, in which electroneutrality is maintained by a dual mechanism: each calcium vacancy is compensated by a hydroxide vacancy together with the protonation of one PO_4^{3-} group into a HPO_4^{2-} group. However, it does not account for the full complexity of CDHA. Three independent lines of experimental evidence reveal this complexity. Solid-state nuclear magnetic resonance (NMR) data suggest that CDHA is made of a crystalline apatitic core coated with a hydrated layer rich in calcium and hydrogenphosphate ions [13–16]. Powder X-ray diffraction (XRD) analysis indicates that the lattice parameters of the CDHA core vary systematically with the Ca/P molar ratio [17–21] consistent with a genuinely non-stoichiometric apatitic core. Fourier transform infrared (FTIR) spectroscopy suggests the presence of additional, non-apatitic domains in CDHA [17]. The hydrated layer is generally considered to be amorphous even though the assumption of a completely amorphous nature has been challenged [11,22]. Taken together, these observations indicate that CDHA composition and structure are not reducible to a single formula and require a more integrated description. This section therefore examines, in turn, the structural and compositional models proposed in the literature, the crystallographic structure and composition of the apatitic core, the nature and organisation of the hydrated layer in five dedicated subsections.

2.1. Structural and compositional models

Various models have been proposed to explain the apparent ability of CDHA lattices to form a continuous series of compositions from a Ca/P of 1.33 to 1.67 [23] (Table 3; Fig. 1). One model describes an epitaxial intergrowth structure comprising stoichiometric OCP and HA [24]. Another model suggests partial replacement of calcium ions by hydrogen ions, resulting in the general formula $Ca_{(10-x)}(H)_{2x}(PO_4)_6(OH)_2$ [25–27]. An expanded concept incorporates calcium and hydroxide defects, expressed as $Ca_{(10-x)}(H)_x(PO_4)_6(OH)_{(2-x)}$ which can also be written as $Ca_{(10-x)}(HPO_4)_x(PO_4)_{(6-x)}(OH)_{(2-x)}$ [28,29]. The latter model of Ca^{2+} vacancies within a HA lattice, where charge balance is maintained via OH^- loss and/or proton addition, is considered by many to best align with experimental evidence [30–32]. Complementary to these lattice-based descriptions, other hypotheses emphasize compositional heterogeneity at the nanoscale, proposing that CDHA may consist of stoichiometric HA coated with surface-adsorbed phosphate groups or

Table 3
Models of lattice substitutions in CDHA as listed by Elliott [347]. Some cells contain two equivalent formula. Please note that the only difference between row 2 and 4 is the range of the x value.

1.	$Ca_{(10-x)}(HPO_4)_{2x}(PO_4)_{(6-2x)}(OH)_2$	$0 \le x \le 2$	[25–27]
2.	$Ca_{(10-x)}(HPO_4)_x(PO_4)_{(6-x)}(OH)_{(2-x)}$	$0 \le x \le 2$	[28,29]
3.	$Ca_{(10-x-y)}(HPO_4)_x(PO_4)_{(6-x)}(OH)_{(2-x-2y)}$	$0 \le x \le 2$ and $y \le (1-x/2)$	[183,348]
4.	$Ca_{(10-x)}(HPO_4)_x(PO_4)_{(6-x)}(OH)_{(2-x)}$	$0 \le x \le 1$	[23,349]
5.	$Ca_{(10-x)}(HPO_4)_x(PO_4)_{(6-x)}(OH)_{(2-x)}(H_2O)_x$	$0 \le x \le 1$	[23,36,61,349]
6.	$Ca_{(9-x)}(HPO_4)_{(1+2x)}(PO_4)_{(5-2x)}(OH)$	1.4 ≤ Ca/P molar ratio ≤ 1.5	[23,349,350]
7.	$Ca_{(9+z)}(HPO_4)_{(5+y+z)}(PO_4)_{(1-y-z)}(OH)_{(1-y+z)}$	-	[351]
8.	$Ca_{(10-x+u)}(PO_4)_{(6-x)}(PO_4)_x(OH)_{(2-x+u)}$	$2-x+2u \le 2$ and $0 \le u \le x/2$	[352]

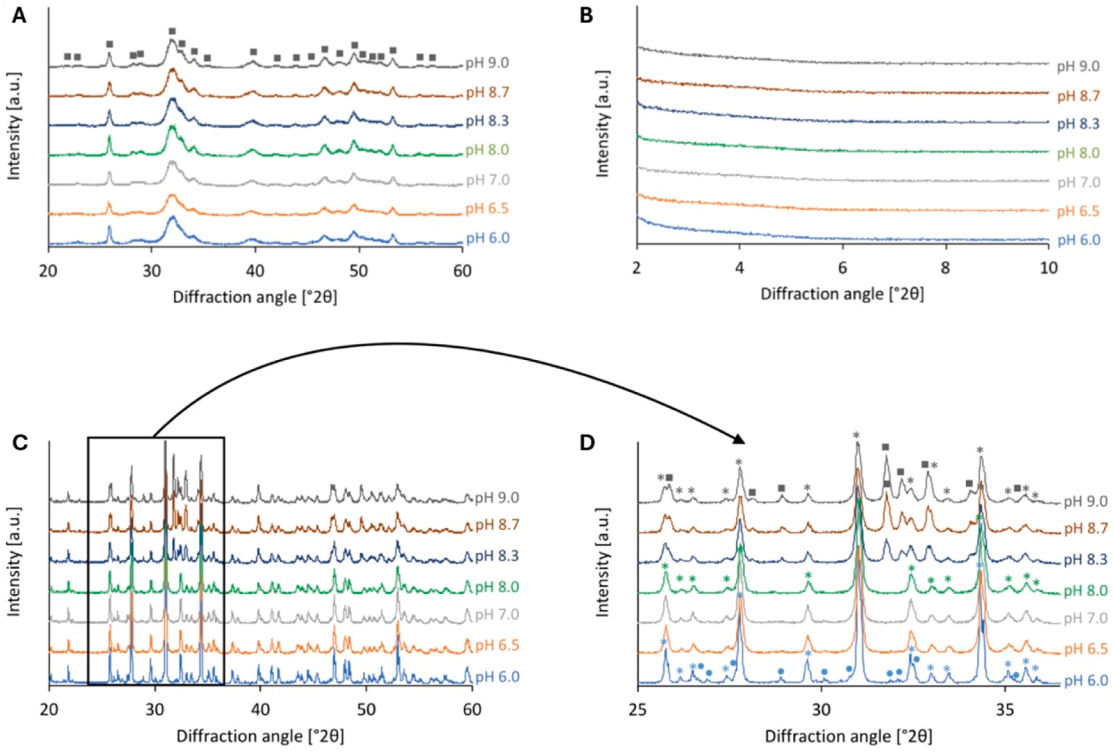

Fig. 1. XRD diffractograms of CDHA powders synthesized at different pH (6.0 to 9.0) showing (A) a typical diffraction pattern of poorly crystallized HA and (B) the absence of foreign phases, particularly OCP at low 2θ angle. After thermal treatment (C)(D), the different Ca/P molar ratios obtained with increasing synthesis pH led to the formation of β-TCP-β-CPP, pure β-TCP, and β-TCP-HA mixtures. The Ca/P molar ratio of these CDHA powders range from 1.44 to 1.56. (●) β-CPP; (*) β-TCP; (■) HA [135].

a mixtures with more acidic phases like dicalcium phosphate dihydrate (DCPD; $CaHPO_4{\cdot}2H_2O$) or anhydrous dicalcium phosphate (DCPA; $CaHPO_4$) [32]. A prevailing view is that CDHA comprises a crystalline CDHA core coated with a hydrated surface layer [11], sometimes referred to as a non-apatitic domain due to its different NMR/IR signature compared to HA [33,34] or even an amorphous-calcium phosphate (ACP)-like layer mostly to highlight the amorphous character of this surface layer [13,14,35]. Nevertheless, despite broad recognition of CDHA as a multiphasic material, its composition is still often approximated using $Ca_{(10-x)}(HPO_4)_x(PO_4)_{(6-x)}(OH)_{(2-x)}$, a convention that can be misleading.

2.2. *Crystallographic structure and composition of the apatitic core*

CDHA exhibits notable structural variations compared to HA, particularly in relation to its crystallographic lattice parameters and structural organization, as influenced by the Ca/P molar ratio. The crystallographic structure of CDHA is closely related to that of stoichiometric HA, but key differences arise. HA has a hexagonal structure with space group P63/m (except in rare cases where ultrapure HA can crystallize in the monoclinic system). Its unit cell contains two formula units of $Ca_5(PO_4)_3OH$ with two types of calcium sites (Ca1 and Ca2), one phosphate site (PO_4), and one hydroxyl site (OH) in the asymmetric unit. The structure can be visualized as PO_4 tetrahedra linked by Ca ions, with columns of OH groups along the c-axis (Fig. 2). As the Ca/P molar ratio decreases from 1.67 to 1.33, systematic changes in the lattice parameters occur, characterized by an increase in the a-axis parameter and a decrease of the c-axis parameter, indicating anisotropic lattice distortions [17–21].

In the literature, several mechanisms have been proposed to account for the observed calcium deficiency and the associated charge compensation. The lack of calcium has been observed primarily at the Ca2 site [21,36], thus at the vicinity of the OH site, leading to calcium

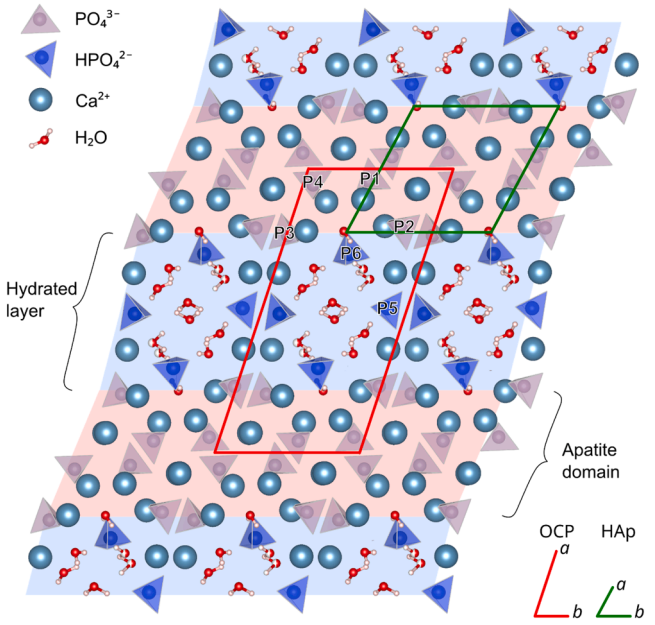

Fig. 2. Crystal structure of triclinic OCP, evidencing the six phosphate groups per unit cell (P1 to P6). The OCP (red) and HA (green) unit cells highlight the structural relationship between the two phases. Adapted from [404]. The lattice parameter "a" in HA (0.954 nm) is 1.6% shorter than the corresponding "b" parameter in OCP (0.97 nm). The "c" parameter of HA (~0.69 nm) corresponds approximately to the thickness of the apatite-like layers in OCP, rather than to the full OCP unit cell parameter. The OCP c-axis (not shown) is associated with the stacking direction of the layered structure and is inclined with respect to the plane of the figure due to the triclinic symmetry.

vacancies that induce structural disorder within the lattice. This results in elongated Ca-O bond distances and a reduced coordination number of calcium atoms compared to stoichiometric HA [19,37,38]. To maintain charge neutrality, various compensatory mechanisms have been proposed, including the incorporation of protons (H^+) from the surrounding aqueous solution. These protons can either be interstitial or substitute for Ca^{2+} ions [36–38]. Interstitial protons may attach to the OH group, forming H_2O [36], or reside between oxygen atoms of adjacent PO_4 groups. Substitutional protons replace Ca ions and attach to neighboring oxygen, forming HPO_4 groups [36–38]. The incorporation of HPO_4^{2-} groups as charge compensators alters the local chemical environment and introduces further structural irregularities. Hydroxide (OH^-) vacancies also contribute to charge compensation, further modifying the structure of CDHA.

Despite these supporting observations, conclusions from XRD studies remain inconclusive. Rietveld refinement often lacks the sensitivity required to accurately resolve the positions of H^+ ions. In addition, pronounced peak overlap in diffraction patterns of nanocrystalline apatites further restricts its suitability for detailed structural refinement. Indeed, inconsistencies between chemically determined compositions and refinement-derived occupancies have been reported [18]. For example, [18] found that Ca/P molar ratios derived from Rietveld occupancies were only slightly lower than the stoichiometric value and significantly higher than chemically determined values. This discrepancy was dismissed as the result of "an incorrect model in the structure refinement." Detailed crystallographic characterization of CDHA is further impeded by its nanometric crystallite size, which limits the resolution of XRD data and precludes the use of single-crystal XRD analysis. Also, internal strains, arising for example from interfacial stresses induced by the hydrated layer, can significantly affect the apparent lattice parameters. Furthermore, the absence of an internal standard in most studies prevents proper calibration of the refined lattice parameters, resulting in correlations with sample-height displacement errors and significantly inflated uncertainties. Consequently, lattice parameter changes observed by XRD cannot be unambiguously attributed to Ca deficiency alone. Beside technical aspects, several XRD studies have omitted chemical composition data, even though carbonate ions, which are common impurities in apatites, can induce calcium vacancies [21] and accordingly modify the lattice parameters [39]. Interestingly, the incorporation of carbonate ions into the HA structure leads to a decrease of the a-axis and increase of c-axis [39], which can confound lattice parameter trends attributed to Ca deficiency [17–21]. In this context, one study reported the presence of ~6 wt% carbonate groups [21], whereas others did not assess carbonate content [17–20]. The presence of sodium ions in CDHA crystals produced in sodium-rich solutions is also often ignored even though it could lead to non-negligible monovalent sodium content in CDHA.

A central and still unresolved question concerns the precise location of HPO_4^{2-} groups: within the crystalline core and/or confined to the hydrated surface layer. Indeed, solid-state NMR studies have sometimes yielded contradictory findings. One study claimed that all hydrogenphosphate ions in a well-crystallized, HPO_4-substituted hydroxyapatite were incorporated into the apatitic lattice [15]. Yet, no evidence was provided to substantiate either the alleged calcium deficiency or the crystalline, non-amorphous nature of the material. Another study reported a spectral signature attributed to defective hydrogenphosphate ions in the crystal bulk, but again without demonstrating chemical purity or calcium deficiency [40]. In contrast, Jäger et al. [16] only took into account in their approximate model the presence of hydrogenphosphate ions on the surface layer while disregarding the copresence of these ions in the core. To add confusion, one study reported that HPO_4^{2-} groups were located exclusively in the non-apatitic, amorphous surface layer of the carbonated apatite and bone mineral [15]. These contradictions have direct quantitative consequences: XRD-based methods quantify the amorphous content without any assumption about its chemistry, whereas the solid-state NMR estimates commonly reported for bone and carbonated apatites rely on the attribution of the hydrogenphosphate NMR signal to a non-apatitic, amorphous environment. If a fraction of the HPO_4^{2-} groups is in fact located within the crystalline CDHA core, solid-state NMR would systematically overestimate the amorphous content relative to XRD. The large gap between XRD values (4–11 wt%) and NMR values (30–70 wt%), which is summarised in Table 4 and discussed in greater detail in Section 4, is therefore consistent with a crystalline core that itself incorporates HPO_4^{2-} groups, rather than being solely attributable to genuine differences between the materials investigated. This point reinforces the need for the careful characterisation advocated in section 4.

2.3. Hydrated layer: structural model

Several structural models have been proposed to describe the spatial arrangement of the hydrated layer (Fig. 3). In the core–shell model, the entire crystal is coated with a hydrated layer; in the core–crown model, only the narrow edges of the crystal plates are coated; and in the core–surface model, only the flat surfaces of the crystal plates are coated. To date, no firm consensus has been reached within the research community. Some authors favor the core-crown configuration [41], others support the core-surface model [15], while some suggest a core-shell structure [14,42]. One study even concluded that the best-fitting model depends on the synthesis conditions [41]. It further suggested that both the position and thickness of the hydrated layer may vary depending on the level of calcium deficiency and

Table 4
Quantitative values reported in the literature for the amorphous phase content and the thickness of the hydrated layer. Most studies are devoted to carbonated or bone apatites. Except for high-resolution transmission electron microscopy (HRTEM), all methods used to determine the thickness of the hydrated layer are indirect.

	Quantity	Method	Ref.	Note
Amorphous phase content	4.0 ± 0.5 wt % 5.5 ± 2.9 wt % 6.5 ± 0.5 wt %	XRD – G method	[138]	Similar values were reported in 2 articles if one considers that the ACP content includes water: 42-44 wt% ACP incl. 40 wt% water in [353] and 35 wt% ACP for 33 wt% water in [354]
	7.1 wt% 11.2 wt%	XRD – Al_2O_3 internal standard	[139]	
	20 wt% to 40 wt%	Solid-state NMR	[199]	Carbonated apatites
	30-65 wt%	Solid-state NMR	[145]	Carbonated apatites
	50 wt%	Solid-state NMR	[15]	2-year sheep bone mineral
	45 wt%	Solid-state NMR	[14]	2-year sheep bone mineral
	55 wt%	Solid-state NMR	[16]	
	23.3 wt% 31.5 wt%	SAXS and WAXS	[41]	2 carbonated apatites
Thickness	0.8 nm	Solid-state NMR	[15]	2-year sheep bone. Estimate based on the fraction of HPO_4^{2-} ions.
	1.2 nm (crown) 0.4 and 0.6 nm (base and crown)	SAXS and WAXS	[41]	2 carbonated apatites
	1 nm	HRTEM	[14]	2-year sheep bone mineral
	1-2 nm	HRTEM	[45]	
	1 nm	Solid-state NMR	[16]	Carbonated apatite

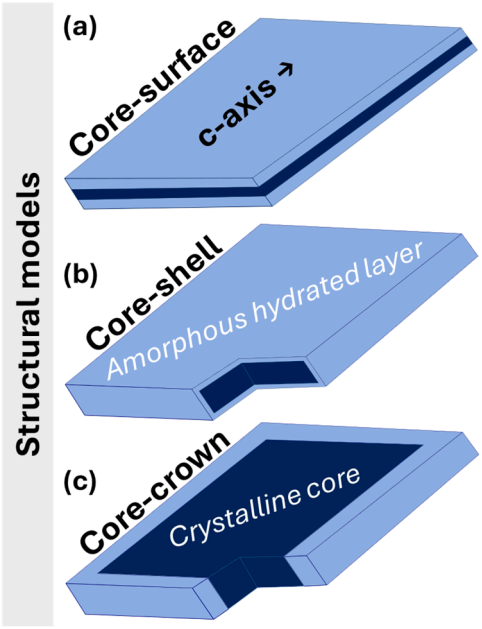

Fig. 3. A diagram illustrating the typical platelet-like structure of CDHA (a) core-surface model. (b) core-crown model; (c) core-shell model. Adapted from [15,42].

maturing/crystallization [41]. Specifically, longer maturation times were associated with thicker platelets and reduced hydrated layer content, thereby highlighting the structural heterogeneity inherent in these biomimetic apatite systems.

2.4. Hydrated layer: thickness and volume fraction

Multiple studies have examined the thickness of the hydrated layer, which is probably variable depending on the precipitation conditions. For platelet-shaped bone mineral particles, it was estimated to be around 0.8 nm on particles 4 nm thick, indicating that nearly half of the inorganic phosphate ions reside in this layer [14–16] (Fig. 3; Table 4). This value (~50%) corresponds to the estimated content of amorphous component, historically considered as ACP in bone [43,44], while this amorphous component is now understood as being essentially due to the hydrated layer itself. Small- and wide-angle X-ray scattering (small-/-wide-angle x-ray scattering, resp. SAXS/WAXS) analyses confirmed that the crystalline plates are coated with a 0.4–1.2 nm thick layer [41], while high resolution transmission electron microscopy (HR-TEM) revealed a thickness of 1–2 nm [45]. Studies on the maturation of the hydrated layer pointed out that its volume fraction, and accordingly its thickness, decreases with increasing maturation time, temperature, and pH [17]. At the same time, the Ca/P molar ratio increased, possibly culminating in the complete disappearance of the hydrated layer in samples produced in hydrothermal conditions.

Taken together, these experimental measurements provide a consistent, if approximate, picture of the hydrated layer's dimensions. A simple order-of-magnitude estimate further illustrates how its thickness relates to the amorphous content and the specific surface area (SSA) of a CDHA sample, and helps place the scattered experimental values into a coherent quantitative framework. For CDHA produced by α-TCP hydrolysis, the SSA is typically 25-30 m^2/g [46]. Assuming platelet-shaped crystals are much longer and wider than they are thick, the surface to volume ratio is approximately $2/h$ were h is the crystal thickness. Combined with an assumed density of 3'000 kg/m^3 for both the apatitic core and the hydrated layer (most calcium phosphates have a density around that value), a SSA of 30'000 m^2/kg corresponds to $h = 2/(30'000 \times 3'000)$ m ≈ 22 nm. If the hydrated layer, is treated as an amorphous coating covering both flat faces of the platelet, its thickness δ on each face is simply δ = (amorphous fraction) × h / 2. For an amorphous content of 5 wt%, this yields δ ≈ 0.55 nm; for 11 wt%, δ ≈ 1.21 nm. Even though these values represent crude approximations and would increase slighthly if the density of the hydrated layer were lower than that of the apatitic core, they fall within the 0.4–1.2 nm range derived from SAXS/WAXS [41] and the 1–2 nm range reported by HR-TEM [45]. This agreement lends internal consistency to the current structural picture of the hydrated layer. It also illustrates that the 4–11 wt% amorphous content reported for CDHA (Section 4) is not a residual impurity but corresponds, at this scale, to a substantial fraction of the total volume. The available quantitative estimates of the hydrated layer are summarized in Table 4. These values should be interpreted with caution, as the hydrated layer is intrinsically fragile/metastable. Even simple washing can induce chemical alterations in the resulting crystals [47]. More generally, many analytical methods used to investigate the hydrated layer may themselves alter or even destroy it due to its intrinsic fragility. For example, HR-TEM observations and similar techniques performed under high vacuum (unless conducted in cryogenic mode) can significantly modify nano-sized calcium phosphate particles under the electron beam.

2.5. Hydrated layer: formation and stability

This fragility and sensitivity to experimental conditions raises a more fundamental question: how does the hydrated layer form in the first place, and what mechanisms account for its persistence? While its presence is widely reported, the underlying mechanisms remain incompletely understood. During maturation, this layer tends to diminish [17], suggesting that it may originate as a remnant of metastable phases formed before CDHA crystallization. As time spent in solution increases, the apatitic core grows by incorporating ions from the hydrated layer, which itself progressively deprotonates and dehydrates [22]. A detailed thermodynamic study quantified the direct role of these maturation conditions – i.e. controlling the amount of hydrated layer through the non-apatitic ionic content – on the enthalpy and thus Gibbs free energy of formation of CDHA samples, and thus their metastability [48].

Christoffersen et al. speculated that the hydrated layer in CDHA could derive from the hydrated layer present in OCP crystals [49]. However, CDHA is not always produced via OCP hydrolysis, indicating that other pathways must exist. One alternative route involves ACP, a known precursor of CDHA. Early studies revealed that freshly synthesized ACP is associated with "relatively labile particles of a calcium acid phosphate-rich ($CaHPO_4 \cdot xH_2O$-like) amorphous phase" located at its surface [47]. This phase decreased as the precipitation reaction progressed. In a purely kinetically driven process, such metastable surface phases would be expected to vanish over time. Yet, the hydrated layer persists, at least partially [17]. This could indicate a diffusion limitation or that the hydrated layer is stabilizing thermodynamically the solid-water interface.

2.6. Hydrated layer: surface charge and interfacial models

Surface complexation frameworks provide a useful conceptual basis for describing interactions between the hydrated layer and the surrounding solution. Such stabilization can be rationalized within this framework [50,51], an extension of the electric double layer (EDL = Stern layer + diffuse layer) model. Such complexation models are commonly used to replicate observed acid-base and ion binding behaviors of mineral surfaces [52]. In this approach, the total charge of a mineral is described as the sum of an intrinsic (permanent) charge, arising mainly from lattice substitutions, and a variable (pH-dependent) surface charge. The latter originates from protonation/deprotonation reactions and the specific adsorption of ions forming inner-sphere complexes with surface sites such as phosphate groups [53,54].

Several authors argue, however, that the hydrated layer of CDHA should not be equated with a classical Stern electrical double layer [55,56], since it represents an integral part of the crystal structure rather than a feature of the surrounding solution. Also, a thickness of about 1 nanometer was reported in the literature for moderately-matured samples [14–16,41,45], which is beyond the scale of the Stern layer, i.e. the compact interfacial layer comprising the inner and outer Helmholtz planes. Together, these interfacial models highlight that the hydrated layer occupies a structurally and chemically intermediate position — strongly bound to the crystal yet in dynamic exchange with the solution. Understanding its precise composition and internal ionic organization is therefore essential to account for its reactivity.

2.7. Hydrated layer: composition and ionic organization

The precise nature of the hydrated layer, typically in terms of local ions organization, and the role of the water molecules is still the subject of debate. It is structurally distinct from the apatite lattice, being hydrated, disordered, and chemically labile [17,49]. In particular, it can incorporate acidic phosphate groups and other ions, making it compositionally closer to CDHA precursor phases such as ACP or OCP [47], although its chemical composition may approach more that of brushite, $CaHPO_4{\cdot}nH_2O$ (with n = 2 for brushite). The FTIR signature of CDHA shows similarities to that of another hydrated calcium phosphate, namely OCP, suggesting that the Ca/P molar ratio of the hydrated layer is low, potentially close to 1.0-1.3 [57]. However, ^{31}P NMR data pointed to clear differences between OCP and CDHA. The authors thus emphasized that the hydrated layer is distinct from these well-crystallized phases, representing instead a transient, non-apatitic, hydrated domain at the crystal surface. Given that this layer is composed of relatively mobile and exchangeable ions, its Ca/P molar ratio is likely dynamic and sensitive to the local ionic environment [58,59]. Variations in the $HPO_4^{2-}/H_2PO_4^-$ ratio of the surrounding solution due to pH change can influence the corresponding ratio within the hydrated layer [58,59]. However, $H_2PO_4^-$ ions are generally considered to be absent from the hydrated layer due to their lower attraction to surface calcium ions and the high solubility of all monocalcium phosphate salts. The possibility of proton hopping was suggested to explain the dynamic behavior of biomimetic apatites in solution, e.g. after drying [60]. To maintain electroneutrality, any compositional shift in the solution would necessitate adjustments in the Ca^{2+} content of the layer, thereby altering its overall Ca/P molar ratio. This dynamic behavior of the hydrated layer offers a plausible explanation for the observed dependence of CDHA's Ca/P molar ratio on the synthesis pH, without requiring changes to the intrinsic composition of the core itself. Indeed, when the Ca/P molar ratio decreases, the surface of CDHA particles becomes increasingly acidic [61,62].

Surface and calorimetry analyses confirmed that the hydrated layer contains water with varying degrees of binding, as well as exchangeable ions, which confer a high reactivity compared to the underlying crystalline core [50,51]. This hydrated layer can be seen as an interphase belonging to the nanocrystals, separating its core from the surrounding solution. It is thus probable that some gradient of physical and chemical properties could exist within this layer. In this view, DSC analyses [22] pointed out the existence of at least two populations of water molecules, with H_2O molecules simply “physisorbed” (and thermodynamically close to liquid water) and H_2O more tightly bound, leaving the surface upon heating at higher temperatures, and corresponding to the “structural” water of the hydrated ionic surface layer. The labile character of the ions in this layer explains for instance its critical role in mineral–solution interactions, including ion exchange, dissolution, and re-precipitation phenomena [53,54,57,63].

These compositional features are not merely static: the exchangeable nature of the ions and the heterogeneity of water binding reflect a layer that is structurally continuous with the crystal yet dynamically coupled to the solution. This dual character, structural yet dynamic, accounts for its central role in determining surface reactivity and bioactivity in both biological apatites and biomimetic apatite-based biomaterials [55,56]. In this context, it is noteworthy that several precursor phases to CDHA also exhibit such intermediate features. In particular, recent studies identified pre-nucleation and ACP species that contain negatively charged complexes with Ca/P molar ratios well below 1.50 [64,65]. These findings support the view that the hydrated layer may be part of a broader spectrum of metastable, ion-rich structures bridging solution chemistry and crystalline apatite.

The ionic organization within this interphase domain is difficult to assess directly, as little structural information is available at that scale. Nevertheless, FTIR and NMR studies suggest the existence of a local ordering rather than a totally erratic ion organization [11,22]. In this view, a recent computational ab initio work based on density functional theory (DFT) and molecular dynamics [66] examined in detail several possible scenarios of ionic organization of the layer with the objective to explain the large set of experimental data available to-date. A plausible scenario, fitting well with experimental results including FTIR additional non-apatitic features, was found when considering an organization close (but not identical) to the hydrated layer found in triclinic OCP, with however some addition of water molecules and allowing the system to relax.

2.8. Compositional heterogeneity and phase assignment

The approximate formula $Ca_{(10-x)}(HPO_4)_x(PO_4)_{(6-x)}(OH)_{(2-x)}$, in which x may vary from 0 to 2, formally permits any Ca/P molar ratio between 1.67 and 1.33, suggesting a wide compositional continuum. Nevertheless, several authors—based on both experimental observations and theoretical considerations—have argued that CDHA with a Ca/P molar ratio of 1.50 is more stable than compositions with slightly lower or higher values [67–71]. More broadly, the literature consistently shows that calcium phosphates tend to crystallize or precipitate as crystalline or amorphous phases with characteristic Ca/P molar ratios, such as 0.5, 1.0, 1.33, 1.50, and 1.67. This raises the possibility that the apparent continuum of compositions implied by the formula $Ca_{(10-x)}(HPO_4)_x(PO_4)_{(6-x)}(OH)_{(2-x)}$ may in practice consist of mixtures of a limited number of discrete crystalline or amorphous phases, for example those with Ca/P molar ratios of 1.00, 1.33, 1.50, and 1.67, in which each phase with a Ca/P molar ratio inferior to 1.67 could be a transient phase towards HA. In this scheme, current analytical tools and characterization methods would have great difficulty distinguishing between, for example, (i) a mixture of ACP and nanocrystalline CDHA, (ii) a homogeneous CDHA phase, or (iii) a core-shell CDHA particle comprising a homogeneous core and a hydrated surface layer—particularly when all exhibit the same overall Ca/P molar ratio (Fig. 4). Even if such differences could be detected, their interpretation would remain challenging. This interpretive ambiguity underscores the need for the careful and systematic characterization as advocated in section 4.

Together, the structural and compositional picture developed in this section provides the foundation for understanding the physicochemical properties of CDHA examined in Section 3, where thermal stability, mechanical behavior, solubility, dissolution, and ion exchange are discussed in turn.

3. Physico-chemical properties of CDHA

The structural complexity established in Section 2, in particular the coexistence of a non-stoichiometric apatitic core and a labile hydrated surface layer, directly governs the physicochemical behavior of CDHA. This section examines the properties that are intrinsic to the material itself, independent of biological context: its thermal stability and the transformations it undergoes upon heating; its mechanical behavior as a macroscopic solid; and its aqueous properties — solubility, dissolution kinetics, and ion exchange capacity — which determine how CDHA

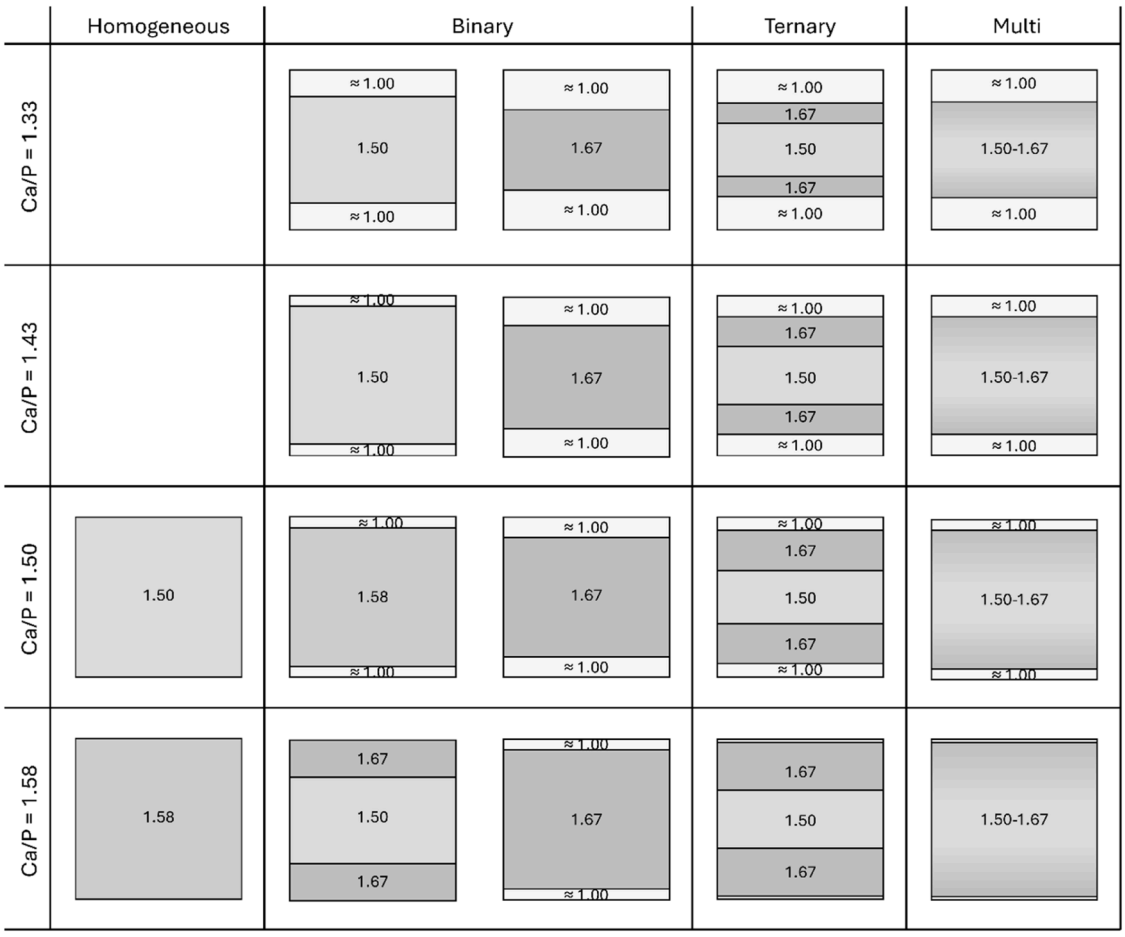

Fig. 4. Schematic representation of possible CDHA particle structures based on the literature. CDHA is generally considered to adopt a core-shell structure with a crystalline core that has a Ca/P molar ratio in the range of 1.50 to 1.67 and a shell made of a hydrated layer with a Ca/P molar ratio below 1.50 (here represented with a ratio close to 1). Accordingly, the latter particles can consist of a mixture of 2 (= binary), 3 (= ternary) or more (= multiple) compositions. However, homogeneous CDHA particles have also been proposed, for example following a hydrothermal process [405–407]. Four Ca/P molar ratios of the CDHA particles are represented. Values of 1.33 and 1.50 are taken because they correspond to an x value of 2 and 1 in the CDHA formula, respectively. The other two values (1.43 and 1.58) are taken arbitrarily. These 4 values correspond to the overall Ca/P molar ratio of the particle. When a Ca/P molar ratio is indicated (e.g. 1.43 or 1.67), it means that the whole "crystal" is homogeneous and has that Ca/P molar ratio. The label "1.50-1.67" refers to a core that contains a mixture of crystals with a Ca/P molar ratio varying between 1.50 and 1.67. For representation purposes, it is assumed that (i) the CDHA particles are prismatic; (ii) the CDHA shell only covers the bottom and top part of the core; (iii) the c-axis is perpendicular to the schemes; (iv) the hydrated layer has a Ca/P molar ratio close to 1.00; (v) when the core is made of more than one composition, the edges have a higher Ca/P molar ratio and the thickness of the central part has an arbitrary thickness; (vi) the density of each phase is identical so that the Ca/P molar ratio of the particle can be inferred from the surface of each respective composition. Here, the hydrated layer thickness decreases with an increase of the Ca/P molar ratio. This effect would be smaller if the Ca/P molar ratio of the hydrated layer increased with increasing Ca/P molar ratio of the core.

interacts with its surrounding ionic environment. These properties provide the essential physicochemical grounding for interpreting CDHA's biological performance, which is taken up in Section 6.

3.1. Thermal stability

The thermal stability of CDHA has been extensively investigated, with a focus on the influence of temperature, time, heating rate, and Ca/P molar ratio [72–81]. As mentioned previously, two endothermic peaks associated with the release of water were identified at 63 °C and 113 °C using differential scanning calorimetry (DSC) [22]. The first peak was attributed to physisorbed liquid-like water, whereas the second peak was attributed to "structural" water bound in the hydrated layer. Interestingly, a rehydrated sample presented almost the same endothermic peaks demonstrating the reversibility of the reaction. No effect of CDHA maturation was observed under the conditions investigated. The amount of liquid water was estimated to be slightly below 2 molecules per unit formula and that of bound water close to 1.5, thus corresponding to about 5% of the total CDHA mass [22]. In contrast, a

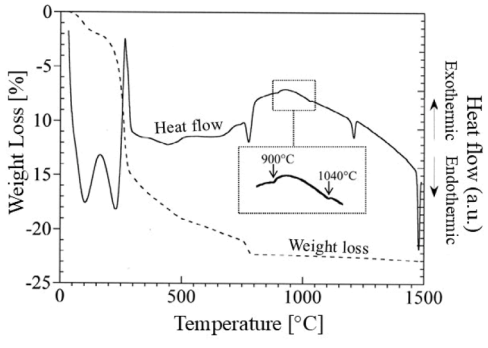

Fig. 5. TG/DTA in air of CDHA raw powder (Ca/P = 1.500). There is a 2 wt% loss close to 100 °C (evaporation of water) and a 13 wt% loss close to 220 °C (removal of bound water). Adapted from [80] and [408].

thermogravimetric analysis revealed a 2 wt% loss close to 100 °C and a 13 wt% loss close to 220 °C (Fig. 5) [80], which happens to be close to the 15 wt% water content of ACP ($Ca_3(PO_4)_2{\cdot}nH_2O$) [82].

Observations show that the condensation of hydrogenphosphate ions occurs within the temperature range of 250–700 °C when samples are heated at a rate of 10 °C/min [73]. This leads to the transient formation of pyrophosphate groups in the 375-600 °C window [73,77,83,84]. Studies on CDHA with a Ca/P molar ratio of 1.50, heated at a slow rate of 2.5 °C/min, detected – as may be expected from the $CaO\text{-}P_2O_5$ phase diagram – the transformation of CDHA into β-tricalcium phosphate (β-TCP; β-$Ca_3(PO_4)_2$) between 720 °C and 730 °C using XRD, with FTIR spectroscopy confirming the disappearance of the OH stretching band at 3569 cm^{-1} between 700 °C and 750 °C [74]. Using a faster heating rate of 5 °C/min and a 10-minute dwell time, the onset of β-TCP formation was observed as early as 700 °C, although most of the transformation occurred between 700 °C and 750 °C [75,80,81]. An earlier onset of transformation, with β-TCP forming around 650 °C during calcination with a 2-hour dwell time, highlights the significant influence of dwell time on the thermal transformation of CDHA [77]. Reports indicate the growth of a Ca-rich metastable phase during CDHA annealing at 750 °C–800 °C, but its chemical nature was not identified [78,79]. These thermal changes can be summarized as follows:

60-200 °C:	Loss of liquid-like water and initiation of the loss of the bound water from the hydrated layer
200-250 °C:	Residual loss of bound water from the hydrated layer
250-700 °C:	Condensation of hydrogenphosphate into pyrophosphate ions ($2HPO_4^{2-} \rightarrow P_2O_7^{4-} + H_2O$)
700-750 °C:	Loss of water upon interaction between the formed pyrophosphate and the present OH^- ($P_2O_7^{4-} + 2OH^- \rightarrow 2PO_4^{3-} + H_2O$) and recrystallization of β-TCP / β-CPP / HA depending on the initial CDHA composition

As previously noted, the hydrated layer is fragile and can be destroyed by drying [57]. However, its ion exchange capacity remains detectable in powders dried at 150 °C [85] and 200 °C [14]. A study on HA suggests that the hydrated layer begins to degrade just above 200 °C [86]. However, a more progressive loss of structural water may be expected and starting below this fixed point. In another study, an irreversible change in conductivity and activation energy was observed from 400 °C, a temperature at the bottom of the formation window of pyrophosphates (375-600 °C) [73,77,83,84]. The authors concluded that these changes were due to “strong microstructural and chemical changes” [87]. While thermal behaviour is governed primarily by the chemistry of the hydrated layer and the $HPO4^{2-}$ content of the core, the mechanical properties of CDHA macroscopic solids are determined largely by their processing history and macroscopic architecture.

3.2. Mechanical properties

CDHA macroscopic solids, which are generally obtained from calcium phosphate cements (CPCs), exhibit mechanical properties that are strongly influenced by its intrinsic porosity and microstructure. Due to the dissolution–precipitation setting reaction, CDHA typically forms a nanocrystalline, highly porous network with limited control over pore size, shape, and interconnectivity. Therefore, the mechanical properties reported in the literature show a wide scatter and depend sensitively on processing parameters, initial cement composition, and porosity [88]. Reported compressive strength values for CPC-derived CDHA materials range from below 1 MPa for highly porous foams up to several tens of MPa for dense formulations [88]. This variability reflects not only differences in formulation but also the dominant role of porosity, which is often intentionally introduced to promote tissue ingrowth. Comparable scatter is observed for other calcium phosphates such as β-TCP, HA, and biphasic calcium phosphate (BCP), though reported values are perhaps slightly higher [89]. Importantly, CDHA and related CPC-based materials are inherently brittle, which precludes their use in load-bearing applications. An exception exists when the mechanical load is transferred to an osteosynthesis plate rather than borne by the cement itself, as in certain craniofacial or maxillofacial reconstructions. In the absence of such fixation, their clinical use is restricted to non-load-bearing situations, where they function as osteoconductive bone graft substitutes. In this context, classical mechanical parameters such as compressive strength or elastic modulus are of secondary importance. Instead, the key practical requirement is sufficient cohesion and integrity of the material to allow handling and implantation without fragmentation or crumbling. Overall, while the mechanical properties of CDHA can be tailored within certain limits through processing and formulation strategies, they remain governed by porosity and brittleness, and must be considered in relation to the intended clinical use, typically non-load-bearing or supported by fixation systems.

3.3. Solubility

The solubility product of CDHA with a molar ratio of 1.50 (i.e. with a global formula of $Ca_9(PO_4)_5(HPO_4)OH$) has been estimated at -85.1 [71,90]. The authors underline the homogeneous nature of the material. This value is considerably higher than the solubility product of stoichiometric HA, reported at –117.2, but still significantly lower than the ionic product found in physiological fluids at pH 7.4 [71,90] (Fig. 6). In practical terms, this implies that a homogeneous CDHA crystal is insoluble under physiological conditions such as those found in serum, cell culture media, or simulated body fluids (SBF) and thus CDHA cannot transform into the thermodynamically stable mixture of HA and DCPA under undersaturated aqueous conditions [91], described by the following reaction:

$$4Ca_9(PO_4)_5(HPO_4)OH + 2H_2O \leftrightarrow 3Ca_{10}(PO_4)_6(OH)_2 + 6CaHPO_4 \quad (1)$$

Nevertheless, experimental data from cell culture media show that CDHA induces a simultaneous decrease in calcium concentration and pH [92–98], along with an increase in phosphate concentration [92–95,98]. Whereas the uptake of calcium could be explained by the precipitation of a calcium-rich mineral or the adsorption of calcium ions on the material surface, the release of phosphate is more difficult to explain. An explanation is based on the assumption that CDHA hydrated layer is more soluble than OCP or DCPA, the phases that are in equilibrium with body fluids [99,100]. The experimental data could then be explained by the dissolution of the hydrated layer and re-precipitation of a more stable, more alkaline phase like CDHA or carbonated apatite. Assuming that the hydrated layer has a composition close to that of amorphous

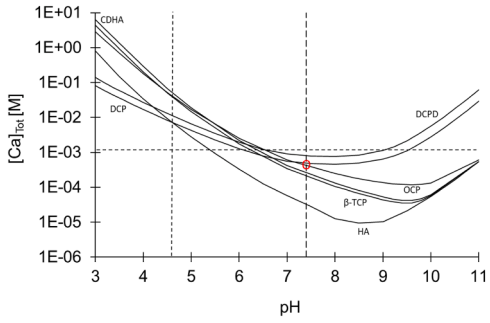

Fig. 6. Solubility isotherms of calcium phosphates in the system $Ca(OH)_2$ – H_3PO_4 – H_2O at 25 °C. The calcium phosphates include DCPA, DCPD, OCP, CDHA (Ca/P = 1.5), β-TCP and HA. The vertical lines show the position of the equilibrium between DCPA and HA (close to pH 4.6), and the physiological pH value (7.4). The horizontal line shows the physiological extracellular calcium level. Experts generally agree that physiological fluids are in equilibrium with OCP or DCPA (red circle). The hypothetical solubility curve of the hydrated layer is expected to be parallel but higher than that of DCPD, consistent with the preferential dissolution of this layer observed experimentally and its role in driving CDHA's faster initial *in vitro* dissolution rates relative to HA.

DCPD [47], the hydrolysis reaction into e.g. CDHA can be tentatively written:

$$(10\text{-}x)\ CaHPO_4{\cdot}nH_2O \leftrightarrow Ca_{(10-x)}(PO_4)_{(6-x)}(HPO_4)_x(OH)_{(2-x)} + (4\text{-}x)\ H_3PO_4 + (10n - 2 + x(1\text{-}n))\ H_2O \quad (2)$$

A similar reaction could also be written in the presence of carbonate ions, for the precipitation of carbonated apatite. Measuring a solubility constant for CDHA is therefore questionable since CDHA is typically heterogeneous and only partially crystalline; however, such measurements were justified at the time by the prevailing assumption (without clear experimental evidence) that a homogeneous CDHA phase existed [71]. The problems related to the determination of the solubility of calcium phosphates due to incongruent dissolution are discussed in more details here [101].

3.4. Dissolution

As already pointed out, CDHA dissolves incongruently, meaning that the Ca/P molar ratio in solution differs from that in the solid bulk phase [47,101,102]. In acidic conditions (pH < 4-5), the incongruency was associated with the precipitation of DCPD on the surface of the particles [59,103]. At higher pH value, the observed incongruency is due to the presence of the calcium phosphate hydrated layer, which is rich in hydrogenphosphate ions and characterized by a Ca/P molar ratio well below 1.67 [13–16]. This labile surface layer is expected to dissolve prior to the thermodynamically more stable crystalline core. Considering the chemical similarity of the hydrated layer to other hydrated phases such as DCPD and OCP [57], one can assume in first approximation that the hydrated layer consists of an amorphous DCPD-like layer and dissolves according to a reaction such as:

$$CaHPO_4{\cdot}nH_2O \leftrightarrow Ca^{2+} + HPO_4^{2-} + nH_2O \quad (3)$$

In this view, the Ca/P molar ratio in the solution should be close to the Ca/P molar ratio of the hydrated layer at early dissolution times. At long dissolution times, when the whole hydrated layer is dissolved, the apatitic core is then expected to start dissolving, thereby raising the Ca/P molar ratio in the solution. Once the crystals are fully dissolved, the Ca/P molar ratio of the solution should match the Ca/P molar ratio of the solid prior to dissolution. If the amount of liquid is too limited to reach full dissolution, the high solubility of the hydrated layer compared to HA solubility may lead to the precipitation of a thermodynamically more stable phase like CDHA and HA (Eq. [2]; Fig. 6). The precipitation would acidify the solution [60] and decrease its Ca/P molar ratio, typically between 0.5 and 1 [104].

The interactions between the CDHA hydrated layer and the solution are expected to be dynamic, meaning that the Ca/P molar ratio observed in suspensions at equilibrium is a function of pH, solid-to-solution ratio, ionic strength, eventual co-presence of circulating ions or molecular species, and finally the history of the CDHA powder [59]. Maturation tests at neutral pH and 37 °C suggest that any change of the maturation solution leads to very long equilibration times [105]. This is particularly true for CDHA porous solids, e.g. produced using a cementitious reaction, which present a nanosized network of pores [106] and accordingly limited ionic diffusion rates within the porous network.

In a closed system, there is not only a decrease in the Ca/P molar ratio of the aqueous solution but also a decrease of pH during maturation (see e.g. Eq. [2]). For example, in a model system where 37.5 g of α-tricalcium phosphate (α-TCP; α-$Ca_3(PO_4)_2$) reacted with 375 mL of deionized water at 37.4 °C, the calcium and phosphate concentrations in the solution increased continuously even after full conversion of α-TCP into CDHA, reaching approximately 2.5 mM and 5.8 mM after 28 days respectively and thus a Ca/P molar ratio of 0.43 [107]. Concurrently, the pH of the solution decreased, with values around 5.6 after 36 hours and 5.0 after 28 days. Similarly, in a system involving a 70 g tetracalcium phosphate (TTCP; $Ca_4(PO_4)_2O$)-DCPA mixture with 350 mL of deionized water at 25 °C, the Ca/P molar ratio of the solution after full conversion to CDHA (24 hours) decreased from 1 to approximately 0.5 after 6 months of reaction [105]. Over the same period, the pH dropped from 6.7 to 4.9. At 37.4 °C, the Ca/P molar ratio and pH values were even lower, reaching approximately 0.29 and 4.5, respectively. These pH values and Ca/P molar ratios are close to the values expected in concentrated systems, at the equilibrium pH between HA and DCPA (or possibly DCPD) [108]. The reason why the Ca/P molar ratio in the solution is close to 0.5, i.e. much lower than the Ca/P molar ratio of HA and DCPA, can be understood considering that there must be a charge balance between the two main anionic and cationic species present in the solution at that pH value namely $H_2PO_4^-$ and Ca^{2+} [60].

As a side note, numerous models have been developed to describe HA dissolution kinetics, though most have achieved only limited predictive success [109]. A common shortcoming is their inability to explain the rapid initial dissolution followed by a near-complete cessation, even under undersaturated conditions [110]. A better understanding of the structure and composition of the hydrated layer, for example using computed models [66], could possibly improve predictions.

3.5. Ion exchange

Beyond its structural role, the hydrated layer plays a crucial function in ionic exchange processes with aqueous solutions, displaying varying degrees of reversibility depending on the exchanged cations [47,111–116]. The exchange is completely reversible for calcium ions (Ca^{2+}) [58,112], partially reversible for strontium (Sr^{2+}) and magnesium ions (Mg^{2+}) [114,117], but irreversible for other cations such as zinc (Zn^{2+}) and cadmium (Cd^{2+}) due to their stronger affinity for the apatite structure [115]. No exchange is generally observed with monovalent cations [118], though exchange with hydronium ions is possible [58] and adsorption of sodium ions (Na^+) has been reported [111]. This selective ion-exchange capability which appears to follow a Langmuir-type isotherm in the case of Sr^{2+} [56] makes biomimetic apatites effective inorganic cation-exchangers, particularly in applications for recovering valuable cations or removing toxic metals from wastewater [115,118–121]. CDHA can also adsorb anions such as carbonate [122] or sulfate ions [111], but the exchange appears at least in some instances irreversible.

Ion-exchange studies report that the affinity of the hydrated layer for cations such as Mg^{2+}, Sr^{2+}, and Ca^{2+} increases as the Ca/P molar ratio decreases [85] while others show that these exchange capacities are not related to this ratio [95]. Beyond the Ca/P molar ratio, the extent and reversibility of ion exchange in apatites particles appear to be strongly influenced by their progressive maturation [22]. As maturation advances, increases in particle size [123], crystallinity and structural ordering [118] reduce the number of exchangeable sites within the hydrated layer, thereby decreasing the overall ion exchange capacity. In media simulating the extracellular fluid of bone, the exchange of calcium and phosphate ions has been shown to significantly modulate the zeta potential [116]. This suggests that these ions are, at least in part, specifically adsorbed onto the mineral surface, likely at the Stern layer (near the shear plane), either before or after undergoing hydrolysis [124]. Additionally, ions such as Sr^{2+} [11,114], CO_3^{2-} [57,125] or toxic metals (as discussed above) may become incorporated into the growing apatitic domains, further limiting their mobility.

The kinetics of calcium exchange at the surface of apatites have long raised questions regarding the underlying incorporation mechanism. In particular, the slow fixation of calcium observed in isotopic exchange experiments cannot be readily explained by a simple solid-state diffusion process within the apatite lattice. Two main hypotheses have historically been proposed to explain the slow fixation of radioactive calcium isotopes (^{45}Ca) in apatite materials. The first, initially proposed by Weikel et al. [126] and subsequently adopted by several authors [112,127], attributes the slow kinetics to the intracrystalline diffusion of calcium ions within the apatite lattice. However, this interpretation was

challenged early on by Neuman et al. [128], who demonstrated that bone mineral crystals can recrystallize rapidly and spontaneously in aqueous media, suggesting that a recrystallization process is more appropriate than simple diffusion. On the basis of the kinetic data reported by Weikel et al. [126], Edgington [129] concluded that the characteristic time constants associated with the slow reaction are incompatible with the laws governing intracrystalline diffusion, and instead support an incorporation of calcium through a dissolution–reprecipitation mechanism. Similar conclusions were later reached by Misra [130] in a reinterpretation of Avnimelech's data [131]. In this framework, calcium "exchange" is not a solid-state substitution process but rather reflects a surface-mediated recrystallization phenomenon. Such recrystallization implies precipitation or coprecipitation processes governed by thermodynamic equilibria, notably the solubility product (K_{SP}), and proceeds through successive steps of nucleation and crystal growth. In the case of heterogeneous systems such as CDHA, these processes are expected to occur preferentially at the crystal–solution interface, i.e. within or through the hydrated surface layer. In this view, the apparent ion-exchange behavior of CDHA emerges from a dynamic interplay between surface dissolution, ion incorporation, and re-precipitation, rather than from bulk diffusion within the apatitic core.

Taken together, these physicochemical properties — governed by the structural duality described in Section 2 — must be reliably measured before any meaningful biological interpretation can be attempted. Section 4 therefore reviews the analytical methods available for characterising CDHA, with particular attention to their limitations and mutual inconsistencies.

4. CDHA characterization

Because the structural and compositional features of CDHA (Section 2) and its intrinsic physicochemical properties (Section 3) cannot be inferred from a single technique, reliable identification of CDHA requires a coordinated set of analytical methods whose strengths, limitations, and mutual inconsistencies must be understood before any biological interpretation (Section 6) can be made — and, as discussed below, many reported controversies in the CDHA literature can be traced to the inappropriate use or over-interpretation of these methods.

The methods used to identify CDHA have evolved significantly over the years. This evolution is evident when comparing the approaches employed in 1987 by a team of experts—who conducted an "international multimethod analysis" of a HA powder precipitated from an aqueous solution [132]—with the more recent techniques discussed below. Nevertheless, given the complex composition of CDHA, there remains a need to define new approaches that can fully characterize CDHA scaffolds intended for biomedical applications. This section provides an overview of the characterization methods most relevant for identifying CDHA. Some of the methods are summarized in Table 5. The focus is not on cataloguing all analytical techniques that can be applied to CDHA, but rather on those that specifically enable its reliable identification [10,132–134]. This section reviews also methods to characterize the 3D structure of CDHA-based scaffolds.

4.1. Determination of chemical purity/identity

A two-step procedure is recommended for the identification of CDHA by X-ray diffraction (XRD) analysis. Initially, the XRD pattern of a CDHA sample should reveal the presence of an HA-like phase without any detectable secondary crystalline phases [135]. Particular attention should be paid to performing a full scan starting at a diffraction angle of 4 ° (2θ) to identify potential OCP remnants. Following firing at 1000 °C in air, a Rietveld refinement of the XRD diffractogram enables estimation of the β-CPP, β-TCP, and HA contents, and thereby calculation of the Ca/P molar ratio [136]. It is important to note that ISO 13779 recommends a long calcination period, specifically 15 hours at 1000 °C, to eliminate all amorphous species, particularly amorphous calcium pyrophosphate species, and allow sufficient time for all species to diffuse adequately as dictated by thermodynamics. Extended firing may also result in phosphate group evaporation, but the effect primarily affects pyrophosphate phases. Orthophosphate phases are less affected [137].

Table 5
Non-exhaustive list of methods used to identify the purity and composition of CDHA. It is advised to refer to [10,132–134] for an in-depth description of analytical techniques of calcium phosphates.

Item	Method	Ref.
Identity	XRD	[148,149,355]
	SS-NMR	[356]
Ca/P molar ratio	ICP	[135,146]
	XRF	[148]
	XRD	[75,135,136,146]
	Ion chromatography	[148,149]
Amorphous content	XRD	[138,139]
	FTIR	[43,357]
Trace elements	ICP	[148,149]
	Atomic absorption	[148,149]
Acid phosphate (HPO_4^{2-})	SS-NMR	[15]
	FTIR	[10,17,144]
	TGA	[132]
	Gee-Deitz	[83]
Hydroxyl (OH^-)	FTIR	[10,132]
	SS-NMR	[151]
Carbonates (CO_3^{2-})	Thermal combustion	[132,150]
	SS-NMR	[358]
Nitrates (NO_3^-)	FTIR	[132]
Leachables	ICP	[154,155,359]

Recent XRD studies have demonstrated the presence of approximately 4–11 wt% amorphous phase in CDHA [138,139] (Table 4). As these values are biologically relevant, accurate quantification of the amorphous content is essential. This can be done by adding an internal standard such as corundum [140] or by applying the G method [138, 139]. However, neither approach can distinguish between ACP, a known precursor to CDHA [141–143] and the hydrated layer. Bone and carbonated apatites are reported to contain substantially larger amorphous fractions, ranging from 30–70% [43,44] (Table 4), but it remains unclear whether CDHA can accommodate amorphous contents exceeding the 4–11 wt% reported here. As discussed in Section 2, part of the apparent discrepancy between XRD and solid-state NMR estimates of the amorphous fraction may be methodological rather than material-related, reflecting the assumption (implicit in the NMR-based quantification) that all HPO_4^{2-} groups reside in a non-apatitic environment.

A complementary approach is to quantify the hydrogenphosphate content using alternative analytical methods, since HPO_4^{2-} groups are expected to be enriched in the hydrated surface layer. This quantification is not without pitfalls either, as ACP itself may contain acidic phosphate species depending on its synthesis conditions [47], which can subsequently undergo partial internal hydrolysis. Several analytical methods have been described [132], including thermal analysis, the Gee-Deitz method [83,144], radioactive and kinetic methods, as well as FTIR spectroscopy [10,144]. Reported values for one specific CDHA powder ranged from 0.6 to 3.5 wt%, depending on the technique employed [132]. In one study, results obtained using the Gee-Deitz and FTIR methods showed good correlation [144]. However, FTIR consistently yielded higher values than the Gee-Deitz method. Moreover, the relative difference between the two techniques increased as the hydrogenphosphate content decreased, approaching a factor of two for powders with the lowest hydrogenphosphate levels. Solid-state NMR provides a more direct quantification of hydrogenphosphate [13,15,35, 145]. Quantitative ^{31}P MAS NMR allows the separation and integration of HPO_4^{2-} and PO_4^{3-} signals, yielding reliable bulk values. Complementary ^{1}H–^{31}P correlation experiments further confirm assignments through the characteristic interaction of HPO_4^{2-} groups with P–OH

protons.

Because ion substitution can occur within the CDHA structure, it is essential to complement crystallographic analysis with chemical characterization to ensure both structural and chemical purity. These include inductively coupled plasma – optical emission spectroscopy (ICP-OES) or ICP-mass spectrometry (ICP-MS) [135,146], X-ray fluorescence (XRF) [147,148], and ion-chromatography [148,149]. A strong correlation ($r^2 > 0.99$) is generally observed between the Ca/P molar ratios determined via chemical analysis and those calculated from Rietveld refinement [135,136] (Fig. 7). Energy-dispersive X-ray spectroscopy (EDX) is a valuable tool for the detection of contaminants, in particular particulate contaminants, but is too inaccurate for the determination of the Ca/P molar ratio [134]. Cationic impurities can be identified using techniques such as ICP-MS or X-ray fluorescence (XRF). Carbonate ions can be detected either by measuring the total inorganic carbon content, typically using a thermal combustion method [150], NMR [151], Raman Spectroscopy [97], or FTIR [22,132,150]. Raman and FTIR offer also a convenient method for identifying other polyatomic ions, such as nitrate [132], fluoride [152], and hydroxyde groups [10]. Notably, Raman spectroscopy has less water vibrations compared to IR spectroscopy, which is an advantage when studying biological or hydrated samples (although fine details observable by FTIR due to the higher intensity of bands in the ν_4PO_4 domain may be more difficult to detect by Raman). An indirect indication of CDHA purity can be obtained by verifying the positions of XRD diffraction peaks by adding a suitable line position standard. However, the interpretation of the results may be difficult considering the effect of the Ca/P molar ratio on the lattice parameters. Bound and adsorbed water contents can be determined through gravimetric analysis, which can also provide an indirect estimate of hydrogenphosphate content [132]. Finally, solid-state NMR and FTIR (e.g. for carbonate and silicate ions) can be used to determine ionic substitutions [13,15].

A recently proposed mechanism for osteoinduction [153] suggests that the presence of ionic species in the environment surrounding CDHA implants may significantly influence their osteoinductive potential. Two recent *in vitro* studies [154,155] have shown that calcium phosphate bone granules can substantially alter the ionic composition of the surrounding incubation medium. In some cases, the medium was found to be nearly depleted of all calcium or phosphate ions [154]. Consequently, conducting a leachable and extractable analysis in accordance with ISO 10993-18:2020 is essential to better understand the biological behavior of CDHA-based materials.

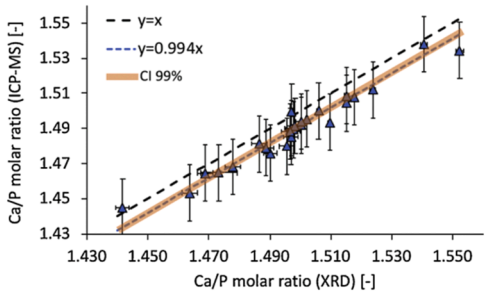

Fig. 7. Correlation between Ca/P molar ratios measured by two independent techniques: XRD (x) and ICP-MS (y). Black dashed curve represents the equation y = x while the blue point dashed curve represents the correlation between XRD and ICP-MS (y = 0.994 x; $R^2 = 0.948$). The 99% confidence interval (CI) is indicated in orange. Error bars for ICP-MS Ca/P molar ratios correspond to Uk=2 values and those for XRD Ca/P molar ratios to repeatability (2.77* estimated standard deviation). (For interpretation of the references to colour in this legend, the reader is referred to the web version of this article). Figure taken from [135].

4.2. 3D structural analysis

A range of analytical techniques is available to characterize the three-dimensional structure of CDHA scaffolds. Among these, micro-computed tomography (μCT) is a valuable tool for evaluating the architecture of these structures; however, its use in ex vivo analysis presents certain challenges, particularly due to the similar radiopacity of CDHA to that of bone mineral [156]. Scanning electron microscopy (SEM) offers higher resolution imaging of structural features. SEM analysis can be conducted on fractured surfaces (e.g., [106,157]) or on polished cross-sections (e.g., [158,159] (Fig. 8). In addition to morphological evaluation, polished sections provide insights into the homogeneity and porosity of the CPC matrix. For a more quantitative and in-depth analysis of porosity, however, mercury intrusion porosimetry remains the gold standard [106,157].

Nitrogen adsorption is widely used to assess the nanoscale textural properties of CDHA, offering valuable information not only on SSA, which reflects crystal fineness, but also on the pore size distribution. These parameters are indeed directly related to the pore network, which governs molecular transport within the materials. Although pores are generally largely interconnected, both pore diameters and pore size distribution are highly dependent on the synthesis conditions. This variability significantly influences the accessibility of the porous structure to biological molecules. Notably, a threshold pore size of approximately 1 μm appears to exist, below which bovine serum albumin (BSA) is unable to penetrate the pore network [106] (Fig. 9). This limitation is likely attributable to pore-entry constrictions as well as adsorption and tortuosity effects. However, particular caution is required when performing nitrogen sorption measurements to determine the SSA, given the thermal and vacuum sensitivity of the hydrated ionic layer covering the nanocrystals. At present, no clear consensus has been established regarding the most appropriate initial outgassing conditions. To preserve the structural integrity of this surface layer, it is advisable to limit the maximum temperature to no more than 100 °C, extend the pretreatment duration if necessary, and apply only primary (mild) vacuum conditions.

5. Synthesis of CDHA powders, granules, and scaffolds

The structural complexity established in Section 2, in particular the coexistence of a non-stoichiometric apatitic core and a hydrated surface layer, directly constrains how CDHA can be produced. Any high-temperature processing route would destroy the very features that define the material; this section therefore focuses on the low-temperature pathways that preserve CDHA's characteristic chemistry. The physicochemical properties reviewed in Section 3 — in particular the thermal instability of the hydrated layer and the solubility relationships governing dissolution and reprecipitation — provide the mechanistic rationale for the synthesis strategies described here.

CDHA powders are typically synthesized through aqueous precipitation [80], but this route alone does not enable the fabrication of the granules, scaffolds, and macroscopic constructs commonly used as bone graft substitutes (Fig. 10). Because CDHA is thermally unstable and transforms into other calcium phosphate phases upon conventional firing, its processing differs fundamentally from that of sintered ceramics. Macroscopic CDHA constructs are generally produced through alternative low-temperature pathways that rely on dissolution–precipitation processes under aqueous or near-aqueous conditions. This section reviews these production routes in the order in which they are typically considered. It first describes the aqueous precipitation of CDHA powders, including the role of transient phases such as ACP and OCP, before discussing the morphology of the resulting particles in dilute and in concentrated systems. The synthesis of macroscopic solids is then examined through three complementary families of reactions — hydrolysis of calcium phosphate precursors, hydraulic cement reactions, and solid–solid conversion routes — followed by the specific strategies

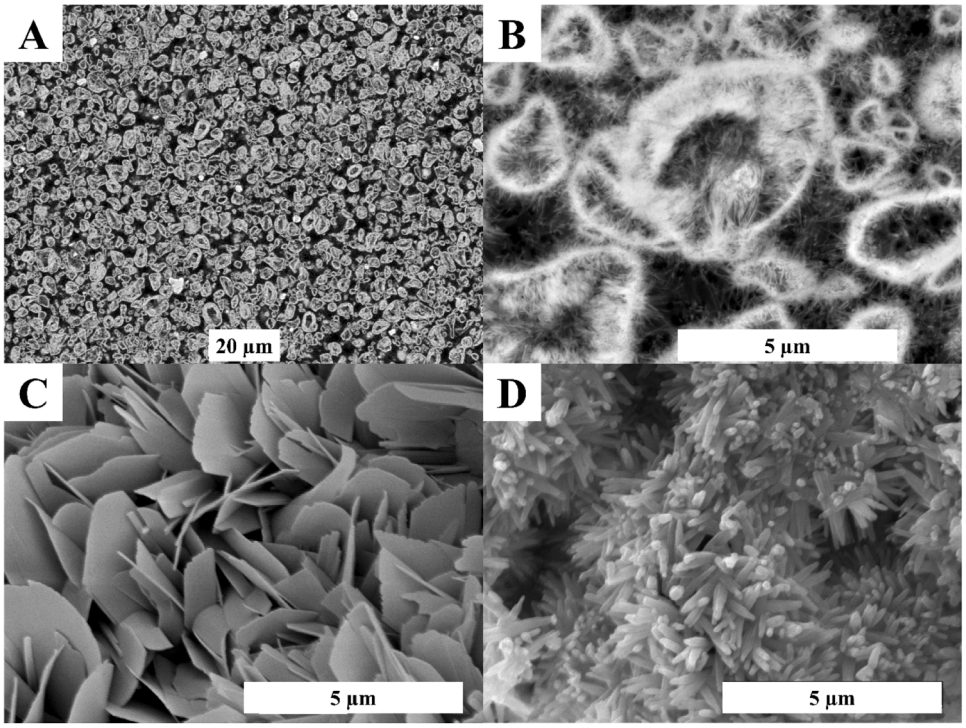

Fig. 8. Diverse CDHA crystal morphologies obtained from α-TCP hydraulic reactions; (a, b) polished sample; (c, d) surface of a pore; Mixing liquid rich in (a-c) phosphate ions and (d) calcium ions. SEM images taken from (a-c) [159] and (d) [202]. ; black = porosity; white = material.

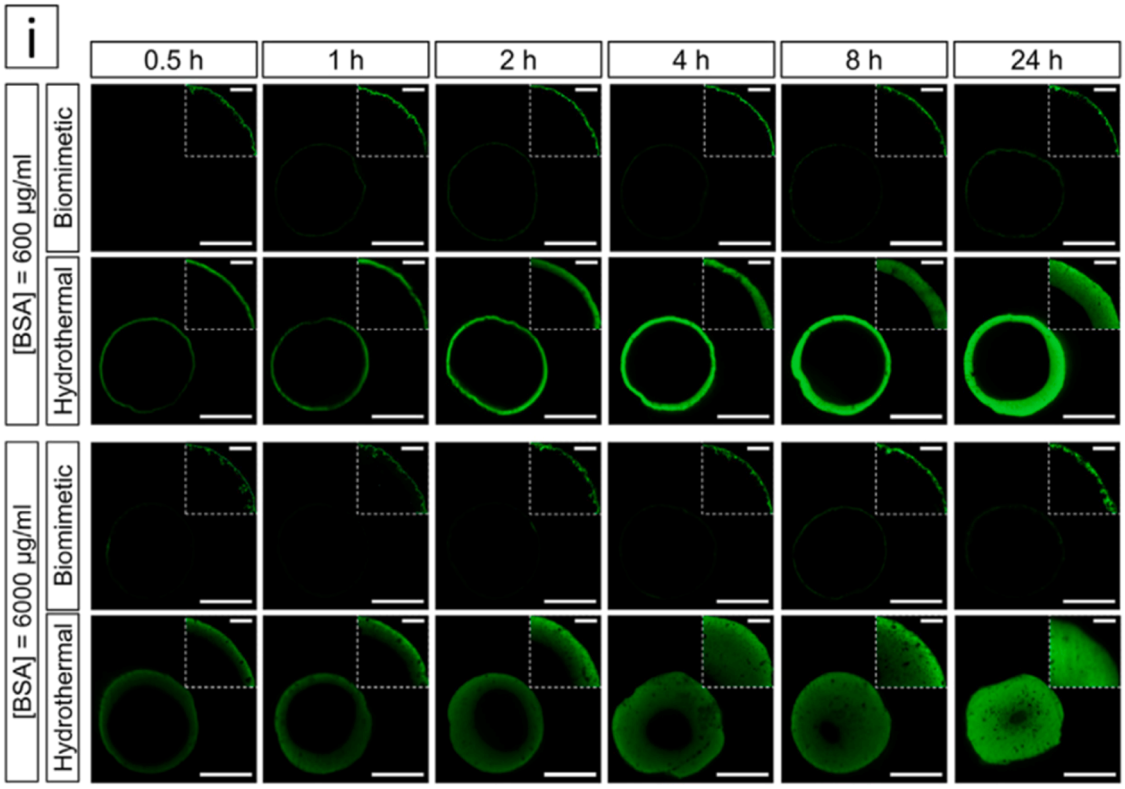

Fig. 9. Comparison of the protein adsorption properties of the biomimetic and hydrothermally treated CDHA samples incubated in two different BSA concentrations. Fluorescent confocal microscopy images of the strand's cross-sections illustrating the penetration of BSA (in green) at different incubation times. Main images acquired with normalised settings for a better comparison between conditions. Scalebar = 200 µm. Inserts showing a close-up view of the surface penetration with optimised settings individually adjusted for each image. Scalebar = 50 µm. Taken from [139];.

used to introduce macroporosity into granules and scaffolds (gas, liquid, and solid pore-forming agents; 3D printing; intergranular templating).

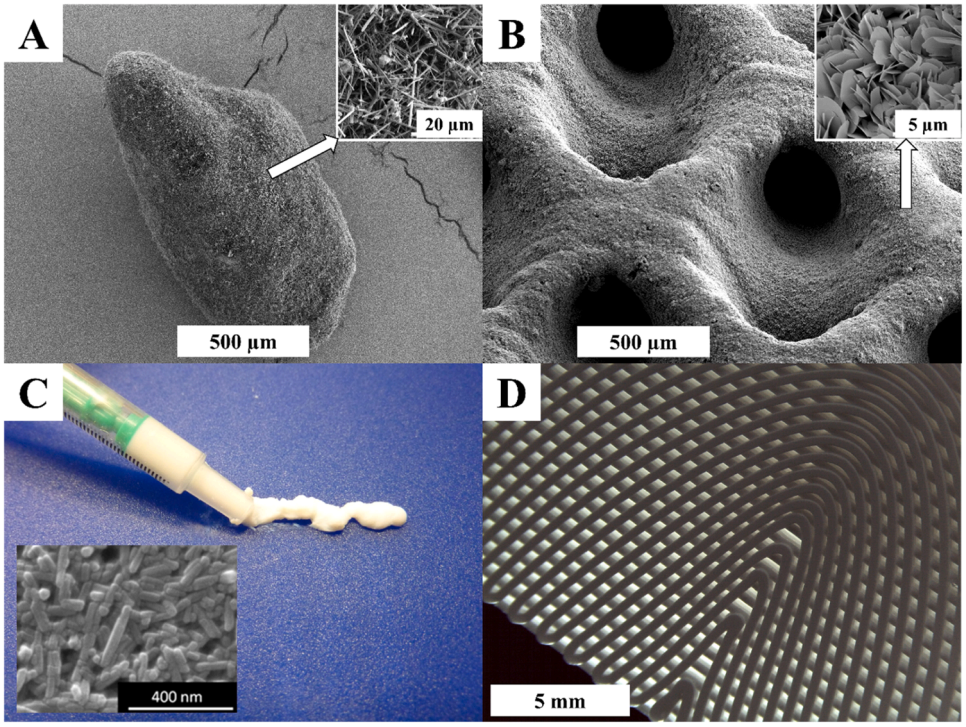

Fig. 10. Some examples of CDHA bone graft substitutes: (a) granule without macroporosity; (b) macroporous scaffold; (c) injectable aqueous paste containing CDHA nanorods [409]; (d) macroporous scaffold obtained by robocasting (scale bar: 5 mm; courtesy of S. Heinemann, InnoTERE GmbH, Germany); taken from [410].

Recent low-temperature densification approaches, most notably spark-plasma sintering and cold-sintering, are then introduced. These methods open new opportunities for consolidating CDHA while avoiding the phase instability associated with traditional sintering [160,161]. The section concludes with an overview of the main CDHA formats derived from these processing strategies and their implications for clinical use.

5.1. CDHA precipitation

Various raw materials can be used to produce CDHA through aqueous precipitation. The calcium source is typically a chloride or nitrate, while the phosphate source is commonly ammonium, potassium, or sodium hydrogenphosphate (Table 6). A key advantage of using calcium nitrate and ammonium hydrogenphosphate is that nitrate and ammonium ions are not included in the CDHA lattice and remain spectator ions. Also, these compounds are eliminated during thermal treatment, enabling the formation of pure α-TCP or β-TCP phases without the incorporation of foreign ions, such as Na [17]. However, this method has drawbacks, including the hazardous nature of raw materials and the corrosive effects of ammonia. Particular attention must be given to the purity of the calcium source, because it often contains divalent cations like Mg^{2+} or sometimes Sr^{2+} [135]. Precautions should also be taken to prevent the incorporation of carbonate ions in alkaline conditions, for example by bubbling nitrogen in the reactor or performing the synthesis in a protected environment [31,58,59]. Although most authors add the phosphate solution to the calcium solution [13,50,61,62,162,163], some leading groups follow the reverse order to use the buffering capacity of phosphate solutions [17,65,117]. Only a few studies have explicitly examined the influence of reagent-addition order on CDHA synthesis [164–166] and even fewer report any measurable effect [164]. This limited attention may reflect the fact that, in many cases, changing the order of addition does not significantly affect the final product [47].

CDHA aqueous precipitation is generally performed at a pH value of 6 to 9 [17,30,79,80,135,167,168]. A lower pH may lead to DCPD or OCP formation [47,59,103,167,169]. The higher the pH and temperature are, the higher the chance of approaching the stoichiometry of HA. Kinetics play an important role since the first formed phase may depend on the reagent addition rate [169,170]. Also, the initial phase formed is typically not CDHA but a metastable phase like ACP [141–143]. ACP particles are often spherical, close to 50-100 nm in diameter, and made of

Table 6
Approaches used for the synthesis of CDHA with two liquid precursors, one calcium rich, one phosphate rich. For the sake of simplicity, the table does not differentiate between dehydrated and hydrated salts, e.g. $Ca(NO_3)_2{\cdot}4H_2O$ instead of $Ca(NO_3)_2$, or between the protonation of the phosphate salt (Na_2HPO_4 vs NaH_2PO_4).

Ca source	P source	Ref
$CaCl_2$	$(NH_4)_2HPO_4$	[142,175–179,196,360]
	K_2HPO_4	[361,362]
	KH_2PO_4	[65]
	Na_2HPO_4	[171,193,360,361,363,364]
$Ca(NO_3)_2$	$(NH_4)_2HPO_4$	[17,21–23,72,80,87,95,104,135,136,168,178,179,194,241,282,321,333,365–373]
	K_2HPO_4	[30,31,132,174,180,181,321]
	Na_2HPO_4	[172,189]
$Ca(OH)_2$	H_3PO_4	[32,45,61,136,167,208,374–376]
	$Ca(H_2PO_4)_2$	[58,59,103,377]
$Ca(CH_3COO)_2$	H_3PO_4	[70,378]
	$(NH_4)_2HPO_4$	[331]

smaller entities such as Posner's clusters [49,143,171]. Notably, the formation of ACP can be prevented by seeding the supersaturated calcium phosphate solution with apatite crystals [172]. The conversion of ACP to CDHA has been claimed to be an autocatalytic process [173]. CDHA crystals typically form on the ACP surface [143,171,172], but an internal hydrolysis process between PO_4^{3-} ions and neighboring H_2O molecules had also been proposed [68]. The conversion proceeds more rapidly by lowering the pH value from alkaline to neutral, at lower Ca/P molar ratios (due to shortened induction times), and in the presence of seed crystals, which eliminate the nucleation barrier [142,173,174]. Conversely, it can be delayed or inhibited by crystallization inhibitors, such as pyrophosphate or magnesium ions [142,175–177].

Some authors have reported that this ACP-to-CDHA transformation follows a 2-stage maturation process [47,80,173,178–180]. However, the definition of a "stage" varies from authors to authors. In some studies, the two stages were related to the change of slope of the Ca/P molar ratio during maturation [80]. In other studies, the two stages were associated with the changes of phases, namely the formation of OCP as another intermediate phase, followed by its conversion to CDHA [49,174,180–184]. The analysis of the chemical species which are present during the conversion of ACP to OCP and then from OCP to CDHA suggests that OCP crystallization is kinetically favorable, but only in slightly acidic conditions, close to neutral pH values (Fig. 11). There is also a report that the ACP to CDHA transformation follows a 3-stage maturation process: a first ACP phase is transformed into a second ACP phase, which eventually convert to OCP and CDHA [49]. In alkaline conditions, ACP is directly converted to CDHA [174,182]. In contrast to Mg^{2+}, the presence of fluoride ions F^- in the solution favors this direct conversion [185,186], possibly due to the greater thermodynamic stability of fluorapatite compared to HA [187].

As the structure of (triclinic) OCP involves a stacking of apatite and hydrated layers (Fig. 2), CDHA could conceptually form by hydrolysis of OCP without the need for new crystal nucleation [24,188–190]. In other words, the OCP-to-CDHA conversion would be a solid-state (i.e. topotactic) reaction during which the phosphate groups of OCP are relocated [189,191]. Various models for the hydrolysis of OCP to an HA structure have been discussed such as an interlayered structure of OCP and HA domains [24,188] (Fig. 12). Experimental evidence favors, however, a core-shell or core-surface model (Fig. 3) with an apatitic crystalline core surrounded by a hydrated layer. The hydrated layer could be a remnant of the OCP hydrated layer [49] and lower the interfacial energy between the crystalline core and an aqueous solution.

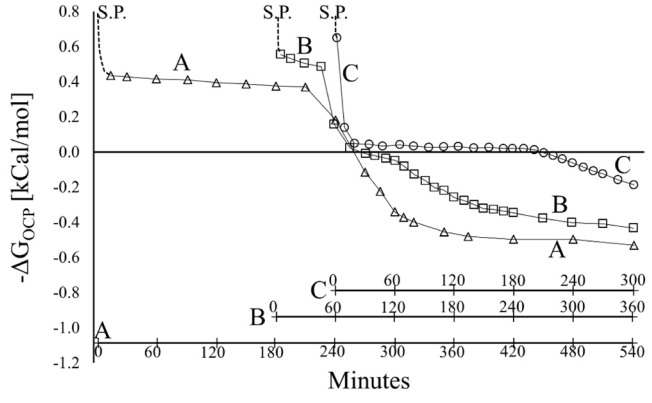

Fig. 11. During the spontaneous precipitation of HA in solution, OCP is sometimes formed as intermediate phase. This can be seen by looking at the evolution of solution saturation towards OCP. At pH 7, the solution is in metastable equilibrium with OCP during roughly 200 minutes (line C is horizontal close to $\Delta G_{OCP} = 0$). At pH 8 (line B), this range is much shorter. At pH 9, there is no inflection of the saturation curve close to $\Delta G_{OCP} = 0$ suggesting that ACP is directly transformed into HA. "S.P." indicates the start of the precipitation. Adapted from [182].

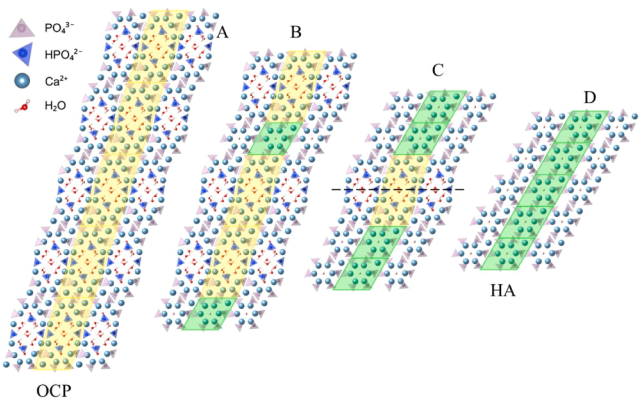

Fig. 12. Schematic transformation of (A) OCP into (D) HA. (B) and (C) represent interlayered mixtures of OCP and HA. Brown et al [188] postulated that the structure shown in (C) could split in the middle (dashed line) due to internal strains provoked by the transformation. Tseng et al [189] proposed that the OCP-HA transformation starts at both ends of the OCP crystal and move towards the center, potentially leaving a "central dark line" in the middle of the crystal (situation shown in C).

Considering the large consumption of calcium vs phosphate during the conversion, it is more likely that the hydrated layer in OCP converts to an HA layer through the release of phosphate (conceptually Eq. [2]: hydrated layer → HA + phosphoric acid) rather than through the uptake of calcium (conceptually: hydrated layer + Ca^{2+} ions → HA + H^+ ions) [189,192].

As maturation progresses, the Ca/P molar ratio increases and stabilizes after 1–2 days in calcium phosphate solutions [17,80,180], or after several weeks in cell culture medium [95,97] (Fig. 13). Zeta potential measurements also indicate that full maturation may take several weeks [124]. If the pH of the mother solution is not regulated, a drop of more than one unit can occur during maturation [95]. The final Ca/P molar ratio of the precipitate tends to increase with higher pH values [17,80], and elevated temperatures further enhance this ratio [17,80,168]. The mechanism underlying the increase in the Ca/P molar ratio remains unclear, although it is often hypothesized to arise from a reduction in the size of the hydrated layer rather than to an increase in the Ca/P molar ratio of the CDHA crystalline core [17].

5.2. *Morphology of precipitated CDHA particles in diluted and concentrated systems*

In the literature, CDHA particles exhibit markedly different morphologies. In some studies [80,135,193–195], they appear as roughly spherical particles with diameters of about 20–50 nm in diameter (Fig. 14). In others [61,70,193–196], they present acicular, needle- or

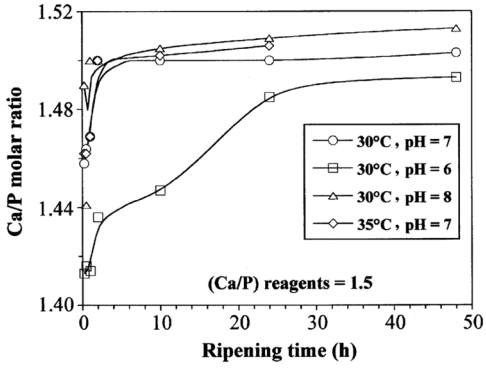

Fig. 13. Ca/P molar ratio of CDHA precipitates vs. the ripening time for different synthesis conditions. Taken from [80].

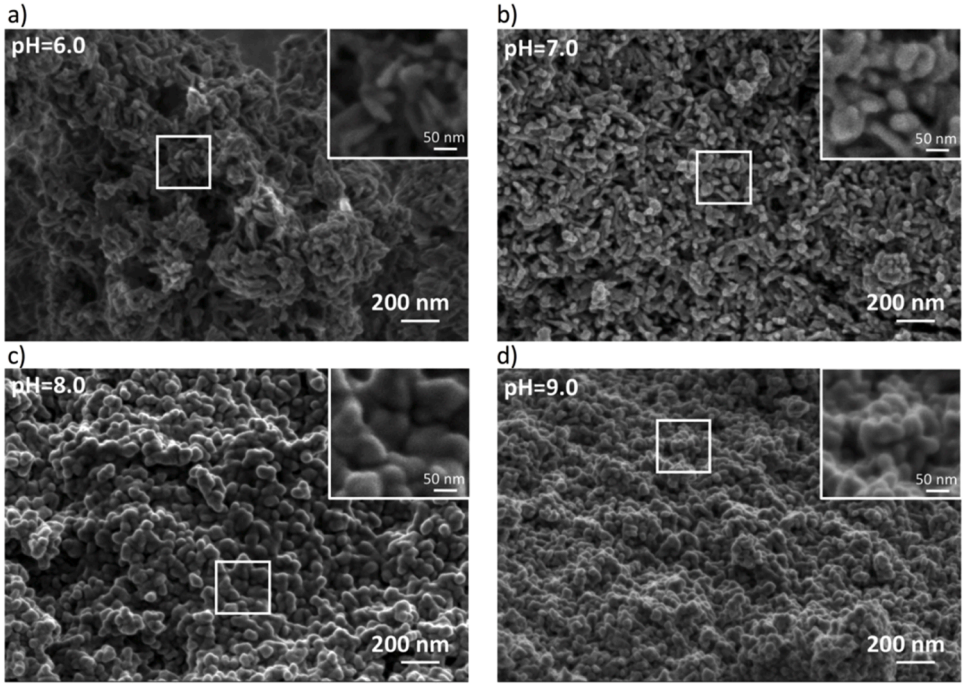

Fig. 14. Morphology of CDHA particles produced by precipitation of calcium nitrate and ammonium phosphate at a pH ranging from (a) 6.0 to (d) 9.0. Taken from [135].

rod-like shapes, with thicknesses below 50 nm and lengths exceeding this value (Fig. 15).

A large body of work has focused on ACP-mediated formation pathways. ACP generally forms as spherules with diameters of 30–100 nm [47,142,172], and its subsequent conversion to crystalline apatite can proceed with or without significant changes in particle morphology [47,171,178] (Fig. 16), as schematically outlined by [42]. Both dissolution–reprecipitation [197] and hydrolysis [198] mechanisms have been proposed to explain the crystallization of amorphous phosphate into apatite, even in cases where morphology is largely preserved. The presence of mixed-phase particles, consisting of a crystalline core intimately associated with a variably thick amorphous surface layer, has been interpreted as evidence for such hydrolysis-driven transformations and could account for the results obtained in several studies [80,135,193,199]. Besides ACP, OCP is another well-established precursor of CDHA, and its transformation pathway also influences the resulting morphology. When CDHA forms through the hydrolytic conversion of OCP, the product frequently adopts a platelet-like morphology rather than a needle- or rod-like shape, reflecting the layered structure of OCP and its progressive rearrangement into an apatite lattice during hydrolysis [190]. After the initial crystallization step, irrespective of whether ACP or OCP is involved, an Ostwald ripening process, describing the growth of larger crystals at the expense of smaller ones [200,201], has occasionally been proposed to explain the continued growth of apatite crystals during the post-conversion phase, i.e., the maturation of the crystallites [179,180]. Finally, slight variations in the morphology of CDHA crystals may result from changes in the solution pH; specifically, CDHA particles tend to become less spherical at lower pH values (Fig. 11).

In concentrated systems, such as in CPCs, the shape and size of the CDHA crystals vary according to the presence of additives, liquid-to-powder ratio, and the SSA of precursors such as α-TCP powder. Increasing the SSA of α-TCP transforms a platelet-like structure into a needle-like structure [106] and leads to finer crystals [157]. The presence of calcium chloride in the mixing liquid favors a needle-like structure (Fig. 8) [202]. This ability to finely tailor the morphology of CDHA crystals, particularly to produce structures with a high aspect ratio, enables significant improvements in several key properties of CDHA materials, including molecular adsorption, ion exchange capacity, catalytic activity, and even the mitigation of the inherent brittleness of ceramics [203]. This has sparked growing interest in a range of application areas, including catalysis, energy storage, and the design of surfaces with antimicrobial properties [204,205].

5.3. CDHA production by calcium phosphate hydrolysis

Instead of starting from solution-precursors, CDHA can be produced by hydrolyzing calcium phosphate powders such as DCPA, DCPD, OCP, α-TCP, and ACP (Table 7). The reaction relies on the dissolution of the calcium phosphate raw material, which is influenced by its solubility. Since the solubility of most calcium phosphates decreases with increasing pH, higher pH levels may inhibit the conversion of the raw material into CDHA [206]. When sodium hydroxide is used to maintain a constant pH, sodium ions may be incorporated into the CDHA particles [207], thereby contaminating CDHA. CDHA can also be obtained from the hydrolysis of other calcium salts, such as calcium oxide or hydroxide [136,208], calcium carbonate [76,165,209–211], and calcium sulfate [212–218], but in the latter case with the risk of incorporating carbonate and sulfate ions.

5.4. CDHA production using hydraulic cement reactions

Different hydraulic cement reactions can be employed to obtain CDHA macroscopic solids. These reactions typically involve either the hydrolysis of ACP, α-TCP, or acid-base reactions (Table 8), like mixtures of TTCP and DCPA powders [219,220]. The concentrated powder-aqueous solution mixtures harden through the entanglement of the precipitating crystals, thereby creating a cohesive macroscopic solid. Examples of hydraulic reactions leading to CDHA formation are as follows:

$$3\ Ca_3(PO_4)_2{\cdot}nH_2O \rightarrow Ca_9(HPO_4)(PO_4)_5OH + (3n\text{-}1)\ H_2O \quad (4)$$

$$3\ \alpha\text{-}Ca_3(PO_4)_2 + H_2O \rightarrow Ca_9(HPO_4)(PO_4)_5OH \quad (5)$$

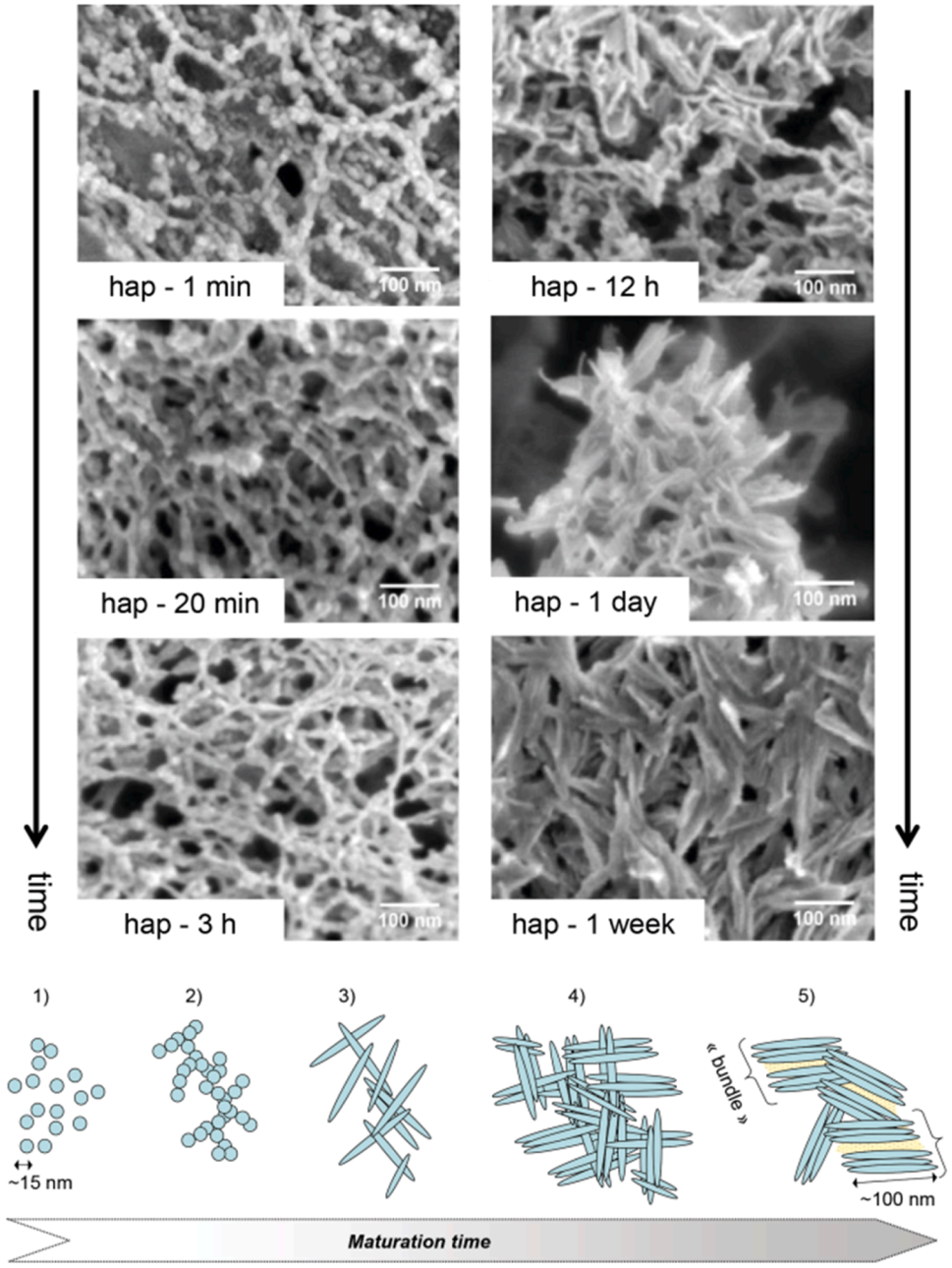

Fig. 15. Cryo-FEG-SEM observations of nanocrystalline apatites matured at 25 °C between 1 min and 1 week and directly analyzed (initial magnification: 150'000x), and schematic representation of the evolutional change of morphology. Taken from [22].

$$3\ Ca_4(PO_4)_2O + 6\ CaHPO_4 \rightarrow 2\ Ca_9(HPO_4)(PO_4)_5OH + H_2O \quad (6)$$

Among these, the hydrolysis of α-TCP is the most used approach to producing CDHA granules and scaffolds, as α-TCP is relatively easier to produce and has a better shelf-life stability compared to ACP and TTCP.

The handling properties of CPCs such as injectability [221,222], cohesion [223], and setting time [224] play a crucial role in their clinical application. However, these aspects are beyond the scope of the present review. In contrast to CDHA powders which are often spherical (Fig. 11), CDHA solids are generally composed of thin needle- or plate-like structures, possibly because CDHA solids are synthesized for several days, leaving time for crystal maturation. SSA values of CDHA scaffolds produced from α-TCP are typically in the range of 15 to 40 m^2/g [106,157,202,225], but values close to 200 m^2/g can be obtained using other raw materials such as ACP [226].

During the aqueous precipitation of CDHA, the formation of intermediate phases commonly precedes its crystallization. Similar phenomena have been observed in CPCs. TEM studies revealed that α-TCP surfaces are initially covered with an amorphous layer [227,228] (Fig. 17). This layer subsequently serves as a substrate for the nucleation of HA crystals, which grow into fine, needle-like structures [228]. The presence of this amorphous phase has been proposed to explain findings from a study investigating the evolution of crystalline phases during the hydraulic setting of α-TCP-based cements [138]. In this context, the ACP content was estimated at approximately 5% in one study [138] and about 10% in another [139].

In a related investigation employing isothermal calorimetry, a delayed endothermic event was attributed to the crystallization of an initially amorphous phase [229]. Furthermore, several authors have speculated on the possible formation of OCP during α-TCP hydrolysis. While OCP is generally not detected [227,230], it may form under near-neutral pH conditions during mixing [231–233]. Beside ACP and OCP, monoclinic HA is the third phase that has been discussed as a

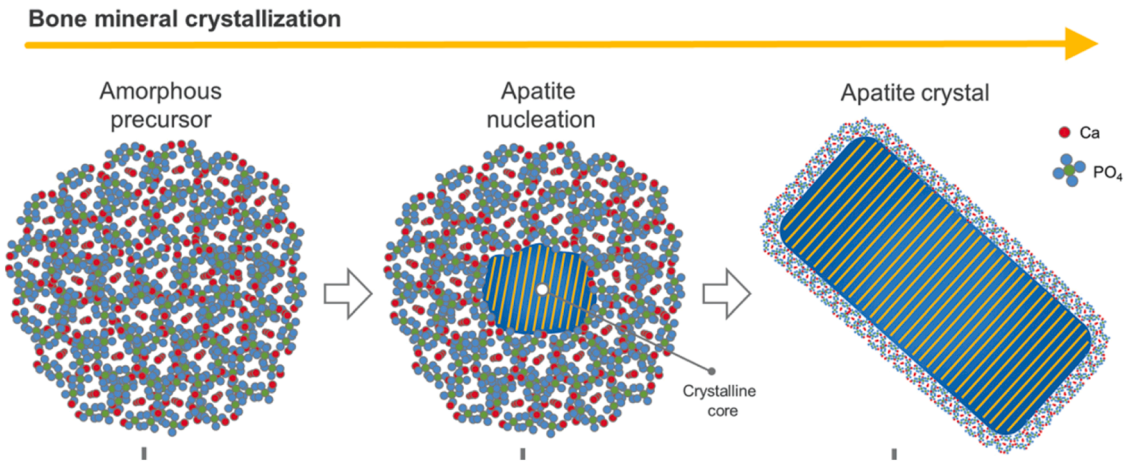

Fig. 16. Schematic of bone mineral crystallization and detection of the conversion of amorphous calcium phosphate (ACP) into apatite. The conversion of ACP into apatite may involve different stages, in which atoms in the center of amorphous particles rearrange into a crystalline core where apatite is nucleated. As the mineral crystallizes, atoms from the ACP component are progressively incorporated into the crystal lattice, leading to the growth of the apatite domain and reduction of the amorphous shell. Taken from [42].

Table 7
Approaches used for the synthesis of CDHA with one solid precursor and one liquid precursor. Calcium phosphates are hydrolyzed in alkaline conditions. Calcium carbonate is combined with phosphoric acid. Calcium sulfates ($CaSO_4$, $CaSO_4{\cdot}0.5H_2O$, $CaSO_4{\cdot}2H_2O$) are combined with ammonium phosphate solutions. It is likely that apatites produced from calcium carbonates and calcium sulfates contain carbonate and sulfate impurities.

Solid precursor	Ref
MCP	[59,377]
MCPM	[103,236]
DCPA	[206,237,320,321]
DCPD	[85,206,207,237,379,380]
OCP	[238–240,381–383]
ACP	[17,22,30,31,47,80,132,135,142,171–180,226,229,241,360,361, 363,364,384,385]
α-TCP	[107,138,228,234,235,242,243,259–261,386–392]
β-TCP	[386]
$CaCO_3$	[76,165,209–211]
$CaSO_4$	[212–218]

Table 8
Approaches used for the synthesis of CDHA with two solid precursors and an aqueous solution. TetCP (Ca/P = 2.0) is combined with a calcium phosphate with a Ca/P molar ratio inferior to 1.50 such as MCPM, DCPA, DCPD and OCP.

Solid 1	Solid 2	Ref
MCPM	TetCP	[393]
DCPA	TetCP	[91,394–399]
DCPD	TetCP	[105]
OCP	TetCP	[400]

potential transient phase occurring during α-TCP hydrolysis into CDHA [230]. However, distinguishing monoclinic from hexagonal HA in nano-crystalline samples is extremely difficult due to severe peak overlap in XRD patterns. Nonetheless, obtaining the monoclinic HA phase is highly improbable, as this structure requires a perfectly ordered antiparallel arrangement of the OH^- ions in adjacent apatitic channels. For HA to appear monoclinic in XRD, the material must be nearly defect-free and within the appropriate temperature range. In all other situations, the structure will almost certainly appear hexagonal.

The hydrolysis of α-TCP is often characterized by an initial pH increase of the solution and/or an alkaline pH range [107,234,235], followed by acidification of the solution down to pH 4-4.5 and a

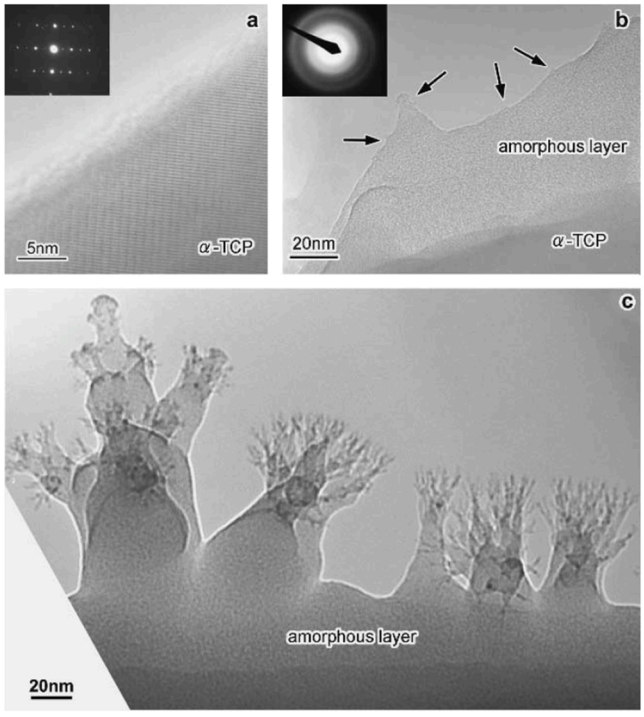

Fig. 17. TEM images of the sintered α-TCP thin film (a) before and after hydrolysis (b) for 2 h and (c) 4 h. Images taken from [228].

simultaneous decrease in the Ca/P molar ratio, which can drop to as low as 0.5 [107,234,235]. As previously discussed, these drops are probably associated with equilibrium between HA and DCPA or DCPD [108].

5.5. CDHA production using solid-solid conversion reactions

One approach to produce CDHA scaffolds is to first produce a calcium phosphate, sulfate or carbonate scaffold and then transform it into a CDHA scaffold. Numerous calcium salts can be converted to CDHA (Table 7), including monocalcium phosphate monohydrate (MCPM; $Ca(H_2PO_4)_2{\cdot}H_2O$) [236], DCPD/brushite [206,207,237], DCPA/monetite [206,237], OCP [238–240], ACP [226,241], α-TCP [242–244], β-TCP [245,246], calcium carbonate ($CaCO_3$; CC) [209,210], and calcium

sulfate dihydrate ($CaSO_4 \cdot 2H_2O$; CSD) [212]. The conversion generally involves a hydrothermal treatment, for example with porite corals [209], α-TCP [242,243] or β-TCP [245,246]. The Ca/P molar ratio can be adjusted by the pH of the reaction [206], i.e. a higher pH value leads to a higher Ca/P value. The templating effect is not always perfect since some of the CDHA crystals are sometimes formed on top of the initial calcium phosphate crystals (Fig. 18).

5.6. Production of macroporous scaffolds and granules

To enhance bone ingrowth, the presence of macropores, defined as pores larger than 50–100 μm, is essential. These macropores are typically introduced into CPC pastes by incorporating gases, immiscible liquids, or solid particles [88]. While the pore size and shape can be influenced by the characteristics of the space fillers, the main challenge lies in controlling the size and morphology of these fillers. When using gas or liquid fillers, pore dimensions are largely governed by the quantity of emulsifier. However, foams and emulsions tend to lack mechanical stability, making it difficult to harden them without altering the size, shape, or distribution of the fillers. In the case of solid fillers, the key limitation is the availability of particles with well-controlled dimensions and shapes.

One example with solid fillers involves the use of water-soluble crystals with defined sizes, added to a hydraulic cement paste composed of TTCP-DCPA mixtures [247]. After the setting reaction between the two calcium phosphates, the resulting CDHA solid was immersed in distilled water to dissolve the filler crystals and form macropores. However, complete removal of the crystals is difficult, leaving behind residues within the scaffold. This issue was addressed in a subsequent approach, where TTCP powder, DCPA powder, and ice particles were pressed together [248]. Upon heating, the ice melted, allowing the hydraulic reaction to proceed and creating a porous CDHA scaffold. Since ice fully sublimates or melts away, this method avoided the problem of residual fillers. Macropores can also be introduced using hydrophobic liquids. For instance, an α-TCP aqueous paste can be mixed with a hydrophobic liquid and an emulsifier to create an oil-in-water emulsion [249–251]. After α-TCP transforms into CDHA and the hydrophobic phase is removed, a porous scaffold remains. Pore size can be tuned by adjusting the emulsifier concentration. A third approach involves the generation of gas within the paste. In [252], an α-TCP-based paste was combined with a gas-releasing agent (e.g., hydrogen peroxide) to form pores. However, achieving a uniform pore structure and size distribution proved challenging. This limitation was overcome by incorporating an emulsifier to stabilize the gas bubbles, resulting in a more homogeneous foam [253,254]. As with emulsions, pore size control is achieved by varying the emulsifier content. To address the presence of organic residues, a thermal treatment at 700 °C has been shown to effectively oxidize organic remnants while limiting the conversion of CDHA into other calcium phosphate phases such as β-TCP, β-calcium pyrophosphate (β-CPP; $\beta\text{-}Ca_2P_2O_7$) or HA [255].

Macroporosity can also be achieved without the use of pore-forming agents. For instance, CDHA scaffolds are often fabricated via 3D printing techniques such as robocasting (see [256–258]. These scaffolds consist of an array of cylindrical CDHA filaments. By modifying the extruder geometry, it is possible to introduce concave pores into the printed structure [258]. Printing can be done with a CPC or with a calcium sulfate cement. In the latter case, the cement must be converted in ammonium phosphate solution into CDHA [214]. Another spacer-free approach involves the hydrothermal conversion of α-TCP granules with controlled geometries into macroporous CDHA scaffolds [259–261]. In this case, macroporosity arises from the intergranular voids between the individual granules. However, the handling of these scaffolds is limited by the poor mechanical properties.

Various methods have been developed to produce CDHA granules, most of which involve fragmentation of a solid precursor followed by size selection via sieving [215,216,262,263]. While the core approach remains similar, notable differences exist in the specifics of each method. One common strategy is the direct crushing of pre-formed CDHA solids. For instance, in one study, a slurry containing CDHA particles was dried, and the resulting solid was gently ground into granules. Based on the description, these granules were likely very fragile due to the soft nature of the starting material. More robust

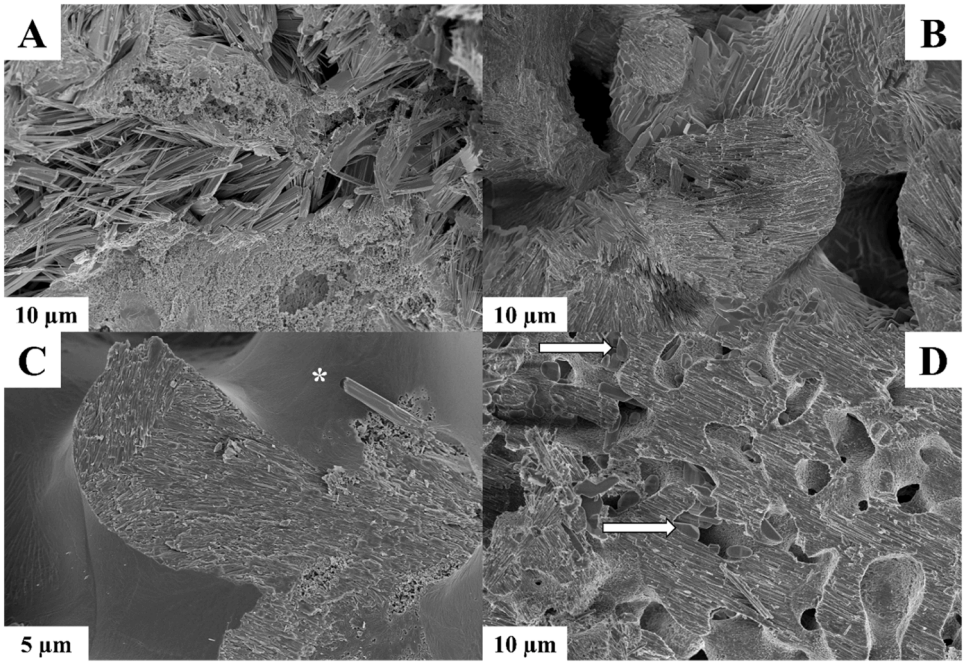

Fig. 18. Production of CDHA scaffold from α-TCP scaffold using hydrothermal treatment. (a) at 125 °C: micropores of α-TCP scaffolds are filled with CDHA crystals after α-TCP conversion; (b) at 175 °C: most micropores of α-TCP scaffolds are free of CDHA crystals after α-TCP conversion; (c) almost perfect templating effect with a smooth surface. Only one needle protrudes into the pore space (shown with a star). The fractured structure shows some aligned CDHA crystals; (d) large zones of identically oriented CDHA crystals. The arrows show some DCPA crystals. Image (a) taken from [411].

granules can be obtained by crushing CDHA solids derived from CPC reactions. Utilizing a macroporous CPC as the starting material offers the advantage of improved biological performance of the resulting granules. However, this approach comes with a trade-off: the production yield tends to decrease due to the lower mechanical strength of the macroporous CPC, which makes it more prone to fragmentation during processing. Another widely used method involves converting pre-formed non-CDHA granules into CDHA. The most straightforward approach is to fabricate α-TCP granules and then convert them into CDHA granules by immersion in an aqueous solution [242,263]. An alternative and less conventional route involves starting from a non-calcium phosphate precursor. For example, calcium sulfate granules, either formed via a cement reaction [215] or by sintering [216], can be crushed, sieved, and then chemically converted into CDHA granules. This conversion is typically performed using an ammonium phosphate solution.

5.7. Spark-plasma sintering and cold sintering

Beyond these aqueous-based processing routes, recent work has explored low-temperature densification strategies to consolidate CDHA and related calcium phosphate phases while minimizing the structural alterations associated with conventional high-temperature sintering. Approaches include spark plasma sintering (SPS) and “cold-sintering” routes [160,161,264]. Even though SPS at low temperature is per se a “cold-sintering” approach, “cold-sintering” typically refers to uniaxially pressing powder-liquid mixtures at temperatures below 200 °C. The latter approaches have enabled the compaction of nanocrystalline apatites with substantial retention of their hydrated, partially non-apatitic surface domains [161]. Similar low-temperature consolidation has also been demonstrated for ACP, both by cold SPS and high-pressure room-temperature compaction, where the metastable character of the precursor can be largely preserved [265,266]. Although ACP and CDHA differ structurally, these results underline a broader principle: calcium phosphates possessing hydrated or metastable domains can undergo substantial densification under mild thermal and mechanical conditions. Such emerging low-temperature processing techniques expand the range of feasible CDHA architectures and may provide new pathways for producing consolidated constructs without compromising the reactivity inherent to nanocrystalline apatites.

5.8. Clinical applicability

The clinical applicability of CDHA strongly depends on its physical form, as different formats provide distinct handling properties, mechanical behavior, and biological responses [267]. Granules, cements, pastes / putties, and porous scaffolds are the most commonly used configurations, each being suited for specific defect types and surgical indications. CDHA granules are widely used due to their ease of handling and ability to conform to irregular defect geometries. Their high SSA promotes rapid interaction with the biological environment and supports bone ingrowth. However, their lack of mechanical cohesion and the potential for particle migration limit their use to contained defects. Injectable CDHA pastes, typically obtained from CPC formulations, offer the advantage of minimally invasive application and excellent defect conformability. These materials can be delivered as a moldable paste that sets *in situ*, allowing for precise filling of complex geometries [223,268]. Nevertheless, their macroporosity is often limited unless specifically engineered, and their mechanical properties remain insufficient for load-bearing applications unless mechanical stability is ensured by fixation systems. Porous CDHA scaffolds and foams are designed to maximize bone ingrowth through interconnected macroporosity and high surface area. These structures can enhance osteoconduction and, in some cases, osteoinductive responses [251,256]. However, their high porosity further compromises mechanical strength and results in brittle behavior, which restricts their use to situations where structural support is not required and careful handling is possible. Overall, these differences illustrate that the choice of CDHA format is primarily dictated by defect geometry, surgical approach, and handling requirements rather than by intrinsic material composition alone. In all cases, the biological performance of these formats, which ultimately determines their clinical value, is examined in section 6.

6. CDHA as bone substitute

The biological and clinical behavior of CDHA cannot be read directly from its structure and composition alone (Sections 2, 3 and 4) as it results from the dynamic interaction between the hydrated surface established in Section 2 and the biological environment. This section interprets the available *in vitro* and *in vivo* evidence in light of those intrinsic material features. It is organised in two parts. The first examines *in vitro* behavior, beginning with the physicochemical interactions between CDHA and cell culture media — which set the ionic context for all subsequent cell studies — and then reviewing the cellular responses relevant to bone regeneration across the main cell populations involved. The second part examines *in vivo* performance, covering biocompatibility, osteoconductivity, osteoinduction, and resorption, before turning to clinical use and CDHA's potential as a drug delivery platform.

6.1. In vitro behavior

CDHA is one of the most intensively studied calcium phosphate biomaterials for bone repair. Its physicochemical resemblance to native bone mineral, versatility across formats — from granules and 3D scaffolds to injectable pastes — and its capacity for ion exchange and therapeutic loading have stimulated broad interest in both basic and translational research. Its biological performance is strongly influenced by its nanocrystalline structure and hydrated surface layer, which govern ion exchange, protein adsorption, and cell–material interactions. Translating these laboratory findings into safe and effective clinical products demands a clear understanding of CDHA's behavior in biological environments, beginning with the *in vitro* context examined here. A prerequisite for interpreting any cell-based study of CDHA is an understanding of how the material modifies the physicochemical composition of its surrounding medium — a process driven by the ion-reactive hydrated surface layer described in Section 2. Particular attention is therefore given to the limitations of static *in vitro* assays, especially those arising from CDHA-induced shifts in medium composition, before reviewing the cellular responses across the main populations involved in bone regeneration: osteoblasts and their precursors, cells of the innate immune system, osteoclasts, and vascular-related cells. This is addressed first, before turning to the cellular responses themselves.

6.1.1. Interactions with cell culture media

The incubation of CDHA in a medium supersaturated with respect to HA, such as SBF or cell culture medium, triggers specific physicochemical processes, including changes in pH, ionic composition, increase in maturation, ion exchange, and surface mineralization. Under these conditions, surface mineralization is likely to occur already during incubation in cell culture media, and the formation of a carbonated apatite layer at the CDHA surface is therefore expected [57,269,270]. According to [271], incubation in Dulbecco’s Modified Eagle Medium (DMEM) and McCoy media initially caused a drop in pH due to the interaction between the CDHA surface and the medium. During the process, sodium (Na^+), potassium (K^+), calcium (Ca^{2+}), and phosphate (PO_4^{3-}) ions were sorbed onto the CDHA surface. However, exchanging the medium every 2 days over a period of 20 days revealed distinct trends for each ion. Sodium and potassium sorption occurred rapidly and ceased early in the experiment. Phosphate ion sorption not only ceased but shifted into a release phase toward the end of the incubation period, indicating a change in equilibrium conditions and suggesting dissolution of a calcium phosphate phase or ionic exchange between phosphate and carbonate groups, as discussed in the solubility section.

Interestingly, the initial acidification observed in the cell culture medium no longer occurred after prolonged incubation, likely due to the equilibration of the new CDHA surface with the surrounding medium, minimizing further ion exchange and buffering pH changes. These findings underscore the dynamic nature of ion interactions at the CDHA surface, particularly during prolonged exposure to supersaturated environments [116]. When cells were present in indirect contact with CDHA materials, not only the material but also the cells modified the ionic levels in the McCoy medium [272]. The authors concluded that "the chemical environment determined by CDHA made minimal damage to the cells but may reduce or delay certain osteoblast-like cellular functions". Additional studies have confirmed that CDHA consumes calcium ions [92–98]. They have also shown that CDHA materials may adsorb [95,96] or release [92–95,98] phosphate ions. Interestingly, a study investigating the *in vitro* evolution of CDHA in physiological fluid over 50 days reported an increase in the Ca/P molar ratio, carbonate content, and crystallinity without any evidence for "the precipitation of new crystalline phase" [97]. The authors suggested that "the changes (of CDHA) occurred in the crystal lattice or in the hydrated layer". Nevertheless, the precise location of the incorporated ions could not be identified from the available data [97], which is not that astonishing considering the nanoscale size of the crystals. Surprisingly, the increase in crystallite size occurring during the incubation period was not discussed in greater detail, a phenomenon that has already been frequently reported [17,47,273,274]. Two distinct growth modes can be envisaged at the CDHA surface: heteroepitaxy (the growth of a new crystal phase with a structure different from the substrate) and homoepitaxy (the growth of the same phase, or of a closely related solid solution, on the substrate). The results argue against heteroepitaxy. Homoepitaxial growth of a carbonated apatite solid solution on the CDHA crystallite, via the hydrated layer, could by contrast explain the enrichment of CO_3^{2-} ions in the apatite lattice, the growth of crystalline domains, and the ion-exchange equilibrium observed after a few days. Finally, it is also worth noting that the nanoscale dimensions of CDHA particles make any direct observation of morphological changes particularly challenging.

6.1.2. *In vitro biocompatibility*

According to the latest ISO 10993 guidance, every biocompatibility evaluation should begin with a comprehensive physico-chemical characterization of the medical device, including extractables and leachables studies. Once the chemical profile has been established (ISO 10993-1:2018, ISO 10993:18:2020), a toxicological risk assessment of the identified substances is performed (ISO 10993-17:2023). Routine cell-culture assays, which were prescribed in earlier editions of the standard, are no longer mandatory. Instead, biological testing should be selected based on a risk-based approach, as correlations between static in-vitro assays and in-vivo performance have been shown to be limited [275].

6.1.3. *Cytocompatibility*

Under static culture conditions, CDHA-based bone-graft substitutes are frequently associated with low proliferation rates or even material-related toxicity (i.e. cell death) [92,97,98,276,277]. These adverse effects are driven by ionic exchanges at the material–medium interface which can drastically modify the composition of the cell culture medium [272]. They can be mitigated by enlarging the medium-to-biomaterial volume ratio and buffering the medium with (4-(2-hydroxyethyl)-1-piperazineethanesulfonic acid) (HEPES) to prevent pH shifts such as the acidification that can occur during CDHA maturation [94], or by pre-incubating CDHA in cell culture medium before cell seeding [97].

Despite these *in vitro* challenges, the cellular response to CDHA has been studied extensively to elucidate the fundamental mechanisms of interaction throughout the critical stages of bone regeneration. This process involves a complex interplay between diverse cell populations; consequently, research has addressed the impact of CDHA not only on the osteogenic lineage, including osteoblasts and their precursors, but also on immune cells, osteoclasts, and vascular-related cells, among others

6.1.4. *Osteogenic potential*

Collectively, the *in vitro* investigations indicate that CDHA enhances osteogenic activity: human BMSCs proliferated readily on CDHA with elevated total protein and alkaline phosphatase activity [278–280], and upregulation of bone-related genes like bone morphogenetic protein-2, osteonectin, osteopontin, and osteocalcin was observed in rat bone marrow stromal cells (BMSCs) cultured on CDHA [94,256]. Moreover, CDHA consistently out-performed β-TCP and other sintered calcium phosphates in osteogenic assays [94,96,98,278,281]. Mouse BMSCs also maintained high proliferation rates on CDHA powders with differing Ca/P molar ratios [95], while primary osteoblasts displayed robust metabolic activity on CDHA pellets, surpassing performance on stoichiometric HA [282]. Comparative studies between bare sintered HA or BCP scaffolds and those coated with hydrothermally derived CDHA nanorods demonstrated that the CDHA-coated variants significantly accelerated cell proliferation and osteogenic differentiation in mouse osteoblast precursor cells (MC3T3-E1) and rabbit BMSCs [281,283]. This enhanced osteogenic outcome was attributed to a combination of ion exchange and surface topography acting through mechanotransduction-related signaling pathways.

6.1.5. *Osteoimmunomodulation and osteoclastogenesis*

The clinical success of bone substitutes depends not only on their osteoconductive properties but also on their ability to modulate the local immune environment. Investigating the interaction between implanted biomaterials and immune cells is critical, as the host early inflammatory response dictates the subsequent recruitment and differentiation of osteoprogenitor cells, a process termed osteoimmunomodulation. Regarding the innate immune response, RAW246.7 macrophages were shown to adopt morphological patterns indicative of a pro-healing M2 polarization when seeded on 3D CDHA scaffolds, accompanied by the downregulation of pro-inflammatory cytokines [284], and this effect was more pronounced in dynamic on-chip culture conditions [285]. While sintered β-TCP demonstrated a greater reduction in inflammatory cytokine release than biomimetic CDHA, the latter generated a more potent osteogenic microenvironment [96]. Specifically, conditioned media from macrophages cultured on CDHA substrates fostered superior osteogenic differentiation in both BMSCs and preosteoblastic SaOS-2 cells, characterized by higher collagen type I production and upregulated expression of key osteogenic markers such as Runx2 and Bone sialoprotein. This pro-osteogenic effect was particularly pronounced when the CDHA possessed a needle-like microstructure [93,96]. Furthermore, a similar trend towards osteogenic differentiation was observed through osteoclastogenic-osteogenic coupling; specifically, the supernatants from osteoclasts cultured on CDHA discs effectively promoted the differentiation of C2C12 osteoblast precursors [243].

The assessment of osteoclastogenesis is essential, as osteoclasts not only drive bone resorption but also communicate with osteoblasts to coordinate new bone deposition [286]. In this context, biomimetic CDHA surfaces have been shown to successfully support the attachment and survival of blood-derived osteoclast precursors [287,288]. However, reports regarding their differentiation and functional maturation are divergent. While certain studies observed higher tartrate-resistant acid phosphatase (TRAP) activity on CDHA compared to sintered HA [242], others reported reduced osteoclastic differentiation on CDHA relative to smoother sintered calcium phosphates, such as β-TCP [288] or HA [287]. Specifically, while osteoclast-like cells on CDHA expressed TRAP, they failed to exhibit functional resorption. Comparative analysis suggest that this inhibition is likely driven by both the micro-topography and the ionic fluctuations inherent to CDHA [287]. Furthermore, it is important to note that the high roughness and intrinsic porosity of CDHA present significant challenges for establishing proper *in vitro*

models of osteoclastic resorption, as these features hinder the formation of the stable sealing zones required to create resorption pits, confounding the interpretation of the material's true resorptive profile [289].

6.1.6. Angiogenesis

Angiogenesis, i.e., the formation of new blood vessels, is vital for the survival of large bone grafts, and CDHA showed promising properties in this respect. Specifically, the needle-like nanostructure of CDHA was found to upregulate key angiogenic genes, such as VEGFA, in endothelial progenitor cells (EPCs) [92]. Furthermore, in BMSC/EPC co-culture models, the CDHA nanoroughness established a synergistic microenvironment that triggered the release of pro-vascularization signals, suggesting that textural properties exert a more profound influence on the angiogenic response than surface chemistry alone [92].

Taken together, although care is needed when interpreting static in-vitro data, the accumulated evidence positions CDHA as a biologically favourable bone-graft material with potential advantages over conventional calcium phosphates when culture conditions are properly controlled.

6.2. In vivo behavior

The *in vitro* evidence reviewed in Section 6.1 provides mechanistic insights into how CDHA interacts with cells and ionic environments under controlled conditions. Translating these findings to the *in vivo* context remains challenging because static *in vitro* assays do not reproduce key biological processes such as immune responses, vascular ingrowth, mechanical loading, and osteoclastic resorption. The following subsections examine CDHA's *in vivo* biocompatibility, osteoconductivity, osteoinductive potential, and resorption behaviour, drawing on orthotopic and ectopic animal models, before turning to the current clinical landscape and CDHA's potential as a local drug-delivery platform.

6.2.1. In vivo biocompatibility

Owing to its strong resemblance to native bone mineral, CDHA consistently demonstrates outstanding *in vivo* behavior [8,139,290–292]. For example, Raymond et al. reported "no evidence of fibrous enCAPsulation nor foreign-body reaction … in any of the samples," highlighting the material's excellent tissue compatibility [139]. In another study, the authors mentioned "no inflammatory signs or adverse tissue reactions" [290]. In a soft-tissue response study [292], an "almost complete absence of inflammatory cells" was observed after 8 weeks of implantation. Small signs of inflammation were only observed in zones of dispersed particles near the cement-soft tissue interface [292].

Bone apposition on CDHA is typically extensive (Fig. 19, Fig. 20) and develops rapidly. In one study using a carbonated-apatite CPC, which is chemically similar to, though not identical with CDHA, nearly the entire cement surface was covered by bone within just two weeks of implantation [290]. The rate of bone apposition seems to depend on porosity: a connective-tissue gap persisted around the non-macroporous cement at two weeks, whereas the macroporous version fostered callus formation at the interface, signalling a more advanced healing response [293]. Given this consistently favorable osteoconductivity, it is unsurprising that macroporous CDHA reliably promotes bone ingrowth [280]

CDHA is frequently reported to exhibit superior osteoconductivity compared to conventional calcium phosphate phases, including BCP, β-TCP, sintered HA and xenograft. For example, in an orthotopic rabbit model, CDHA granules promoted greater bone ingrowth than BCP granules [263]. Similarly, in a sheep interbody fusion model using titanium cages, histological evaluation revealed significantly better fusion outcomes in cages pre-filled with CDHA granules compared to those filled with β-TCP granules [251]. Additional support for CDHA's enhanced osteoconductive properties comes from rabbit studies in femoral and tibial condyle defect models, where a higher amount of new bone was observed in CDHA granule-treated sites compared to those treated with HA granules [242,243]. Based on a series of *in vitro* and *in vivo* studies conducted in both orthotopic and ectopic models [278,279,

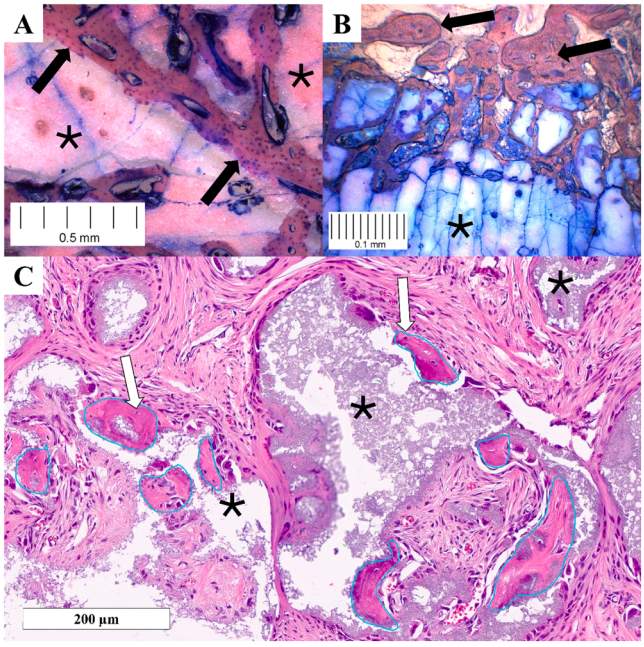

Fig. 19. Illustration of bone apposition on CDHA in contrasting implantation sites. Top: bone apposition on Norian Skeletal Repair System cement. The asterisk and the arrows indicate the position of the material and bone, respectively. Courtesy of A. Gisep, AO Research Foundation, Davos. Bottom: ectopic bone formation in CDHA macroporous granules implanted in Friend leukemia virus B (FVB) mice. The bone areas are delineated by thin green lines. The asterix and the white arrows show the position of the material and osteocytes, respectively.

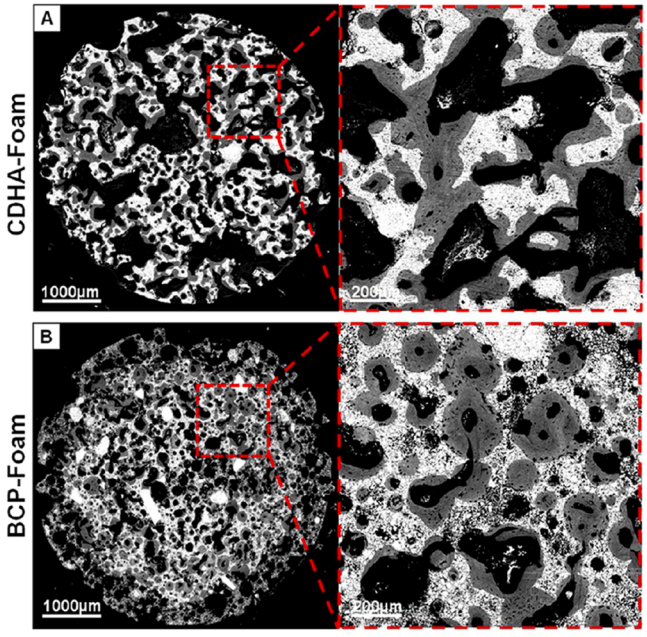

Fig. 20. Backscattered scanning electron micrographs of (A) CDHA and (B) BCP Foams after 12 weeks ectopic implantation in beagle dogs, showing distinct patterns of bone formation. In BCP foams, bone grew appositionally on the scaffold surface, progressively filling the macropores, whereas in CDHA foams, scaffold resorption preceded bone deposition. Images taken from [256].

294], CDHA was found to possess more favorable properties for bone regeneration than β-TCP. In one of these studies [279], CDHA scaffolds also demonstrated superior performance compared to HA scaffolds, further highlighting the material's enhanced osteoconductive potential. Finally, CDHA granules were found to have significantly more bone coverage than an apatite xenograft (Bio-Oss) [295].

Beyond the well-established formats of granules, scaffolds, and cements, CDHA injectable pastes have emerged as promising candidates for bone regeneration [296–300]. These pastes contain nanocrystalline HA particles produced by precipitation (and therefore classified as CDHA) dispersed in an aqueous carrier. While their developers report good biocompatibility, the supporting evidence is still limited. This is particularly true given clinical observations of aseptic paste leakage through the skin after tibial-plateau augmentation [301], something that is also observed with calcium sulfate use [302]. Particle release is a recognised concern: debris from calcium-phosphate bone-graft substitutes has previously provoked adverse tissue responses [292,303]. To mitigate such effects, viscous additives are often incorporated into CPC pastes, reducing direct blood–cement interactions and thereby improving biocompatibility [303].

Despite or perhaps because of the widespread use of CDHA and HA particles in the pharmaceutical, food, and cosmetic industries (in food applications, calcium phosphates are designated as “E341”, including “tricalcium phosphate”), their nanoscale size has raised concerns about potential safety risks. However, hydroxyapatite is phagocytosed by cells, and its degradation products, calcium and phosphate ions, are naturally abundant in the human body. A recent expert assessment [304] concluded that nano-hydroxyapatite is safe for use in toothpaste and mouthwash at the assessed concentrations.

6.2.2. Osteoinduction

CDHA was first shown to be osteoinductive in 2000 [291]. Later investigations could not reproduce this finding [305,306]: Gosain et al. attributed their minimal bone formation to the absence of macroporosity [305], whereas Bodde et al. speculated that complete failure was caused by loss of implant integrity [306]. A more recent study confirmed not only the osteoinductive potency of CDHA compared to β-TCP and BCP, but also the importance of architecture [256] (Fig. 19). CDHA foams also exhibited improved bone bridging in a femoral dog model compared to robocast CDHA-based scaffolds [257], a difference that may be attributed to the osteoinductive properties of the foam scaffolds [256].

The mechanism behind osteoinduction remains contentious. Some authors emphasize protein adsorption [307]; others focus on surface topography, particularly needle-like features [308]; still others point to the surrounding ionic medium [309]. Uniquely, CDHA satisfies all three conditions: its large specific surface favours protein adsorption, its plate- or needle-like micro-roughness offers topographical cues, and its labile hydrated layer modifies local calcium and phosphate levels (see sections 2, 4 and 6.1). Together, these attributes make CDHA one of the most promising osteoinductive bone-graft substitutes.

A question that naturally arises concerns whether CDHA's well-documented sequestration of calcium from the biological environment (demonstrated so far *in vitro*) might attenuate CaSR-mediated osteogenic signalling and thereby diminish osteogenic potential. However, no published study has demonstrated such a negative effect, and the experimental record consistently shows that CDHA outperforms more chemically inert calcium phosphates in osteogenic assays. A mechanistic framework that may explain this is suggested by the convergence of three lines of evidence. First, as described in Sections 2 and 5, CDHA not only depletes local calcium but also releases phosphate and generates local acidification through the dissolution and maturation reactions of its hydrated surface layer [22]. Second, both sub-physiological calcium and local acidification are established activators of osteoclasts: low extracellular calcium stimulates CaSR-expressing osteoclasts through well-characterized signaling pathways [153,310], while acidosis is a potent promoter of osteoclastogenesis and osteoclast resorptive activity [311]. Consistent with this, a recent study identified the acidic, phosphate-rich interfacial microenvironment (precisely the signature created by CDHA) as the strongest predictor of osteoinduction, and explicitly attributed this effect to osteoclastogenesis [312]. The study quantitatively correlated the physicochemical properties of a range of calcium phosphate bone graft substitutes with their ectopic bone-forming capacity in a standardized mouse model. Third, osteoclasts have recently been shown to be sufficient on their own to initiate de novo bone formation ectopically with 100% incidence, through paracrine secretion of osteogenic factors including (BMP-2, clastokines, and extracellular vesicles [313]. Together, these observations suggest a coherent mechanism in which CDHA's ionic reactivity (calcium depletion and local acidification) activates osteoclasts, which then drive the osteogenic cascade. In this view, the local calcium depletion created by CDHA is not a liability that reduces osteogenic potential but a potential physicochemical trigger of osteoclast-mediated bone formation, consistent with CDHA's consistently superior osteogenic performance relative to more chemically inert calcium phosphates. This mechanistic interpretation remains to be directly verified for CDHA specifically and represents a compelling avenue for future investigation.

6.2.3. Resorption

Comparative animal studies demonstrate that CDHA resorption is not a passive physicochemical process but is governed by osteoclastic activity [242,243,256,257,263,288,291,314]. Relative to stoichiometric HA, CDHA granules recruit significantly more osteoclasts and undergo more pronounced resorption, while simultaneously stimulating greater new bone formation [242,243] — a property that HA, owing to its near-insolubility, largely lacks. A causal link between osteoclastic activity and subsequent bone regeneration has been proposed [242,243] and further supported by independent findings [255]. This mechanism is also consistent with the observations of Barba et al. [256,257], who reported that CDHA scaffolds, which exhibited higher resorption than sintered BCP scaffolds, also stimulated more intensive bone formation. Importantly, several studies have noted the absence of a connective tissue layer between CDHA and bone [291], which further supports the interpretation that scaffold degradation is directly coupled to new bone deposition: rather than simply being filled around, CDHA is progressively resorbed and replaced by newly formed bone.

From a thermodynamic perspective, if CDHA has the composition $Ca_9(HPO_4)(PO_4)_5OH$ and adopting the solubility constant calculated by Driessens [71,90], its solubility isotherm can be derived accordingly. This isotherm closely matches that of β-TCP (Fig. 6), suggesting that the *in vivo* behavior of CDHA may be comparable to that of β-TCP. However, caution should be exercised because CDHA is generally considered to be heterogeneous: two CDHA materials with the same nominal Ca/P molar ratio may nonetheless differ in their true chemical composition and structural characteristics (Fig. 4), with consequences for both solubility and biological performance.

Beyond its intrinsic material properties, the resorption of CDHA is also shaped by scaffold architecture, implantation site, biological environment, and observation time. In vitro, CDHA scaffolds with high specific surface area (SSA) showed the highest degradation rates among β-TCP, HA, and CDHA [150], though these differences cannot be attributed to surface area alone, as CDHA also differs from sintered calcium phosphate ceramics in surface chemistry. In vivo, the picture is equally complex: an ectopic implantation study reported higher resorption rates for CDHA than for β-TCP foamed scaffolds at 6 weeks, with similar levels reached by 12 weeks [256], while a calvarial defect study found a slightly higher resorption rate for β-TCP than for CDHA [288]. Scaffold architecture adds a further layer of variability — robocast CDHA scaffolds degraded significantly more slowly than foamed counterparts, regardless of ceramic composition [256,257], suggesting that architecture can exert a greater influence on degradation behavior than material composition itself.

6.2.4. Clinical use

Assessing the clinical performance of CDHA is currently difficult because no commercial product consists strictly of CDHA as defined in this review. Nevertheless, a number of marketed bone graft substitutes are chemically closely related, including self-setting CPCs that yield nanocrystalline apatite after *in situ* hydrolysis, pre-mixed non-setting pastes based on precipitated HA/CDHA particles dispersed in an aqueous or hydrogel carrier, and granules obtained by autoclaving or low-temperature conversion of calcium phosphate precursors (Table 9). Several limitations complicate the translation of such products into a reliable clinical evidence base. First, the composition of these materials is often poorly documented. FDA 510(k) clearance relies on demonstrating substantial equivalence to a legally marketed predicate device, rather than on disclosing the full formulation or proving comparative efficacy. As a result, publicly available information rarely specifies key parameters such as the Ca/P molar ratio, the residual amounts of precursor phases (e.g., α-TCP, ACP, DCPA), or the carbonate and sodium content. As a result, materials grouped under umbrella terms such as "nanocrystalline HA" or "biomimetic apatite" may differ substantially from one another and from the CDHA materials characterized in the

Table 9

List of commercial products composed predominantly of synthetic nanocrystalline apatite / unsintered apatite. Most of the products listed below were identified in the U.S. Food and Drug Administration (FDA) 510(k) Premarket Notification database with a classification code "MQV" ("https://www.accessdata.fda.gov/scripts/cdrh/cfdocs/cfpmn/pmn.cfm"). The commercial availability of the products was then checked in the "GUDID" website of the NIH National Library of Medicine ("https://accessgudid.nlm.nih.gov/"). Product types are differentiated between hardening pastes ("Cement"), non-hardening pastes ("Paste"), scaffolds, and granules. Some of the non-hardening pastes are pre-mixed, whereas others need to be mixed during the surgery. The FDA website provides limited information about the composition of the products. For each product, interventional and observational studies were identified on ClinicalTrials.gov (query on product trade name, April 20, 2026).

Type	Name	Producer	Composition	Clinical trial No / Note
CEMENTS	Tactoset®	Annika Therapeutics	Powder: α-TCP, calcium carbonate, monocalcium phosphate. Liquid: sodium phosphate dibasic, citric acid, hyaluronic acid and water.	
	Arthrex® Quickset	Arthrex®	Powder: calcium phosphate salts and hydroxypropylmethyl cellulose (HPMC); Liquid: di-sodium phosphate aqueous solution	
	Cerasorb® CPC	Curasan	Pre-mixed paste made of a reactive calcium phosphate powder + non-aqueous liquid carrier	
	Norian® SRS Fast Set Putty Norian® CRS Fast Set Putty	DePuy Synthes	Likely close to Norian® SRS composition: Powder: α-TCP (85%), $CaCO_3$ (12%) MCPM (3%); Solution: H_2O, Na_2HPO_4	
	Norian® Drillable	DePuy Synthes	Composition: calcium phosphate powder, bioresorbable fibers and sodium hyaluronate solution	NCT01132508
	ColoSSIS™	DSM Biomed	Calcium phosphate powder with bovine collagen mixed with saline, patient's blood or patient's bone marrow to form hydroxyapatite	
	Graftys® Quickset	Graftys	Composition: calcium phosphate salts, hydroxypropylmethylcellulose (HPMC), and phosphate-based aqueous solution	NCT02575352
	Heracure One	Heraeus Medical	Powder: 60 wt.% α-TCP, 26 wt.% DCPA, 10 wt.% CC, and 4 wt. % precipitated HA [401]	Ready-to-use paste
	Biopex®-R	HOYA Technosurgical	Powder: α-TCP, TetCP, DCPD, HA, $Mg_3(PO_4)_2$, $NaHSO_3$ [402] Solution: H_2O, Sodium succinate, sodium chondroitin sulfate	Four product types are listed: Biopex R "Advance", "Quick", "Excellent" and "Long"
	Callos™ Skaffold™ OsteoVation® EX	Skeletal Kinetics	Composition: α-TCP, $CaCO_3$, MCPM; Solution: sodium silicate	
	HydroSet™	Stryker	Powder: TetCP, DCPD, trisodium citrate; Solution: H_2O, polyvynilpyrrolidone, sodium phosphate [403]	NCT02918344
	Mimix™ Mimix™ QS	Zimmer Biomet	Powder: TetCP, α-TCP, trisodium citrate ($C_6H_5O_7Na_3{\cdot}2H_2O$); Solution: H_2O, citric acid ($C_6H_8O_7$)	The "quick set" ("QS") version has a faster setting time
	AccuFill® β-BSM γ-BSM CarriGen® CalciGen™	Zimmer Biomet	Probably ACP as main components	AccuFill and β-BSM are injectable; γ-BSM is moldable Clinical trials for AccuFill®: NCT03494660, NCT03110224, NCT06027697
	Equivabone	Zimmer Biomet	Probably ACP as main component	Contains Demineralized Bone Matrix (DBM)
PASTES	NanoBone® SBX Putty NanoBone® QD	Biocomposite	Nanoparticles + aqueous gel	NCT04439032, NCT04503759, NCT06256458, NCT04615260, NCT04559841, NCT03331159, NCT02836678, NCT03536260, NCT02613663
	SintLife®	Fin-Ceramica	Mg-doped HA + aqueous solution	NCT03407560
	nanoXIM HAp	Fluidinova	HA (5, 15, 30, or 40%) and water	Two consistencies: nanoXIM HAp102 (more liquid) and nanoXIM HAp103 (more pasty). Also a paste with Sr-substituted HA (nanoXIM SrHAp102)
	Nanostim™	Medtronic	Nanocrystalline HA and water	
	OssDsign® Catalyst	OssDsign	5.8 wt% Si-substituted nanoapatite	NCT05329129
	Nanogel	Teknimed	Nanocrystalline HA (100-200nm) (30%) and water (70%)	NCT06374342
	nanOss®	Xtant medical	Nano-structured HA granules with a collagen carrier	NCT01829997, NCT01968993
GRANULES	OsteoGen® (HA Resorb)®	Impladent	>90% HA	Obtained by autoclaving.
	Cytrans®	GC Biomaterials	Non-sintered carbonated apatite	
	Creos™ Syntogain	Nobel Biocare	80% HA and 20% β-TCP	Obtained by autoclaving an α-TCP-based paste; NCT03374813, NCT04773847

laboratory studies cited in this review. Second, only a limited number of these products have been evaluated in prospective clinical trials, and the available studies are typically small, single-arm, industry-sponsored, and heterogeneous in indication (spine fusion, trauma, craniomaxillofacial, dental), which hinders pooled analyses and head-to-head comparisons with autograft, the clinical gold standard. Third, in contrast to total hip and knee arthroplasty, for which national and international implant registries (e.g., National Joint Registry, Australian Orthopaedic Association National Joint Replacement Registry, Swedish Arthroplasty Register) enable long-term post-market surveillance, no comparable registry exists for bone graft substitutes. Post-market evidence is therefore fragmented across case series, retrospective cohorts, and adverse-event databases such as the "Manufacturer and User Facility Device Experience" (MAUDE), which are ill-suited to benchmarking comparative efficacy or resorption behavior across products. Overall, these gaps underscore the need for more transparent compositional reporting, standardized pre-clinical characterization aligned with the CDHA definition proposed here, and coordinated clinical data collection to allow an evidence-based appraisal of CDHA-based bone graft substitutes.

6.2.5. *Drug carrier for bone applications*

CDHA has emerged as a promising carrier for therapeutic proteins and drugs because it combines an interconnected porous network, a high SSA, and a strong affinity for organic molecules [315–321]. Proteins such as Transforming Growth Factor β1 (TGF-β1) and BMP-2 have for example been succesfully incorporated into CPC pastes [317,322–324]. Due to their size, HA and CDHA micro and nanoparticles have been considered for a broad range of applications, such as gene delivery and vaccines [325,326], cancer treatment [327,328], and dental applications [329].

The mechanisms by which CDHA sequesters proteins and growth factors are multiple and interrelated. At the most basic level, CDHA's surface presents an array of functional sites (phosphate groups, hydroxyl groups, and exposed calcium ions) that interact with charged domains on proteins through electrostatic attraction, hydrogen bonding, and coordinative binding [315–321]. The hydrated, ion-rich surface layer plays a particularly important role in this regard: owing to its compositional lability and high surface reactivity, it provides a dynamic interface at which protein adsorption can occur rapidly and with high capacity [56,57]. Release kinetics are governed by a combination of factors: the solubility and resorption rate of the CDHA carrier itself, the depth of protein penetration into the pore network, the strength of the protein–surface interaction, and the local ionic environment *in vivo*. Materials with larger pore-entry diameters allow deeper protein penetration and consequently more sustained release, while finer pore networks retain proteins near the surface and may favor a more rapid initial burst [106,139]. This tunability, which is achievable through control of synthesis conditions, liquid-to-powder ratio, and scaffold architecture, positions CDHA as a versatile platform for the controlled local delivery of growth factors in bone regeneration applications.

Because osteoinduction is thought to depend at least in part on the adsorption of circulating proteins, several studies have examined how CDHA microstructure influences protein uptake. In particular, increasing the pore-entry diameter enhances protein adsorption and allows deeper penetration into the pore network [106,139] (Fig. 21). Such enlargement can be achieved by using a higher liquid-to-powder ratio during paste preparation [106] or by adopting a hydrothermal rather than a biomimetic synthesis route [139]. A complementary strategy relies on templated synthesis, in which elongated CSD microcrystals are converted into highly porous CDHA scaffolds optimized for protein loading [216].

7. Challenges and future directions

CDHA remains a complex and evolving field of study, with several unresolved challenges that continue to limit a unified understanding of its structure and properties. This section outlines key issues and perspectives for future research, focusing in particular on reproducibility, the still uncertain composition of both the crystalline core and the hydrated surface layer, the propensity of CDHA to incorporate contaminants, and the ambiguities associated with current terminology. The

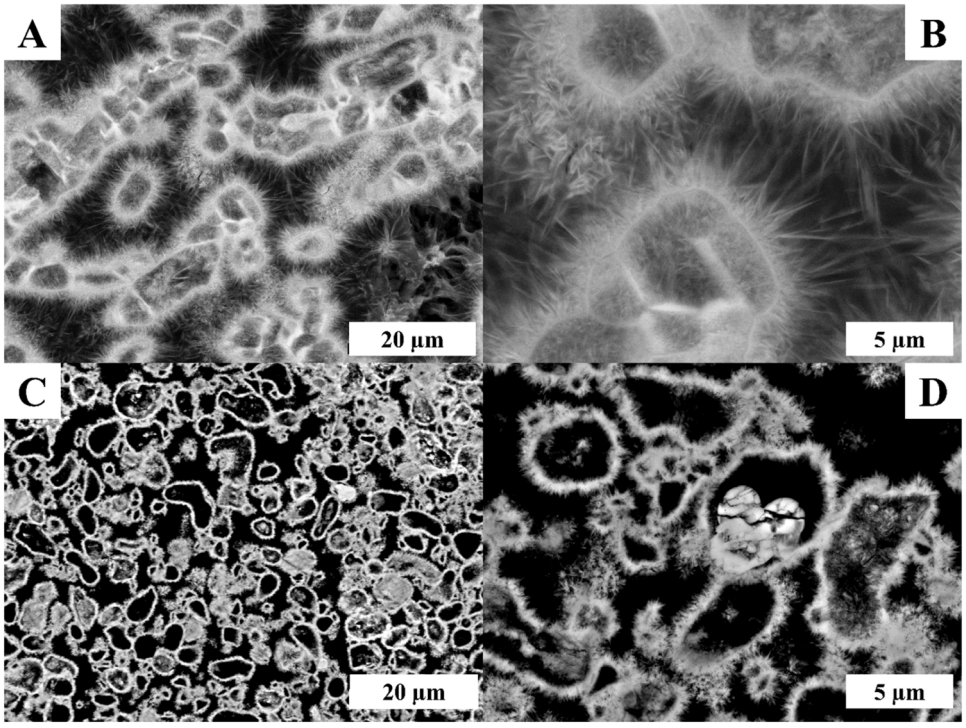

Fig. 21. CDHA microstructure made from anhydrous calcium sulfate template. Courtesy of A. de Gasparo, RMS Foundation; bottom: "standard" CDHA structure obtained from an α-TCP-based hydraulic cement. Black = porosity; white = material. Produced in the study [159].

following discussion is not exhaustive but highlights areas where further clarification is essential to advance the field.

7.1. Reproducibility

A major challenge in the study of CDHA materials lies in the limited reproducibility and comparability between studies. Reported structural, compositional, and interfacial properties are highly sensitive to synthesis parameters, including pH, temperature, reactant concentrations, maturation time, and post-synthesis treatments such as drying or aging. In addition, the metastable nature of these materials and the presence of a hydrated surface layer further complicate their characterization, as measurements may depend strongly on the hydration state and the analytical technique employed. As a result, discrepancies between studies are common and may not necessarily reflect intrinsic material differences but rather variations in preparation. A closely related issue concerns the analytical methods used to identify and characterise CDHA, which are themselves subject to important methodological caveats that can confound the interpretation of reported data; these are discussed in detail in Section 4.

To improve reproducibility and facilitate meaningful comparisons between studies, it is essential that a minimum set of parameters be systematically reported. These include the synthesis conditions (such as pH, temperature, precursor concentrations, and addition rate), as well as maturation and aging conditions, and any drying and storage procedures applied. In addition, the overall Ca/P ratio should be provided together with the method used for its determination, along with information on crystallinity and crystallite size (e.g., from XRD). Whenever possible, the characteristics of the hydrated surface layer should also be described. Finally, particular attention should be paid to the reporting of measurement conditions, especially the hydration state during analysis, given its strong influence on the observed properties. Without such information, the term “CDHA” remains difficult to interpret and to compare across different studies.

7.2. Composition of the CDHA core

To date, the precise composition of the CDHA crystal core remains uncertain, although available evidence places its Ca/P molar ratio between 1.50 and 1.67. Indeed, during prolonged α-TCP hydrolysis, low pH values and Ca/P molar ratios near 0.5 have been measured in solution [107,234,235]. These observations indicate that α-TCP transforms into a more alkaline phase than itself, namely an apatitic phase with a Ca/P molar ratio higher than that of α-TCP (1.50). This transformation can be represented as:

$$(10\text{-}x)\ \alpha\text{-}Ca_3(PO_4)_2 + (6\text{-}3x)\ H_2O \rightarrow 3Ca_{(10\text{-}x)}(PO_4)_{(6\text{-}x)}(HPO_4)_x(OH)_{(2\text{-}x)} + (2\text{-}2x)\ H_3PO_4 \quad (7)$$

In reaction (7), phosphoric acid is released, and the resulting CDHA has a Ca/P molar ratio of (10-x)/6, which is greater than 9/6 = 1.50 since $0 < x < 1$. However, in this type of reaction, only an overall composition is given for the formed CDHA where the distinction between the core and surface layer compositions is not visible. If the crystalline core is calcium-deficient, an important question is whether it follows a fixed stoichiometry, or whether the crystal core can accommodate a range of compositions. TEM imaging has revealed the presence of central dark lines [186,189,330,331] and axial zones [70] in CDHA crystals, which may be related to the incorporation of OCP remnants during CDHA formation [189,330]. However, whether these remnants are the sole cause of any observed calcium deficiency is unclear. Furthermore, OCP is only a transient intermediate in the formation of CDHA under near-neutral pH conditions [231–233], with most CDHA crystals forming directly from ACP. Another study [332] has proposed that the dark lines observed in TEM images may be due to bend contours within the crystals, rather than actual voids or structural defects. Taken together, these uncertainties surrounding the composition and structure of the crystalline core create substantial interpretive flexibility within the literature, permitting a wide array of structural models to be attributed to CDHA (Fig. 4).

7.3. Composition of the hydrated layer

Characterizing the hydrated layer is as complex as determining the composition of the CDHA crystal core itself, and it remains a subject of active investigation for over 60 years. Theoretical frameworks, such as surface complexation models, have been proposed to capture its behavior [66]. A central question concerns its (meta)stability. Some authors suggested that the layer may readily dissolve, especially in carbonate-free environments. Yet experimental evidence suggests that it never disappears entirely, even after extended maturation [22,239]. Efforts to eliminate it, for example chemically in alkaline solution or thermally at 200 °C, only reduced its thickness without removing it completely [14]. Such persistence suggests a role in thermodynamic stabilization of the underlying crystal lattice in aqueous media.

Recent work further highlights that the hydrated layer may not be unique to CDHA but part of a broader spectrum of metastable surface structures. For instance, as soon as apatite particles are immersed in aqueous media, surface modifications occur and a labile layer having a Ca/P molar ratio inferior to 1.67 forms at their surface [102,333]. As discussed in section 2, this places the hydrated layer within a broad continuum of metastable, ion-rich interfacial structures common to several calcium-phosphate systems. Within this framework, the hydrated layer can be understood as a dynamic interfacial zone: it may grow in supersaturated solutions and shrink under undersaturated conditions, while maintaining a characteristic equilibrium thickness that reflects the balance between surface reactivity and thermodynamic stabilization. Three open questions are particularly pressing: the dynamic balance between growth and dissolution of the layer, its structural nature, and its contribution to thermodynamic stabilization. Whether the apparent dissolution in undersaturated media is genuine or corresponds instead to a destabilization of the hydrogen-bond network that structures the hydrated layer [334] is itself not yet resolved. Answering these questions will be essential for understanding not only biomimetic apatites but also mineralization processes in biological systems. This need is underscored by experimental evidence showing that the hydrated layer accounts for ~4–11 wt% of CDHA [16,138,139] where it forms the interface between the crystalline core and the external environment. The actual weight fraction of the hydrated layer in CDHA remains uncertain, as neither the precise composition of the crystalline core nor that of the hydrated layer is fully established. Moreover, only a few studies have attempted to quantify the amorphous fraction in CDHA. Considering that related materials such as bone and calcium phosphate cements can contain substantially higher amorphous contents (30–70%) [15,35,43,44,145,199], it is plausible that CDHA, under certain synthesis conditions, may also incorporate significantly larger fractions than the 4–11 wt% reported so far (Table 4). This may especially be the case when apatite growth inhibitors such as Mg^{2+} and CO_3^{2-} are also present in the medium.

Given its solubility in physiological fluids, the hydrated layer likely plays a central role in modulating the local ionic milieu around CDHA implants *in vivo*. For example, several static *in vitro* studies have reported that calcium concentrations in the culture medium can decrease by more than 50% in the presence of CDHA [92–98]. Such fluctuations are biologically consequential because extracellular Ca^{2+} acts as a hormone-like signal through the calcium-sensing receptor (CaSR), which is expressed in numerous tissues and regulates the function of the parathyroid and thyroid glands, kidney, and bone cells [335]. Understanding local fluctuations in extracellular calcium and phosphate concentrations is therefore a challenging yet essential step in elucidating the biological response to CDHA implants. This challenge is further compounded by the dynamic nature of the hydrated layer, which, as

explained previously, can evolve over time or in response to environmental conditions [58,59]. This aspect is particularly relevant in the context of osteoinduction, as the local ionic environment is widely considered a critical factor in the osteoinductive potential of biomaterials [153,309,310]. In view of the above, not only experimental but also theoretical modeling (typically through DFT and molecular dynamic approaches) and their cross-validation may help to progress on the fine structuration of this hydrated layer and better understand its dynamic character with its environment.

7.4. Contaminants

Determining the exact composition of both the hydrated layer and the CDHA core is complicated by the fact that a variety of ions can be incorporated into CDHA particles, either within the hydrated layer or the crystal core itself. Among these, carbonate ions are particularly relevant, as they are readily incorporated into HA structures, particularly in alkaline conditions. Their inclusion can be minimized by conducting the synthesis in a controlled atmosphere [31,58,59], yet the majority of studies are performed in unprotected environments. Moreover, most reports do not quantify the levels of impurities present in the resulting CDHA crystals, and only a few addresses carbonate content specifically. Nevertheless, carbonate levels tend to remain low in materials synthesized at room temperature. For example, carbonate ions were detected at levels of only 0.03–0.05 wt% in a CPC sample based on α-TCP [150,336]. Although such considerations were considered in preparing this review, some studies were still included under the umbrella of CDHA research despite the presence of contaminants. Notably, many CPCs contain additives such as carbonate ions [219,268,337] or other calcium phosphates, including DCPA [168,338,339] and DCPD [340,341].

7.5. CDHA terminology

Although the term "CDHA" is widely used to describe the material's overall composition, it can be misleading if interpreted as referring to a single, structurally homogeneous phase. In practice, such CDHA materials are heterogeneous, comprising distinct structural and chemical regions, and are frequently associated with biological apatites. This association further contributes to ambiguity, particularly because biological apatites commonly contain carbonate ions and other substitutions that induce calcium deficiency and structural disorder within the apatite lattice. To address this complexity, alternative terminology has been proposed in the literature, including “biomimetic apatite” [11,41], “biomimetic hydroxyapatite” [97,342,343], and in some cases “precipitated hydroxyapatite” [249,344,345]. Within this terminology, the qualifier “biomimetic” is used with different emphases across the field. In some studies, it refers primarily to chemical similarity to biological apatites, including ionic substitutions such as carbonate, while in others it denotes a broader resemblance to biological apatites, encompassing features such as nanocrystal size, platelet- or needle-like morphology, low crystallinity, and surface chemistry conducive to biological interactions. In this context, particular attention must also be paid to the use of the term “hydroxyapatite”. From a strict crystallographic and compositional perspective, the term hydroxyapatite does not fully capture materials that may exhibit significant structural defects (e.g. lattice vacancies) or pronounced chemical heterogeneity. In fact, given the many open questions surrounding the composition and structure of CDHA, it may be prudent to defer adopting new terminology until more precise characterizations of both the crystalline core and the hydrated layer become available. Such insights may ultimately clarify whether materials currently grouped under the term CDHA represent a single compound or several distinct phases. If the latter proves true, a differentiated nomenclature would likely be necessary to avoid further conceptual ambiguity. This distinction could also account for the broad and sometimes contradictory range of reported observations.

In the absence of a definitive structural model, it is useful to adopt a minimal operational definition of CDHA. In this review, the term “CDHA” is used to describe calcium phosphate materials belonging to the Ca–P–O–H system, with an overall Ca/P molar ratio lower than 1.67, and exhibiting an apatite-like structure, irrespective of whether this structure corresponds to a single phase, a multiphasic assembly, or a core–shell organization involving a hydrated surface layer. Under this definition, “CDHA” should be regarded as a compositional and structural descriptor rather than as a well-defined compound. Whenever possible, additional information on composition, crystallinity, and presence of secondary phases should be provided to avoid ambiguity. This definition intentionally avoids assuming the existence of a continuous solid solution or a unique crystallographic phase, as current evidence does not allow such a conclusion.

8. Conclusion and outlook

CDHA has been extensively investigated as a bone graft substitute due to its compositional resemblance to natural bone mineral and its versatility in biomedical applications. This review highlighted the structural complexity of CDHA, emphasizing its dual nature: a crystalline apatite core enveloped by a hydrated, ion-rich surface layer. While the core often mirrors stoichiometric HA, debates persist regarding potential calcium vacancies and the influence of carbonate (as well as sodium) incorporation, which together complicate any precise determination of its composition. The hydrated layer, although amorphous to the X-rays and dynamic in aqueous media, plays a crucial role in modulating ion exchange as well as molecular sorption processes at physiological interfaces, thereby influencing CDHA’s apparent solubility, surface reactivity, and interaction with biological systems.

A deliberate feature of this review is its restriction of the term "CDHA" to materials belonging to the Ca–P–O–H system, with an overall Ca/P molar ratio below 1.67 and an apatite-like structure. This operational definition, intentionally narrower than the one most commonly used in the literature, allowed us to isolate a chemically coherent family of materials and to avoid the analytical ambiguities introduced by ionic substitutions, while acknowledging that the resulting corpus may correspond to a single phase, a multiphasic asSEMbly, or a core–shell organisation.

The structural duality of CDHA — a non-stoichiometric core and a labile hydrated surface layer — directly governs its physicochemical properties, including thermal instability, incongruent dissolution, and ion exchange capacity, which in turn constrain the synthesis routes by which macroscopic constructs can be produced.

The synthesis of CDHA can be achieved through diverse pathways including aqueous precipitation, hydrolysis of calcium phosphates, hydraulic cement reactions, solid–solid conversion, and, more recently, low-temperature densification approaches such as cold-sintering, each offering unique advantages depending on the intended application. These routes do not simply differ in processing convenience: they often follow complex formation mechanisms involving transient phases such as ACP and, under certain conditions, OCP.

A consistent finding across the review is that the three-dimensional architecture of CDHA constructs often exerts a stronger influence on biological performance than the intrinsic composition of the apatite itself. In particular, macroporosity, pore interconnectivity, and pore-entry size shape resorption dynamics, protein transport, and bone ingrowth at least as much as the Ca/P ratio or the hydrated-layer content. The rational design of CDHA-based biomaterials must therefore integrate architectural control as a central parameter rather than as a secondary refinement.

Biologically, CDHA consistently demonstrates biocompatibility and osteoconductivity outperforming sintered HA, β-TCP, and biphasic calcium phosphates. Its resorption is mediated by osteoclastic activity rather than by passive dissolution, aligning its degradation with natural bone remodeling. Building on this observation, the review proposes a

mechanistic framework in which the ionic microenvironment created by the hydrated surface layer, characterized by local calcium depletion, phosphate release, and mild acidification, activates osteoclasts, which in turn drive de novo bone formation through paracrine factors. This hypothesis, which directly connects the chemistry developed in Section 2 to the biological behaviour reviewed in Section 6, offers a coherent explanation for CDHA's consistently superior osteogenic performance relative to more chemically inert calcium phosphates, and identifies an avenue for targeted experimental verification. CDHA's high SSA and tailored microstructure further make it an effective carrier for therapeutic agents, opening additional avenues for combined drug-delivery and bone-regeneration strategies.

In this biological context, it is essential to note that current ISO 10993 guidance places chemical and physical characterization (together with a leachable–extractable assessment) at the foundation of biocompatibility evaluation, while deemphasizing the routine use of static cytotoxicity assays. This evolution is particularly relevant for CDHA, whose hydrated surface layer can profoundly alter the ionic composition and pH of culture media and drive misleading *in vitro* results that do not reflect *in vivo* performance. A chemistry-first approach is therefore indispensable for interpreting the biological behavior of CDHA and for designing meaningful in-vitro systems that properly account for its strong ion-exchange reactivity. This point is developed in detail section 4 of this review, which argues that no single technique is sufficient and that a coordinated combination of XRD, solid-state NMR, FTIR, and chemical analysis represents the minimum necessary toolkit for reliable compositional identification.

The translation of CDHA from the laboratory to the clinic remains more partial than the volume of preclinical work would suggest. No commercial product consists strictly of CDHA as defined here. The chemically related products currently on the market (self-setting cements, non-setting nanocrystalline apatite pastes, and converted granules) are poorly characterised in the public domain, predominantly cleared through substantial-equivalence pathways, and studied in small, single-arm, indication-heterogeneous trials. The absence of a bone-graft-substitute registry analogous to those used in arthroplasty leaves post-market evidence fragmented and ill-suited to comparative benchmarking. Closing this translational gap will require more transparent compositional reporting by manufacturers, standardised pre-clinical characterisation aligned with the definition proposed here, and coordinated clinical data collection.

Several structural and mechanistic questions therefore remain open. The precise composition and structural organization of both the crystalline core and the hydrated layer warrant further investigation by advanced characterization techniques and computational chemistry. Additionally, the dynamic interactions between the hydrated surface and the biological environment require direct experimental probing under physiological conditions; and the proposed osteoclast-mediated osteogenic mechanism requires targeted *in vivo* verification with well-characterised CDHA. Addressing these challenges is vital both for refining CDHA's clinical performance and for developing a next-generation of bone graft substitutes that fully exploit its distinctive reactivity.

A final limitation highlighted by this review concerns the inconsistent and often conceptually ambiguous terminology used across the literature. Terms such as "CDHA", "biomimetic apatite", "biomimetic hydroxyapatite", "precipitated hydroxyapatite", "nanoapatite", "nano-hydroxyapatite", or even "tricalcium phosphates" are frequently applied to materials that are chemically similar, and in some cases, indistinguishable, yet these labels are used interchangeably without a clear structural or compositional rationale. This inconsistency stems partly from the unresolved composition of the CDHA, including its hydrated surface layer, and partly from the difficulty in distinguishing CDHA from precursor or coexisting phases such as ACP or OCP with current characterization methods. As a result, studies may refer to different materials using the same term, or conversely, to essentially the same material using different terms. Meaningful harmonization of the nomenclature will require not only precise definitions, but also rigorous and standardized characterization capable of unambiguously establishing the phases actually present. Only with such clarity can future studies ensure reproducibility and enable consistent comparisons across the field.

CDHA already holds a prominent place among calcium phosphate biomaterials for bone regeneration. Its future depends less on incremental formulation work than on three concrete advances: a resolved compositional model of the crystalline core and its hydrated surface layer, experimental verification of the osteoclast-mediated osteogenic mechanism proposed here, and a clinical evidence base commensurate with the volume of preclinical data. Delivering these is well within the reach of the field, and doing so would convert CDHA from a promising biomimetic apatite into the first fully rationalised bioactive bone graft substitute.

Declaration of Generative AI and AI-assisted technologies in the writing process

During the preparation of this manuscript, the authors used ChatGPT (OpenAI) and Claude (Anthropic) to assist with language refinement and improvement of text clarity. These tools were not used to generate scientific content, data, or interpretations. All AI-assisted suggestions were carefully reviewed and approved by the authors, who take full responsibility for the manuscript.

CRediT authorship contribution statement

Marc Bohner: Writing – original draft, Supervision, Project administration, Conceptualization. **Nicola Döbelin:** Writing – review & editing, Writing – original draft. **Christophe Drouet:** Writing – review & editing, Writing – original draft. **Maria-Pau Ginebra:** Writing – review & editing, Writing – original draft. **Yassine Maazouz:** Writing – review & editing, Writing – original draft. **David Marchat:** Writing – review & editing, Writing – original draft.

Declaration of competing interest

The authors declare that they have no known competing financial interests or personal relationships that could have appeared to influence the work reported in this paper.

The author is an Editorial Board Member/Editor-in-Chief/Associate Editor/Guest Editor for this journal and was not involved in the editorial review or the decision to publish this article.

Acknowledgments

The authors thank Farida Elahrouni for the preparation of Fig. 3. This work was supported by the European Research Council (project 101055053) and the Agencia Estatal de Investigación (project CEX2023-001300-M / funded by MCIN/AEI /10.13039/501100011033).

References

[1] T.W. Bauer, G.F. Muschler, Bone graft materials. an overview of the basic science, Clin. Orthop. 371 (2000) 10–27, https://doi.org/10.1097/00003086-200002000-00003.
[2] A. Beswick, A.W. Blom, Bone graft substitutes in hip revision surgery: a comprehensive overview, Injury 42 (2011) S40–S46, https://doi.org/10.1016/j.injury.2011.06.009.
[3] R.W. Bucholz, Nonallograft osteoconductive bone graft substitutes, Clin. Orthop. 395 (2002) 44–52, https://doi.org/10.1097/00003086-200202000-00006.
[4] C.J. Damien, J.R. Parsons, Bone graft and bone graft substitutes: a review of current technology and applications, J. Appl. Biomater. 2 (1991) 187–208, https://doi.org/10.1002/jab.770020307.
[5] P.V. Giannoudis, H. Dinopoulos, E. Tsiridis, Bone substitutes: an update, Injury 36 (3) (2005) S20–S27, https://doi.org/10.1016/j.injury.2005.07.029.

[6] R.Z. LeGeros, Properties of osteoconductive biomaterials: calcium phosphates, Clin. Orthop. 395 (2002) 81–98, https://doi.org/10.1097/00003086-200202000-00009.
[7] M. Bohner, L. Galea, N. Doebelin, Calcium phosphate bone graft substitutes: failures and hopes, J. Eur. Ceram. Soc. 32 (2012) 2663–2671, https://doi.org/10.1016/j.jeurceramsoc.2012.02.028.
[8] C.M. Müller-Mai, S.I. Stupp, C. Voigt, U. Gross, Nanoapatite and organoapatite implants in bone: histology and ultrastructure of the interface, J. Biomed. Mater. Res. 29 (1995) 9–18, https://doi.org/10.1002/jbm.820290103.
[9] S.V. Dorozhkin, Nanosized and nanocrystalline calcium orthophosphates, Acta Biomater. 6 (2010) 715–734, https://doi.org/10.1016/j.actbio.2009.10.031.
[10] C. Rey, C. Combes, C. Drouet, D. Grossin, G. Bertrand, J. Soulié, 1.11 Bioactive calcium phosphate compounds: physical chemistry ☆. Compr. Biomater. II, Elsevier, 2017, pp. 244–290, https://doi.org/10.1016/B978-0-12-803581-8.10171-7.
[11] J. Gómez-Morales, M. Iafisco, J.M. Delgado-López, S. Sarda, C. Drouet, Progress on the preparation of nanocrystalline apatites and surface characterization: overview of fundamental and applied aspects, Prog. Cryst. Growth Charact. Mater. 59 (2013) 1–46, https://doi.org/10.1016/j.pcrysgrow.2012.11.001.
[12] H. Zhou, J. Lee, Nanoscale hydroxyapatite particles for bone tissue engineering, Acta Biomater. 7 (2011) 2769–2781, https://doi.org/10.1016/j.actbio.2011.03.019.
[13] S. Von Euw, W. Ajili, T.H.C. Chan-Chang, A. Delices, G. Laurent, F. Babonneau, N. Nassif, T. Azaïs, Amorphous surface layer versus transient amorphous precursor phase in bone – a case study investigated by solid-state NMR spectroscopy, Acta Biomater. 59 (2017) 351–360, https://doi.org/10.1016/j.actbio.2017.06.040.
[14] Y. Wang, S. Von Euw, F.M. Fernandes, S. Cassaignon, M. Selmane, G. Laurent, G. Pehau-Arnaudet, C. Coelho, L. Bonhomme-Coury, M.M. Giraud-Guille, F. Babonneau, T. Azaïs, N. Nassif, Water-mediated structuring of bone apatite, Nat. Mater. 12 (2013) 1144–1153, https://doi.org/10.1038/nmat3787.
[15] S. Von Euw, Y. Wang, G. Laurent, C. Drouet, F. Babonneau, N. Nassif, T. Azaïs, Bone mineral: new insights into its chemical composition, Sci. Rep. 9 (2019) 1–11, https://doi.org/10.1038/s41598-019-44620-6.
[16] C. Jäger, T. Welzel, W. Meyer Zaika, M. Epple, A solid state NMR investigation of the structure of nano crystalline hydroxyapatite, Magn. Reson. Chem. 44 (2006) 573–580, https://doi.org/10.1002/mrc.1774.
[17] N. Vandecandelaere, C. Rey, C. Drouet, Biomimetic apatite-based biomaterials: on the critical impact of synthesis and post-synthesis parameters, J. Mater. Sci. Mater. Med. 23 (2012) 2593–2606, https://doi.org/10.1007/s10856-012-4719-y.
[18] R.M. Wilson, J.C. Elliott, S.E.P. Dowker, L.M. Rodriguez-Lorenzo, Rietveld refinements and spectroscopic studies of the structure of CA-deficient apatite, Biomaterials 26 (2005) 1317–1327, https://doi.org/10.1016/j.biomaterials.2004.04.038.
[19] M. Tamai, A. Nakahira, EXAFS studies on structural disorder in calcium deficient hydroxyapatite, Phosphorus Res. Bull. 17 (2004) 69–74, https://doi.org/10.3363/prb1992.17.0_69.
[20] C. Mochales, R.M. Wilson, S.E.P. Dowker, M.P. Ginebra, Dry mechanosynthesis of nanocrystalline calcium deficient hydroxyapatite: structural characterisation, J. Alloys Compd. 509 (2011) 7389–7394, https://doi.org/10.1016/j.jallcom.2011.04.033.
[21] R.M. Wilson, J.C. Elliott, S.E.P. Dowker, Formate incorporation in the structure of Ca-deficient apatite: Rietveld structure refinement, J. Solid State Chem. 174 (2003) 132–140, https://doi.org/10.1016/S0022-4596(03)00188-9.
[22] C. Drouet, M. Aufray, S. Rollin-Martinet, N. Vandecandelaère, D. Grossin, F. Rossignol, E. Champion, A. Navrotsky, C. Rey, Nanocrystalline apatites: the fundamental role of water, Am. Mineral. 103 (2018) 550–564, https://doi.org/10.2138/am-2018-6415.
[23] E.E. Berry, The structure and composition of some calcium-deficient apatites, J. Inorg. Nucl. Chem. 29 (1967) 317–327, https://doi.org/10.1016/0022-1902(67)80033-2.
[24] W.E. Brown, J.P. Smith, J.R. Lehr, A.W. Frazier, Crystallographic and chemical relations between octocalcium phosphate and hydroxyapatite, Nature 196 (1962) 1050–1055, https://doi.org/10.1038/1961050a0.
[25] A.S. Posner, A. Perloff, Apatites deficient in divalent cations, J. Res. Nat. Bur. Stand. 58 (1957) 279.
[26] A.S. Posner, J.M. Stutman, E.R. Lippincott, Hydrogen-bonding in calcium-deficient hydroxyapatites, Nature 188 (1960) 486–487, https://doi.org/10.1038/188486a0.
[27] J.M. Stutman, A.S. Posner, E.R. Lippincott, Hydrogen bonding in the calcium phosphates, Nature 193 (1962) 368–369, https://doi.org/10.1038/193368a0.
[28] L. Winand, M.J. Dallemagne, G. Duyckaerts, Hydrogen bonding in apatitic calcium phosphates [9], Nature 190 (1961) 164–165, https://doi.org/10.1038/190164a0.
[29] L. Winand, M.J. Dallemagne, Hydrogen bonding in the calcium phosphates, Nature 193 (1962) 369–370, https://doi.org/10.1038/193369a0.
[30] S.J. Zawacki, J.C. Heughebaert, G.H. Nancollas, The growth of nonstoichiometric apatite from aqueous solution at 37 °C. II. effects of pH upon the precipitated phase, J. Colloid Interface Sci. 135 (1990) 33–44, https://doi.org/10.1016/0021-9797(90)90286-w.
[31] J.C. Heughebaert, S.J. Zawacki, G.H. Nancollas, The growth of nonstoichiometric apatite from aqueous solution at 37 °C. I. methodology and growth at pH 7.4, J. Colloid Interface Sci. 135 (1990) 20–32, https://doi.org/10.1016/0021-9797(90)90285-V.
[32] W.P. Rothwell, J.S. Waugh, J.P. Yesinowski, High-Resolution variable-temperature 31P NMR of solid calcium phosphates, J. Am. Chem. Soc. 102 (1980) 2637–2643, https://doi.org/10.1021/ja00528a020.
[33] C. Rey, C. Combes, C. Drouet, M.J. Glimcher, Bone mineral: update on chemical composition and structure, Osteoporos. Int. 20 (2009) 1013–1021, https://doi.org/10.1007/s00198-009-0860-y.
[34] C. Rey, C. Combes, Physical chemistry of biological apatites. Biominer. Biomater. Fundam. Appl., 2016, pp. 95–127, https://doi.org/10.1016/B978-1-78242-338-6.00004-1.
[35] S. Von Euw, T.H.C. Chan-Chang, C. Paquis, B. Haye, G. Pehau-Arnaudet, F. Babonneau, T. Azaïs, N. Nassif, Organization of bone mineral: the role of mineral–water interactions, Geosci. Switz. 8 (2018) 466, https://doi.org/10.3390/geosciences8120466.
[36] D. Zahn, O. Hochrein, On the composition and atomic arrangement of calcium-deficient hydroxyapatite: an ab-initio analysis, J. Solid State Chem. 181 (2008) 1712–1716, https://doi.org/10.1016/j.jssc.2008.03.035.
[37] K. Matsunaga, Theoretical investigation of the defect formation mechanism relevant to nonstoichiometry in hydroxyapatite, Phys. Rev. B - Condens. Matter Mater. Phys. 77 (2008), https://doi.org/10.1103/PhysRevB.77.104106.
[38] K. Matsunaga, Theoretical defect energetics in calcium phosphate bioceramics, J. Am. Ceram. Soc. 93 (2010) 1–14, https://doi.org/10.1111/j.1551-2916.2009.03485.x.
[39] M. Safarzadeh, S. Ramesh, C.Y. Tan, H. Chandran, Y.C. Ching, A.F.M. Noor, S. Krishnasamy, W.D. Teng, Sintering behaviour of carbonated hydroxyapatite prepared at different carbonate and phosphate ratios, Bol. Soc. Esp. Cerámica Vidr. 59 (2020) 73–80, https://doi.org/10.1016/j.bsecv.2019.08.001.
[40] M. Ben Osman, S. Diallo-Garcia, V. Herledan, D. Brouri, T. Yoshioka, J. Kubo, Y. Millot, G. Costentin, Discrimination of surface and bulk structure of crystalline hydroxyapatite nanoparticles by NMR, J. Phys. Chem. C 119 (2015) 23008–23020, https://doi.org/10.1021/acs.jpcc.5b08732.
[41] F. Bertolotti, F.J. Carmona, G. Dal Sasso, G.B. Ramírez-Rodríguez, J.M. Delgado-López, J.S. Pedersen, F. Ferri, N. Masciocchi, A. Guagliardi, On the amorphous layer in bone mineral and biomimetic apatite: a combined small- and wide-angle X-ray scattering analysis, Acta Biomater. 120 (2021) 167–180, https://doi.org/10.1016/j.actbio.2020.04.026.
[42] W. Querido, N. Shanas, S. Bookbinder, M.C. Oliveira-Nunes, B. Krynska, N. Pleshko, Fourier transform infrared spectroscopy of developing bone mineral: from amorphous precursor to mature crystal, Analyst 145 (2020) 764–776, https://doi.org/10.1039/c9an01588d.
[43] R.A. Harper, A.S. Posner, Measurement of non-crystalline calcium phosphate in bone mineral, Proc. Soc. Exp. Biol. Med. 122 (1966) 137–142, https://doi.org/10.3181/00379727-122-31073.
[44] J.D. Termine, A.S. Posner, Amorphous/crystalline interrelationships in bone mineral, Calcif. Tissue Res. 1 (1967) 8–23, https://doi.org/10.1007/BF02008070.
[45] L. Bertinetti, A. Tampieri, E. Landi, C. Ducati, P.A. Midgley, S. Coluccia, G. Martra, Surface structure, hydration, and cationic sites of nanohydroxyapatite: UHR-TEM, IR, and microgravimetric studies, J. Phys. Chem. C 111 (2007) 4027–4035, https://doi.org/10.1021/jp066040s.
[46] M. Bohner, Modulating the nanotopography of apatites, Key Eng. Mater. 254-256 (2004) 895–898, https://doi.org/10.4028/www.scientific.net/KEM.254-256.895.
[47] J.D. Termine, E.D. Eanes, Comparative chemistry of amorphous and apatitic calcium phosphate preparations, Calcif. Tissue Res. 10 (1972) 171–197, https://doi.org/10.1007/BF02012548.
[48] S. Rollin-Martinet, A. Navrotsky, E. Champion, D. Grossin, C. Drouet, Thermodynamic basis for evolution of apatite in calcified tissues, Am. Mineral. 98 (2013) 2037–2045, https://doi.org/10.2138/am.2013.4537.
[49] J. Christoffersen, M.R. Christoffersen, W. Kibalczyc, F.A. Andersen, A contribution to the understanding of the formation of calcium phosphates, J. Cryst. Growth 94 (1989) 767–777, https://doi.org/10.1016/0022-0248(89)90102-4.
[50] Å. Bengtsson, A. Shchukarev, P. Persson, S. Sjöberg, A solubility and surface complexation study of a non-stoichiometric hydroxyapatite, Geochim. Cosmochim. Acta 73 (2009) 257–267, https://doi.org/10.1016/j.gca.2008.09.034.
[51] Å. Bengtsson, S. Sjöberg, Surface complexation and proton-promoted dissolution in aqueous apatite systems, Pure Appl. Chem. 81 (2009) 1569–1584, https://doi.org/10.1351/PAC-CON-08-10-02.
[52] A.P. Robertson, J.O. Leckie, Cation binding predictions of surface complexation models: effects of pH, ionic strength, cation loading, surface complex, and model fit, J. Colloid Interface Sci. 188 (1997) 444–472, https://doi.org/10.1006/jcis.1996.4752.
[53] S. Goldberg, Application of surface complexation models to anion adsorption by natural materials, Environ. Toxicol. Chem. 33 (2014) 2172–2180, https://doi.org/10.1002/etc.2566.
[54] J.E. Groenenberg, S. Lofts, Recent developments in surface complexation modeling, Environ. Toxicol. Chem. 33 (2014) 2170–2171, https://doi.org/10.1002/etc.2690.
[55] V. Uskoković, The role of hydroxyl channel in defining selected physicochemical peculiarities exhibited by hydroxyapatite, RSC Adv. 5 (2015) 36614–36633, https://doi.org/10.1039/C4RA17180B.
[56] C. Rey, C. Combes, C. Drouet, S. Cazalbou, D. Grossin, F. Brouillet, S. Sarda, Surface properties of biomimetic nanocrystalline apatites; applications in biomaterials, Prog. Cryst. Growth Charact. Mater. 60 (2014) 63–73, https://doi.org/10.1016/j.pcrysgrow.2014.09.005.

[57] C. Rey, C. Combes, C. Drouet, H. Sfihi, A. Barroug, Physico-chemical properties of nanocrystalline apatites: implications for biominerals and biomaterials, Mater. Sci. Eng. C 27 (2007) 198–205, https://doi.org/10.1016/j.msec.2006.05.015.
[58] L.C. Bell, H. Mika, The pH dependence of the surface concentrations of calcium and phosphorus on hydroxyapatite in aqueous solutions, J. Soil Sci. 30 (1979) 247–258, https://doi.org/10.1111/j.1365-2389.1979.tb00982.x.
[59] H. Mika, L.C. Bell, B.J. Kruger, The role of surface reactions in the dissolution of stoichiometric hydroxyapatite, Arch. Oral. Biol. 21 (1976) 697–701, https://doi.org/10.1016/0003-9969(76)90145-X.
[60] C. Drouet, N. Vandecandelaère, A. Burger-Kentischer, I. Trick, C.G. Kohl, T. Maucher, M. Mueller, F.E. Weber, Nanocrystalline apatites: post-immersion acidification and how to avoid it—application to antibacterial bone substitutes, Bioeng. 10 (2023) 220, https://doi.org/10.3390/bioengineering10020220.
[61] J.A.S. Bett, L.G. Christner, W.Keith. Hall, Hydrogen held by solids. XII. hydroxyapatite catalysts, J. Am. Chem. Soc. 89 (1967) 5535–5541, https://doi.org/10.1021/ja00998a003.
[62] B. Yan, L.-Z. Tao, Y. Liang, B.-Q. Xu, Sustainable production of acrylic acid: catalytic performance of hydroxyapatites for gas-phase dehydration of lactic acid, ACS. Catal. 4 (2014) 1931–1943, https://doi.org/10.1021/cs500388x.
[63] B.J. Alloway, Heavy Metals in Soils, 3rd Edition, 2013, https://doi.org/10.1007/978-94-007-4470-7.
[64] W.J.E.M. Habraken, J. Tao, L.J. Brylka, H. Friedrich, L. Bertinetti, A.S. Schenk, A. Verch, V. Dmitrovic, P.H.H. Bomans, P.M. Frederik, J. Laven, P. Van Der Schoot, B. Aichmayer, G. De With, J.J. DeYoreo, N.A.J.M. Sommerdijk, Ion-association complexes unite classical and non-classical theories for the biomimetic nucleation of calcium phosphate, Nat. Commun. 4 (2013), https://doi.org/10.1038/ncomms2490. Article number 1507.
[65] B. Xie, T.J. Halter, B.M. Borah, G.H. Nancollas, Tracking amorphous precursor formation and transformation during induction stages of nucleation, Cryst. Growth Des. 14 (2014) 1659–1665, https://doi.org/10.1021/cg401777x.
[66] Y. Hajji, C. Drouet, S. Sarda, O. Marsan, C. Lacaze-Dufaure, First atomic-scale models of biomimetic apatites developed from combined computational and experimental studies, Surf. Interfaces. 62 (2025) 106176, https://doi.org/10.1016/j.surfin.2025.106176.
[67] D.G.A. Nelson, H. Salimi, G.H. Nancollas, Octacalcium phosphate and apatite overgrowths: a crystallographic and kinetic study, J. Colloid Interface Sci. 110 (1986) 32–39, https://doi.org/10.1016/0021-9797(86)90350-4.
[68] J.C. Heughebaert, G. Montel, Conversion of amorphous tricalcium phosphate into apatitic tricalcium phosphate, Calcif. Tissue Int. 34 (1982) S103–S108.
[69] A. Delay, Comportement thermique et composition des phosphates de calcium basiques. II. phosphates calciques basiques de Ca/P supérieur à 3/2, Bull. Soc. Chim. Fr. (1974) 839–844.
[70] S.C. Liou, S.Y. Chen, H.Y. Lee, J.S. Bow, Structural characterization of nano-sized calcium deficient apatite powders, Biomaterials 25 (2004) 189–196, https://doi.org/10.1016/s0142-9612(03)00479-4.
[71] F.C.M. Driessens, Physiology of hard tissues in comparison with the solubility of synthetic calcium phosphates, Ann. NY Acad. Sci. 523 (1988) 131–136, https://doi.org/10.1111/j.1749-6632.1988.tb38507.x.
[72] H. Zhang, M. Zhang, Characterization and thermal behavior of calcium deficient hydroxyapatite whiskers with various Ca/P ratios, Mater. Chem. Phys. 126 (2011) 642–648, https://doi.org/10.1016/j.matchemphys.2010.12.067.
[73] A. Mortier, J. Lemaitre, P.G. Rouxhet, Temperature-programmed characterization of synthetic calcium-deficient phosphate apatites, Thermochim. Acta 143 (1989) 265–282, https://doi.org/10.1016/0040-6031(89)85065-8.
[74] I.R. Gibson, I. Rehman, S.M. Best, W. Bonfield, Characterization of the transformation from calcium-deficient apatite to beta-tricalcium phosphate, J. Mater. Sci.-Mater. Med. 11 (2000) 799–804, https://doi.org/10.1023/A:1008905613182.
[75] S. Raynaud, E. Champion, D. Bernache-Assollant, P. Thomas, Calcium phosphate apatites with variable Ca/P atomic ratio I. synthesis, characterisation and thermal stability of powders, Biomaterials 23 (2002) 1065–1072, https://doi.org/10.1016/s0142-9612(01)00218-6.
[76] D. Pham Minh, M. Galera Martínez, A. Nzihou, P. Sharrock, Thermal behavior of apatitic calcium phosphates synthesized from calcium carbonate and orthophosphoric acid or potassium dihydrogen orthophosphate, J. Therm. Anal. Calorim. 112 (2013) 1145–1155, https://doi.org/10.1007/s10973-012-2695-6.
[77] A. Siddharthan, S.K. Seshadri, T.S.S. Kumar, Microwave accelerated synthesis of nanosized calcium deficient hydroxyapatite, J. Mater. Sci. Mater. Med. 15 (2004) 1279–1284, https://doi.org/10.1007/s10856-004-5735-3.
[78] M. Tamai, T. Isshiki, K. Nishio, M. Nakamura, A. Nakahira, H. Endoh, Transmission electron microscopic observation of a metastable phase on the thermal decomposition process of Ca-deficient hydroxyapatite, J. Mater. Sci. 41 (2006) 525–530, https://doi.org/10.1007/s10853-005-2458-x.
[79] M. Tamai, M. Nakamura, T. Isshiki, K. Nishio, H. Endoh, A. Nakahira, A metastable phase in thermal decomposition of Ca-deficient hydroxyapatite, J. Mater. Sci.-Mater. Med. 14 (2003) 617–622, https://doi.org/10.1023/A:1024075008165.
[80] A. Destainville, E. Champion, D. Bernache-Assollant, E. Laborde, Synthesis, characterization and thermal behavior of apatitic tricalcium phosphate, Mater. Chem. Phys. 80 (2003) 269–277, https://doi.org/10.1016/s0254-0584(02)00466-2.
[81] L. Yubao, C.P.A.T. Klein, J. Dewijn, S. Vandemeer, K. Degroot, Shape change and phase-transition of needle-like nonstoichiometric apatite crystals, J. Mater. Sci.-Mater. Med. 5 (1994) 263–268, https://doi.org/10.1007/BF00122395.
[82] E.D. Eanes, Thermochemical studies on amorphous calcium phosphate, Calcif. Tissue Res. 5 (1970) 133–145, https://doi.org/10.1007/bf02017543.
[83] A. Gee, V.R. Deitz, Pyrophosphate formation upon ignition of precipitated basic calcium phosphates, J. Am. Chem. Soc. 77 (1955) 2961–2965, https://doi.org/10.1021/ja01616a009.
[84] D.J. Greenfield, E.D. Eanes, Formation chemistry of amorphous calcium phosphates prepared from carbonate containing solutions, Calcif. Tissue Res. 9 (1972) 152–162, https://doi.org/10.1007/BF02061953.
[85] Y. Sekine, R. Motokawa, N. Kozai, T. Ohnuki, D. Matsumura, T. Tsuji, R. Kawasaki, K. Akiyoshi, Calcium-deficient hydroxyapatite as a potential sorbent for strontium, Sci. Rep. 7 (2017) 1–8, https://doi.org/10.1038/s41598-017-02269-z.
[86] H. Füredi-Milhofer, V. Hlady, F.S. Baker, R.A. Beebe, N.Wolejko Wikholm, J. S. Kittelberger, Temperature-programmed dehydration of hydroxyapatite, J. Colloid Interface Sci. 70 (1979) 1–9, https://doi.org/10.1016/0021-9797(79)90002-X.
[87] M. Andrés-Vergés, C. Fernández-González, M. Martínez-Gallego, J.D. Solier, I. Cachadiña, E. Matijević, A new route for the synthesis of calcium-deficient hydroxyapatites with low Ca/P ratio: both spectroscopic and electric characterization, J. Mater. Res. 15 (2000) 2526–2533, https://doi.org/10.1557/JMR.2000.0362.
[88] M.P. Ginebra, M. Espanol, E.B. Montufar, R.A. Perez, G. Mestres, New processing approaches in calcium phosphate cements and their applications in regenerative medicine, Acta Biomater. 6 (2010) 2863–2873, https://doi.org/10.1016/j.actbio.2010.01.036.
[89] A.J. Wagoner Johnson, B.A. Herschler, A review of the mechanical behavior of CAP and CAP/polymer composites for applications in bone replacement and repair, Acta Biomater. 7 (2011) 16–30, https://doi.org/10.1016/j.actbio.2010.07.012.
[90] F.C.M. Driessens, The mineral in bone, dentin and tooth, Bull. Soc. Chim. Belg. 89 (1980) 663–689.
[91] R.I. Martin, P.W. Brown, Aqueous formation of hydroxyapatite, J. Biomed. Mater. Res. 35 (1997) 299–308, https://doi.org/10.1002/(SICI)1097-4636(19970605)35:3%3C299::AID-JBM4%3E3.0.CO;2-C.
[92] J.M. Sadowska, J. Guillem-Marti, M.-P. Ginebra, The influence of physicochemical properties of biomimetic hydroxyapatite on the in vitro behavior of endothelial progenitor cells and their interaction with mesenchymal stem cells, Adv. Healthcare Mater. 8 (2019), https://doi.org/10.1002/adhm.201801138.
[93] J.M. Sadowska, F. Wei, J. Guo, J. Guillem-Marti, M.P. Ginebra, Y. Xiao, Effect of nano-structural properties of biomimetic hydroxyapatite on osteoimmunomodulation, Biomaterials 181 (2018) 318–332, https://doi.org/10.1016/j.biomaterials.2018.07.058.
[94] J.M. Sadowska, J. Guillem-Marti, M. Espanol, C. Stähli, N. Döbelin, M.-P. Ginebra, In vitro response of mesenchymal stem cells to biomimetic hydroxyapatite substrates: a new strategy to assess the effect of ion exchange, Acta Biomater. 76 (2018) 319–332, https://doi.org/10.1016/j.actbio.2018.06.025.
[95] L. Zhang, T. Lu, F. He, W. Zhang, X. Yuan, X. Wang, J. Ye, Physicochemical and cytological properties of poorly crystalline calcium-deficient hydroxyapatite with different Ca/P ratios, Ceram. Int. 48 (2022) 24765–24776, https://doi.org/10.1016/j.ceramint.2022.05.126.
[96] J.M. Sadowska, F. Wei, J. Guo, J. Guillem-Marti, Z. Lin, M.-P. Ginebra, Y. Xiao, The effect of biomimetic calcium deficient hydroxyapatite and sintered β-tricalcium phosphate on osteoimmune reaction and osteogenesis, Acta Biomater. 96 (2019) 605–618, https://doi.org/10.1016/j.actbio.2019.06.057.
[97] J. Konka, M. Espanol, B.M. Bosch, E. de Oliveira, M.-P. Ginebra, Maturation of biomimetic hydroxyapatite in physiological fluids: a physicochemical and proteomic study, Mater. Today Bio 12 (2021) 100137, https://doi.org/10.1016/j.mtbio.2021.100137.
[98] J.-M. Sadowska, J. Guillem-Marti, E.B. Montufar, M. Espanol, M.-P. Ginebra, Biomimetic versus sintered calcium phosphates: the in vitro behavior of osteoblasts and mesenchymal stem cells, Tissue Eng., Part A 23 (2017) 1297–1309, https://doi.org/10.1089/ten.tea.2016.0406.
[99] F.C. Driessens, R.M. Verbeeck, J.W. van Dijk, J.M. Borggreven, Degree of saturation of blood plasma in vertebrates with octocalcium phosphate, Z. Naturforsch. [C] 43 (1988) 74–76, https://doi.org/10.1515/znc-1988-1-215.
[100] M. Bohner, J. Lemaitre, Can bioactivity be tested in vitro with SBF solution? Biomaterials 30 (2009) 2175–2179, https://doi.org/10.1016/j.biomaterials.2009.01.008.
[101] H.B. Pan, B.W. Darvell, Calcium phosphate solubility: the need for re-evaluation, Cryst. Growth Des. 9 (2009) 639–645, https://doi.org/10.1021/cg801118v.
[102] P.W. Brown, R.I. Martin, An analysis of hydroxyapatite surface layer formation, J. Phys. Chem. B 103 (1999) 1671–1675, https://doi.org/10.1021/jp982554i.
[103] A.N. Smith, A.M. Posner, J.P. Quirk, Incongruent dissolution and surface complexes of hydroxyapatite, J. Colloid Interface Sci. 48 (1974) 442–449, https://doi.org/10.1016/0021-9797(74)90188-X.
[104] E. Mavropoulos, A.M. Rossi, N.C.C. Da Rocha, G.A. Soares, J.C. Moreira, G. T. Moure, Dissolution of calcium-deficient hydroxyapatite synthesized at different conditions, Mater. Charact. 50 (2003) 203–207, https://doi.org/10.1016/S1044-5803(03)00093-7.
[105] K.S. TenHuisen, P.W. Brown, Variations in solution chemistry during calcium-deficient and stoichiometric hydroxyapatite formation from CaHPo4.2H2O and Ca4(PO4)2O, J. Biomed. Mater. Res. 36 (1997) 233–241, https://doi.org/10.1002/(sici)1097-4636(199708)36:2%3C233::aid-jbm12%3E3.0.co;2-h.
[106] M. Espanol, R.A. Perez, E.B. Montufar, C. Marichal, A. Sacco, M.P. Ginebra, Intrinsic porosity of calcium phosphate cements and its significance for drug

delivery and tissue engineering applications, Acta Biomater. 5 (2009) 2752–2762, https://doi.org/10.1016/j.actbio.2009.03.011.
[107] K.S. TenHuisen, P.W. Brown, Formation of calcium-deficient hydroxyapatite from alpha-tricalcium phosphate, Biomaterials 19 (1998) 2209–2217, https://doi.org/10.1016/s0142-9612(98)00131-8.
[108] G. Vereecke, J. Lemaitre, Calculation of the solubility diagrams in the system Ca (OH)2-H3Po4-KOH-HNo3-CO2-H2O, J. Cryst. Growth 104 (1990) 820–832, https://doi.org/10.1016/0022-0248(90)90108-W.
[109] S.V. Dorozhkin, A review on the dissolution models of calcium apatites, Prog. Cryst. Growth Charact. Mater. 44 (2002) 45–61, https://doi.org/10.1016/S0960-8974(02)00004-9.
[110] R. Tang, G.H. Nancollas, New mechanism for the dissolution of sparingly soluble minerals, Pure Appl. Chem. 74 (2002) 1851–1857, https://doi.org/10.1351/pac200274101851.
[111] S. Shimabayashi, M. Matsumoto, Non-stoichiometric dissolution of hydroxyapatite in the presence of simple salts, Nippon Kagaku Kaishi 1993 (1993) 1118–1122, https://doi.org/10.1246/nikkashi.1993.1118.
[112] C.Y.C. Pak, F.C. Bartter, Ionic interaction with bone mineral. I. evidence for an isionic calcium exchange with hydroxyapatite, Biochim. Biophys. Acta 141 (1967) 401–409, https://doi.org/10.1016/0304-4165(67)90115-8.
[113] W.F. Neuman, B.J. Mulryan, Synthetic hydroxyapatite crystals - IV. magnesium incorporation, Calcif. Tissue Res. 7 (1971) 133–138, https://doi.org/10.1007/bf02062601.
[114] S. Cazalbou, D. Eichert, X. Ranz, C. Drouet, C. Combes, M.F. Harmand, C. Rey, Ion exchanges in apatites for biomedical application, J. Mater. Sci. Mater. Med. 16 (2005) 405–409, https://doi.org/10.1007/s10856-005-6979-2.
[115] T. Suzuki, T. Hatsushika, Y. Hayakawa, Synthetic hydroxyapatites employed as inorganic cation-exchangers, J. Chem. Soc. Faraday Trans. 1 Phys. Chem. Condens. Phases 77 (1981) 1059, https://doi.org/10.1039/f19817701059.
[116] R.M. Kowalchuk, S.R. Pollack, P. Ducheyne, L.A. King, Particle microelectrophoresis of calcium-deficient hydroxyapatite: solution composition and kinetic effects, J. Biomed. Mater. Res. 27 (1993) 783–790, https://doi.org/10.1002/jbm.820270611.
[117] C. Drouet, M.T. Carayon, C. Combes, C. Rey, Surface enrichment of biomimetic apatites with biologically-active ions Mg2+ and Sr2+: a preamble to the activation of bone repair materials, Mater. Sci. Eng. C 28 (2008) 1544–1550, https://doi.org/10.1016/j.msec.2008.04.011.
[118] C. Stötzel, F.A. Müller, F. Reinert, F. Niederdraenk, J.E. Barralet, U. Gbureck, Ion adsorption behaviour of hydroxyapatite with different crystallinities, Colloids Surf. B Biointerfaces 74 (2009) 91–95, https://doi.org/10.1016/j.colsurfb.2009.06.031.
[119] A.I. Ivanets, N.V. Kitikova, I.L. Shashkova, M.Yu. Roshchina, V. Srivastava, M. Sillanpää, Adsorption performance of hydroxyapatite with different crystalline and porous structure towards metal ions in multicomponent solution, J. Water Process Eng. 32 (2019) 100963, https://doi.org/10.1016/j.jwpe.2019.100963.
[120] B. Sandrine, N. Ange, B.-A. Didier, C. Eric, S. Patrick, Removal of aqueous lead ions by hydroxyapatites: equilibria and kinetic processes, J. Hazard. Mater. 139 (2007) 443–446, https://doi.org/10.1016/j.jhazmat.2006.02.039.
[121] D. Marchat, D. Bernache-Assollant, E. Champion, Cadmium fixation by synthetic hydroxyapatite in aqueous solution—Thermal behaviour, J. Hazard. Mater. 139 (2007) 453–460, https://doi.org/10.1016/j.jhazmat.2006.02.040.
[122] S. Cazalbou, C. Combes, D. Eichert, C. Rey, Adaptative physico-chemistry of bio-related calcium phosphates, J. Mater. Chem. 14 (2004) 2148, https://doi.org/10.1039/b401318b.
[123] U. Szałaj, A. Chodara, S. Gierlotka, J. Wojnarowicz, W. Łojkowski, Enhanced release of calcium ions from hydroxyapatite nanoparticles with an increase in their specific surface area, Materials 16 (2023) 6397, https://doi.org/10.3390/ma16196397.
[124] P. Somasundaran, Zeta potential of apatite in aqueous solutions and its change during equilibration, J. Colloid Interface Sci. 27 (1968) 659–666, https://doi.org/10.1016/0021-9797(68)90098-2.
[125] C. Rey, O. Marsan, C. Combes, C. Drouet, D. Grossin, S. Sarda, Characterization of calcium phosphates using vibrational spectroscopies. Adv. Calcium Phosphate Biomater., 2014, pp. 229–266, https://doi.org/10.1007/978-3-642-53980-0_8.
[126] J.H. Weikel, W.F. Neuman, I. Feldman, The surface chemistry of bone. VIII. on the mechanism of ionic exchange[1], J. Am. Chem. Soc. 76 (1954) 5202–5207, https://doi.org/10.1021/ja01649a078.
[127] V.E. Badillo-Almaraz, J. Ly, Calcium sorption on hydroxyapatite in aqueous solutions: reversible and nonreversible components, J. Colloid Interface Sci. 258 (2003) 27–32, https://doi.org/10.1016/S0021-9797(02)00178-9.
[128] W.F. Neuman, M.W. Neuman, The chemical dynamics of bone mineral. https://ia801407.us.archive.org/9/items/in.ernet.dli.2015.552958/2015.552958.The-chemical_text.pdf, 1958.
[129] D.N. Edgington, A proposed mechanism for the uptake of radioactive tracers by an in vitro hydroxyapatite system, Radiat. Res. 25 (1965) 257, https://doi.org/10.2307/3571969.
[130] D.N. Misra, Isoionic isotope exchange with hydroxylapatite and the dilution effect, J. Res. Natl. Bur. Stand. 84 (1979) 395, https://doi.org/10.6028/jres.084.020.
[131] Y. Avnimelech, Analysis of P 32 and Ca 45 exchange between hydroxyapatite and its equilibrium solution, Isr. J. Chem. 6 (1968) 375–385.
[132] J. Arends, J. Christoffersen, M.R. Christoffersen, H. Eckert, J.C. Heughebaert, G. H. Nancollas, J.P. Yesinowski, S.J. Zawacki, A calcium hydroxyapatite precipitated from an aqueous solution: an international multimethod analysis, J. Cryst. Growth 84 (1987) 515–532, https://doi.org/10.1016/0022-0248(87)90284-3.
[133] M. Markovic, B.O. Fowler, M.S. Tung, Preparation and comprehensive characterization of a calcium hydroxyapatite reference material, J. Res. Natl. Inst. Stand. Technol. 109 (2004) 553, https://doi.org/10.6028/jres.109.042.
[134] C. Drouet, Apatite formation: why it may not work as planned, and how to conclusively identify apatite compounds, Biomed. Res. Int. 2013 (2013) 1–12, https://doi.org/10.1155/2013/490946.
[135] B.Le Gars Santoni, L. Niggli, G.A. Sblendorio, D.T.L. Alexander, C. Stähli, P. Bowen, N. Döbelin, M. Bohner, Chemically pure β-tricalcium phosphate powders: evidence of two crystal structures, J. Eur. Ceram. Soc. 41 (2021) 1683–1694, https://doi.org/10.1016/j.jeurceramsoc.2020.09.055.
[136] K. Ishikawa, P. Ducheyne, S. Radin, Determination of the Ca/P ratio in calcium-deficient hydroxyapatite using X-Ray-Diffraction analysis, J. Mater. Sci.-Mater. Med. 4 (1993) 165–168, https://doi.org/10.1007/BF00120386.
[137] N. Döbelin, Y. Maazouz, R. Heuberger, M. Bohner, A.A. Armstrong, A.J. Wagoner Johnson, C. Wanner, A thermodynamic approach to surface modification of calcium phosphate implants by phosphate evaporation and condensation, J. Eur. Ceram. Soc. 40 (2020) 6095–6106, https://doi.org/10.1016/j.jeurceramsoc.2020.07.028.
[138] K. Hurle, J. Neubauer, M. Bohner, N. Doebelin, F. Goetz-Neunhoeffer, Effect of amorphous phases during the hydraulic conversion of α-TCP into calcium-deficient hydroxyapatite, Acta Biomater. 10 (2014) 3931–3941, https://doi.org/10.1016/j.actbio.2014.03.017.
[139] Y. Raymond, M. Bonany, C. Lehmann, E. Thorel, R. Benítez, J. Franch, M. Espanol, X. Solé-Martí, M.-C. Manzanares, C. Canal, M.-P. Ginebra, Hydrothermal processing of 3D-printed calcium phosphate scaffolds enhances bone formation in vivo: a comparison with biomimetic treatment, Acta Biomater. 135 (2021) 671–688, https://doi.org/10.1016/j.actbio.2021.09.001.
[140] T. Westphal, T. Füllmann, H. Pöllmann, Rietveld quantification of amorphous portions with an internal standard—Mathematical consequences of the experimental approach, Powder Diffr. 24 (2009) 239–243, https://doi.org/10.1154/1.3187828.
[141] A.S. Posner, Crystal chemistry of bone mineral, Physiol. Rev. 49 (1969) 760–792, https://doi.org/10.1152/physrev.1969.49.4.760.
[142] A.S. Posner, F. Betts, Synthetic amorphous calcium phosphate and its relation to bone mineral structure, Acc. Chem. Res. 8 (1975) 273–281, https://doi.org/10.1021/ar50092a003.
[143] K. He, M. Sawczyk, C. Liu, Y. Yuan, B. Song, R. Deivanayagam, A. Nie, X. Hu, V. P. Dravid, J. Lu, C. Sukotjo, Y.-P. Lu, P. Král, T. Shokuhfar, R. Shahbazian-Yassar, Revealing nanoscale mineralization pathways of hydroxyapatite using in situ liquid cell transmission electron microscopy, Sci. Adv. 6 (2020) 7524–7542, https://doi.org/10.1126/sciadv.aaz7524.
[144] C. Combes, C. Rey, S. Mounic, Identification and evaluation of HPO4 ions in biomimetic poorly crystalline apatite and bone mineral, Key Eng. Mater. 192-195 (2001) 143–146, https://doi.org/10.4028/www.scientific.net/KEM.192-195.143.
[145] Y. Wang, S. Von Euw, G. Laurent, C. Crevant, L. Bonhomme-Coury, M.-M. Giraud-Guille, F. Babonneau, N. Nassif, T. Azaïs, Impact of collagen confinement vs. ionic substitutions on the local disorder in bone and biomimetic apatites, Mater. Horiz. 1 (2014) 224–231, https://doi.org/10.1039/C3MH00071K.
[146] B.Le Gars Santoni, L. Niggli, S. Dolder, O. Loeffel, G.A. Sblendorio, R. Heuberger, Y. Maazouz, C. Stähli, N. Döbelin, P. Bowen, W. Hofstetter, M. Bohner, Effect of minor amounts of β-calcium pyrophosphate and hydroxyapatite on the physico-chemical properties and osteoclastic resorption of β-tricalcium phosphate cylinders, Bioact. Mater. 10 (2022) 222–235, https://doi.org/10.1016/j.bioactmat.2021.09.003.
[147] M.A. Scapin, S.N. Guilhen, M.E.B. Cotrim, M.A.F. Pires, Determination of Ca/P molar ratio in hydroxyapatite (HA) by x-ray fluorescence technique, in: são paulo, 2015.
[148] ASTM F1088-23, Standard specification for medical-grade beta-tricalcium phosphate raw material for implantable medical devices, (2023).
[149] ASTM, Standard specification for composition of medical-grade hydroxylapatite for surgical implants, (2023).
[150] A. Diez-Escudero, M. Espanol, S. Beats, M.P. Ginebra, In vitro degradation of calcium phosphates: effect of multiscale porosity, textural properties and composition, Acta Biomater. 60 (2017) 81–92, https://doi.org/10.1016/j.actbio.2017.07.033.
[151] L. Pajchel, W. Kolodziejski, Solid-state MAS NMR, TEM, and TGA studies of structural hydroxyl groups and water in nanocrystalline apatites prepared by dry milling, J. Nanoparticle Res. 15 (2013) 1868, https://doi.org/10.1007/s11051-013-1868-y.
[152] M. Campillo, P.D. Lacharmoise, J.S. Sebastián Reparaz, A.R. Goñi, M. Valiente, On the assessment of hydroxyapatite fluoridation by means of Raman scattering, J. Chem. Phys. 132 (2010) 244501, https://doi.org/10.1063/1.3428556.
[153] M. Bohner, R.J. Miron, A proposed mechanism for material-induced heterotopic ossification, Mater. Today 22 (2019) 132–141, https://doi.org/10.1016/j.mattod.2018.10.036.
[154] Y. Maazouz, G. Chizzola, N. Döbelin, M. Bohner, Cell-free, quantitative mineralization measurements as a proxy to identify osteoinductive bone graft substitutes, Biomaterials 275 (2021) 120912, https://doi.org/10.1016/j.biomaterials.2021.120912.
[155] Y. Maazouz, I. Rentsch, B. Lu, B.Le Gars Santoni, N. Doebelin, M. Bohner, In vitro measurement of the chemical changes occurring within β-tricalcium phosphate bone graft substitutes, Acta Biomater. 102 (2020) 440–457, https://doi.org/10.1016/j.actbio.2019.11.035.
[156] S. Lewin, A. Barba, C. Persson, J. Franch, M.P. Ginebra, C. Öhman-Mägi, Evaluation of bone formation in calcium phosphate scaffolds with μcT-method

validation using SEM, Biomed. Mater. Bristol 12 (2017) 065005, https://doi.org/10.1088/1748-605X/aa801d.
[157] D. Pastorino, C. Canal, M.-P. Ginebra, Multiple characterization study on porosity and pore structure of calcium phosphate cements, Acta Biomater. 28 (2015) 205–214, https://doi.org/10.1016/j.actbio.2015.09.017.
[158] C. Mellier, F.-X. Lefèvre, F. Fayon, V. Montouillout, C. Despas, M. Le Ferrec, F. Boukhechba, A. Walcarius, P. Janvier, M. Dutilleul, O. Gauthier, J.-M. Bouler, B. Bujoli, A straightforward approach to enhance the textural, mechanical and biological properties of injectable calcium phosphate apatitic cements (CPCs): CPC/blood composites, a comprehensive study, Acta Biomater. 62 (2017) 328–339, https://doi.org/10.1016/j.actbio.2017.08.040.
[159] M. Bohner, F. Bigolin, I. Bohner, T. Imwinkelried, Y. Maazouz, P. Michel, C. Stähli, Y. Viecelli, N. Döbelin, The reactivity of α-tricalcium phosphate powders is affected by minute amounts of β-calcium pyrophosphate and by the synthesis temperature, Open Ceram. 19 (2024) 100647, https://doi.org/10.1016/j.oceram.2024.100647.
[160] Y. Seo, T. Goto, S. Cho, T. Sekino, Densification of transparent hydroxyapatite ceramics via cold sintering process combined with biomineralization, J. Eur. Ceram. Soc. 44 (2024) 4285–4293, https://doi.org/10.1016/j.jeurceramsoc.2023.12.092.
[161] M. Kumar, M.A. Ben Achour, M. Lasgorceix, P. Quadros, R. Mincheva, J.-M. Raquez, A. Leriche, Densification of hydroxyapatite through cold sintering process: role of liquid phase chemistry and physical characteristic of Ha powder, Open Ceram. 17 (2024) 100566, https://doi.org/10.1016/j.oceram.2024.100566.
[162] E. Kukleva, P. Suchánková, K. Štamberg, M. Vlk, M. Šlouf, J. Kozempel, Surface protolytic property characterization of hydroxyapatite and titanium dioxide nanoparticles, RSC Adv. 9 (2019) 21989–21995, https://doi.org/10.1039/C9RA03698A.
[163] J.A. Stammeier, B. Purgstaller, D. Hippler, V. Mavromatis, M. Dietzel, In-situ Raman spectroscopy of amorphous calcium phosphate to crystalline hydroxyapatite transformation, MethodsX. 5 (2018) 1241–1250, https://doi.org/10.1016/j.mex.2018.09.015.
[164] T. Zhai, Y. Lin, Y. Chen, Z. Lian, Preparation and morphology control of hydroxyapatite by aqueous precipitation, Sci. J. Technol. 6 (2024) 37–41, https://doi.org/10.54691/p46chn44.
[165] D. Pham Minh, H. Sebei, A. Nzihou, P. Sharrock, Apatitic calcium phosphates: synthesis, characterization and reactivity in the removal of lead(II) from aqueous solution, Chem. Eng. J. 198-199 (2012) 180–190, https://doi.org/10.1016/j.cej.2012.05.083.
[166] C. García, C. Paucar, J. Gaviria, A. Durán, Effect of some physical–chemical variables in the synthesis of hydroxyapatite by the precipitation route, Key Eng. Mater. 284-286 (2005) 47–50, https://doi.org/10.4028/www.scientific.net/KEM.284-286.47.
[167] J.G. Neves, D. Navarro Da Rocha, C.C. Lopes, M.H. Prado Da Silva, M.A. C. Sinhoreti, L. Correr-Sobrinho, M.A.A. Fraga, A.B. Correr, Effect of pH level and calcination on the production of calcium phosphates by acidic route of wet precipitation, Cerâmica 67 (2021) 236–243, https://doi.org/10.1590/0366-69132021673822965.
[168] I.-H. Lee, J.-A. Lee, J.-H. Lee, Y.-W. Heo, J.-J. Kim, Effects of pH and reaction temperature on hydroxyapatite powders synthesized by precipitation, J. Korean Ceram. Soc. 57 (2020) 56–64, https://doi.org/10.1007/s43207-019-00004-0.
[169] D.P. McDonogh, P. Kirupananthan, D. Gebauer, Counterintuitive crystallization: rate effects in calcium phosphate nucleation at near-physiological pH, Cryst. Growth Des. 23 (2023) 7037–7043, https://doi.org/10.1021/acs.cgd.3c00851.
[170] M. Iijima, H. Kamemizu, N. Wakamatsu, T. Goto, Y. Doi, Y. Moriwaki, Effects of Ca addition on the formation of octacalcium phosphate and apatite in solution at pH 7.4 and at 37 °C, J. Cryst. Growth 193 (1998) 182–188, https://doi.org/10.1016/S0022-0248(98)00455-2.
[171] E.D. Eanes, J.D. Termine, M.U. Nylen, An electron microscopic study of the formation of amorphous calcium phosphate and its transformation to crystalline apatite, Calcif. Tissue Res. 12 (1973) 143–158, https://doi.org/10.1007/BF02013730.
[172] E.D. Eanes, The interaction of supersaturated calcium phosphate solutions with apatitic substrates, Calcif. Tissue Res. 20 (1976) 75–89, https://doi.org/10.1007/BF02546399.
[173] A.L. Boskey, A.S. Posner, Conversion of amorphous calcium phosphate to microcrystalline hydroxyapatite. a pH-dependent, solution-mediated, solid-solid conversion, J. Phys. Chem. 77 (1973) 2313–2317, https://doi.org/10.1021/j100638a011.
[174] J.L. Meyer, E.D. Eanes, A thermodynamic analysis of the secondary transition in the spontaneous precipitation of calcium phosphate, Calcif. Tissue Res. 25 (1978) 209–216, https://doi.org/10.1007/BF02010771.
[175] H. Fleisch, R.G.G. Russell, S. Bisaz, J.D. Termine, A.S. Posner, Influence of pyrophosphate on the transformation of amorphous to crystalline calcium phosphate, Calcif. Tissue Res. 2 (1968) 49–59, https://doi.org/10.1007/BF02279193.
[176] N.C. Blumenthal, A.S. Posner, Hydroxyapatite: mechanism of formation and properties, Calcif. Tissue Res. 13 (1973) 235–243, https://doi.org/10.1007/bf02015413.
[177] A.L. Boskey, A.S. Posner, Magnesium stabilization of amorphous calcium phosphate: a kinetic study, Mater. Res. Bull. 9 (1974) 907–916, https://doi.org/10.1016/0025-5408(74)90169-X.
[178] E.D. Eanes, I.H. Gillessen, A.S. Posner, Intermediate states in the precipitation of hydroxyapatite, Nature 208 (1965) 365–367, https://doi.org/10.1038/208365a0.
[179] E.D. Eanes, A.S. Posner, A note on the crystal growth of hydroxyapatite precipitated from aqueous solutions, Mater. Res. Bull. 5 (1970) 377–383, https://doi.org/10.1016/0025-5408(70)90075-9.
[180] E.D. Eanes, J.L. Meyer, The maturation of crystalline calcium phosphates in aqueous suspensions at physiologic pH, Calcif. Tissue Res. 23 (1977) 259–269, https://doi.org/10.1007/BF02012795.
[181] T.P. Feenstra, P.L. De Bruyn, Formation of calcium phosphates in moderately supersaturated solutions, J. Phys. Chem. 83 (1979) 475–479, https://doi.org/10.1021/j100467a010.
[182] J.L. Meyer, Hydroxyl content of solution-precipitated calcium phosphates, Calcif. Tissue Int. 27 (1979) 153–160, https://doi.org/10.1007/BF02441178.
[183] J.L. Meyer, B.O. Fowler, Lattice defects in nonstoichiometric calcium hydroxylapatites. a chemical approach, Inorg. Chem. 21 (1982) 3029–3035, https://doi.org/10.1021/ic00138a021.
[184] G.H. Nancollas, B. Tomažič, Growth of calcium phosphate on hydroxyapatite crystals. effect of supersaturation and ionic medium, J. Phys. Chem. 78 (1974) 2218–2225, https://doi.org/10.1021/J100615a007.
[185] E.D. Eanes, J.L. Meyer, The influence of fluoride on apatite formation from unstable supersaturated solutions at pH 7.4, J. Dent. Res. 57 (1978) 617–624, https://doi.org/10.1177/00220345780570041501.
[186] T. Aoba, H. Komatsu, Y. Shimazu, H. Yagishita, Y. Taya, Enamel mineralization and an initial crystalline phase, Connect. Tissue Res. 38 (1998) 129–137, https://doi.org/10.3109/03008209809017029.
[187] C. Drouet, A comprehensive guide to experimental and predicted thermodynamic properties of phosphate apatite minerals in view of applicative purposes, J. Chem. Thermodyn. 81 (2015) 143–159, https://doi.org/10.1016/j.jct.2014.09.012.
[188] W.E. Brown, M. Mathew, M.S. Tung, Crystal chemistry of octacalcium phosphate, Prog. Cryst. Growth Charact. 4 (1981) 59–87, https://doi.org/10.1016/0146-3535(81)90048-4.
[189] Y.-H. Tseng, C.-Y. Mou, J.C.C. Chan, Solid-State NMR study of the transformation of octacalcium phosphate to hydroxyapatite: a mechanistic model for central dark line formation, J. Am. Chem. Soc. 128 (2006) 6909–6918, https://doi.org/10.1021/ja060336u.
[190] M. Robin, S. Von Euw, G. Renaudin, S. Gomes, J.-M. Krafft, N. Nassif, T. Azaïs, G. Costentin, Insights into OCP identification and quantification in the context of apatite biomineralization, CrystEngComm. 22 (2020) 2728–2742, https://doi.org/10.1039/C9CE01972C.
[191] M. Mathew, W.E. Brown, L.W. Schroeder, B. Dickens, Crystal structure of octacalcium bis(hydrogenphosphate) tetrakis(phosphate)pentahydrate, Ca8 (HPO4)2(PO4)4 x 5H2O, J. Crystallogr. Spectrosc. Res. 18 (1988) 235–250, https://doi.org/10.1007/BF01194315.
[192] T. Yokoi, T. Goto, T. Kato, S. Takahashi, J. Nakamura, T. Sekino, C. Ohtsuki, M. Kawashita, Hydroxyapatite formation from octacalcium phosphate and its related compounds: a discussion of the transformation mechanism, Bull. Chem. Soc. Jpn. 93 (2020) 701–707, https://doi.org/10.1246/bcsj.20200031.
[193] Y. Ma, J. Zhang, S. Guo, J. Shi, W. Du, Z. Wang, L. Ye, W. Gu, Biomimetic mineralization of nano-sized, needle-like hydroxyapatite with ultrahigh capacity for lysozyme adsorption, Mater. Sci. Eng. C 68 (2016) 551–556, https://doi.org/10.1016/j.msec.2016.06.021.
[194] P. Wang, C. Li, H. Gong, X. Jiang, H. Wang, K. Li, Effects of synthesis conditions on the morphology of hydroxyapatite nanoparticles produced by wet chemical process, Powder Technol. 203 (2010) 315–321, https://doi.org/10.1016/j.powtec.2010.05.023.
[195] E. Bouyer, F. Gitzhofer, M.I. Boulos, Morphological study of hydroxyapatite nanocrystal suspension, J. Mater. Sci. Mater. Med. 11 (2000) 523–531, https://doi.org/10.1023/A:1008918110156.
[196] Y.X. Pang, X. Bao, Influence of temperature, ripening time and calcination on the morphology and crystallinity of hydroxyapatite nanoparticles, J. Eur. Ceram. Soc. 23 (2003) 1697–1704, https://doi.org/10.1016/S0955-2219(02)00413-2.
[197] E.D. Eanes, A.S. Posner, Kinetics and mechanism of conversion of non-crystalline calcium phosphate to crystalline hydroxyapatite, Trans. NY Acad. Sci. 28 (1965) 233–241, https://doi.org/10.1111/j.2164-0947.1965.tb02877.x.
[198] J.C. Heughebaert, G. Montel, Etude de l'évolution de l'orthophosphate tricalcique non cristallin en phosphate apatitique à la faveur d'une réaction chimique, à température ordinaire, Rev. Phys. Appl. 12 (1977) 691–694, https://doi.org/10.1051/rphysap:01977001205069100.
[199] S. Von Euw, K.F. Eichholz, O.R. Mahon, T. Georges, A. Teahan, J. Charliac, M. Merle, C. Chareyron, G. Laurent, T. Azaïs, N. Nassif, D.J. Kelly, The hydrophilic amorphous layer around bone apatite promotes osteogenesis, Acta Biomater. 210 (2026) 604–616, https://doi.org/10.1016/j.actbio.2025.12.004.
[200] W. Ostwald, Studien über die bildung und umwandlung fester körper, Z. F Phys. Chem. 22U (1897) 289–330.
[201] S.C. Jain, A.E. Hughes, Ostwald ripening and its application to precipitates and colloids in ionic crystals and glasses, J. Mater. Sci. 13 (1978) 1611–1631, https://doi.org/10.1007/BF00548725.
[202] M. Bohner, H. Tiainen, P. Michel, N. Döbelin, Design of an inorganic dual-paste apatite cement using cation exchange, J. Mater. Sci. Mater. Med. 26 (2015) 63, https://doi.org/10.1007/s10856-015-5400-z.
[203] A. Diez-Escudero, M. Espanol, M.-P. Ginebra, High-aspect-ratio nanostructured hydroxyapatite: towards new functionalities for a classical material, Chem. Sci. 15 (2024) 55–76, https://doi.org/10.1039/d3sc05344j.
[204] M. Iglesias-Fernandez, J. Buxadera-Palomero, J.-M. Sadowska, M. Espanol, M.-P. Ginebra, Implementation of bactericidal topographies on biomimetic calcium phosphates and the potential effect of its reactivity, Biomater. Adv. 136 (2022) 212797, https://doi.org/10.1016/j.bioadv.2022.212797.

[205] L. Degli Esposti, D. Squitieri, C. Fusacchia, G. Bassi, R. Torelli, D. Altamura, E. Manicone, S. Panseri, A. Adamiano, C. Giannini, M. Montesi, F. Bugli, M. Iafisco, Bioinspired oriented calcium phosphate nanocrystal arrays with bactericidal and osteogenic properties, Acta Biomater. 186 (2024) 470–488, https://doi.org/10.1016/j.actbio.2024.08.001.
[206] H. Monma, T. Kamiya, Preparation of hydroxyapatite by the hydrolysis of brushite, J. Mater. Sci. 22 (1987) 4247–4250, https://doi.org/10.1007/bf01132015.
[207] J.M. Bouler, R.Z. LeGeros, G. Daculsi, Biphasic calcium phosphates: influence of three synthesis parameters on the Ha/Beta-TCP ratio, J. Biomed. Mater. Res. 51 (2000) 680–684, https://doi.org/10.1002/1097-4636(20000915)51:4%3C680::aid-jbm16%3E3.0.co;2-%23.
[208] G.M.L. Dalmônico, D. Ihiawakrim, N. Ortiz, A.G. Barreto Junior, C.F. Curitiba Marcellos, M. Farina, O. Ersen, A.L. Rossi, Live visualization of the nucleation and growth of needle-like hydroxyapatite crystals in solution by in situ tem, Cryst. Growth Des. 22 (2022) 4828–4837, https://doi.org/10.1021/acs.cgd.2c00296.
[209] D.M. Roy, S.K. Linnehan, Hydroxyapatite formed from coral skeletal carbonate by hydrothermal exchange, Nature 247 (1974) 220–222, https://doi.org/10.1038/247220a0.
[210] N. Mohan, R. Palangadan, F.B. Fernandez, H. Varma, Preparation of hydroxyapatite porous scaffold from a 'coral-like' synthetic inorganic precursor for use as a bone substitute and a drug delivery vehicle, Mater. Sci. Eng. C 92 (2018) 329–337, https://doi.org/10.1016/j.msec.2018.06.064.
[211] F. Scalera, A. Quarta, D.M. Tobaldi, R.C. Pullar, C. Piccirillo, Cork-derived hierarchically porous hydroxyapatite with different stoichiometries for biomedical and environmental applications, Mater. Chem. Front. 5 (2021) 5071–5081, https://doi.org/10.1039/D1QM00584G.
[212] C.T. Zaman, A. Takeuchi, S. Matsuya, Q.H.M.S. Zaman, K. Ishikawa, Fabrication of B-type carbonate apatite blocks by the phosphorization of free-molding gypsum-calcite composite, Dent. Mater. J. 27 (2008) 710–715, https://doi.org/10.4012/dmj.27.710.
[213] I. Mayer, S. Wahnon, S. Cohen, Preparation of hydroxyapatites via the MSO4 sulphates (M = Ca, Sr, Pb and Eu), Mater. Res. Bull. 14 (1979) 1479–1483, https://doi.org/10.1016/0025-5408(79)90092-8.
[214] R. Lowmunkong, T. Sohmura, Y. Suzuki, S. Matsuya, K. Ishikawa, Fabrication of freeform bone-filling calcium phosphate ceramics by gypsum 3D printing method, J. Biomed. Mater. Res. B Appl. Biomater. 90B (2009) 531–539, https://doi.org/10.1002/jbm.b.31314.
[215] I. Grigoraviciute-Puroniene, Y. Tanaka, V. Vegelyte, Y. Nishimoto, K. Ishikawa, A. Kareiva, A novel synthetic approach to low-crystallinity calcium deficient hydroxyapatite, Ceram. Int. 45 (2019) 15620–15623, https://doi.org/10.1016/j.ceramint.2019.05.072.
[216] H.J. Seeherman, S.P. Berasi, C.T. Brown, R.X. Martinez, Z.S. Juo, S. Jelinsky, M. J. Cain, J. Grode, K.E. Tumelty, M. Bohner, O. Grinberg, N. Orr, O. Shoseyov, J. Eyckmans, C. Chen, P.R. Morales, C.G. Wilson, E.J. Vanderploeg, J.M. Wozney, A BMP/activin a chimera is superior to native BMPs and induces bone repair in nonhuman primates when delivered in a composite matrix, Sci. Transl. Med. 11 (2019) 1–21, https://doi.org/10.1126/scitranslmed.aar4953.
[217] Y. Suzuki, S. Matsuya, K.I. Udoh, M. Nakagawa, Y. Tsukiyama, K. Koyano, K. Ishikawa, Fabrication of hydroxyapatite block from gypsum block based on (NH4)2HPO4 treatment, Dent. Mater. J. 24 (2005) 515–521, https://doi.org/10.4012/dmj.24.515.
[218] R. Lowmunkong, T. Sohmura, J. Takahashi, Y. Suzuki, S. Matsuya, K. Ishikawa, Transformation of 3DP gypsum model to Ha by treating in ammonium phosphate solution, J. Biomed. Mater. Res. - Part B Appl. Biomater. 80B (2007) 386–393, https://doi.org/10.1002/jbm.b.30609.
[219] M. Bohner, U. Gbureck, J.E. Barralet, Technological issues for the development of more efficient calcium phosphate bone cements: a critical assessment, Biomaterials 26 (2005) 6423–6429, https://doi.org/10.1016/j.biomaterials.2005.03.049.
[220] J. Zhang, W. Liu, V. Schnitzler, F. Tancret, J.M. Bouler, Calcium phosphate cements for bone substitution: chemistry, handling and mechanical properties, Acta Biomater. 10 (2014) 1035–1049, https://doi.org/10.1016/j.actbio.2013.11.001.
[221] M. Bohner, G. Baroud, Injectability of calcium phosphate pastes, Biomaterials 26 (2005) 1553–1563, https://doi.org/10.1016/j.biomaterials.2004.05.010.
[222] R. O'Neill, H.O. McCarthy, E. Montufar, M.P. Ginebra, D.I. Wilson, A. Lennon, N. Dunne, Critical review: injectability of calcium phosphate pastes and cements, Acta Biomater. 50 (2017) 1–19, https://doi.org/10.1016/j.actbio.2016.11.019.
[223] M. Bohner, Design of ceramic-based cements and putties for bone graft substitution, Eur. Cell Mater. 20 (2010) 1–12, https://doi.org/10.22203/eCM.v020a01.
[224] M. Bohner, Reactivity of calcium phosphate cements, J. Mater. Chem. 17 (2007) 3980–3986, https://doi.org/10.1039/B008889K.
[225] M. Bohner, New hydraulic cements based on alpha-tricalcium phosphate-calcium sulfate dihydrate mixtures, Biomaterials 25 (2004) 741–749, https://doi.org/10.1016/s0142-9612(03)00573-8.
[226] T.J. Brunner, M. Bohner, C. Dora, C. Gerber, W.J. Stark, Comparison of amorphous TCP nanoparticles to micron-sized alpha-TCP as starting materials for calcium phosphate cements, J. Biomed. Mater. Res. B Appl. Biomater. 83B (2007) 400–407, https://doi.org/10.1002/jbm.b.30809.
[227] X. Wei, O. Ugurlu, M. Akinc, Hydrolysis of α-Tricalcium phosphate in simulated body fluid and dehydration behavior during the drying process, J. Am. Ceram. Soc. 90 (2007) 2315–2321, https://doi.org/10.1111/j.1551-2916.2007.01682.x.
[228] M. Tamai, T. Isshiki, K. Nishio, M. Nakamura, A. Nakahira, H. Endoh, Transmission electron microscopic studies on an initial stage in the conversion process from α-tricalcium phosphate to hydroxyapatite, J. Mater. Res. 18 (2003) 2633–2638, https://doi.org/10.1557/JMR.2003.0368.
[229] M. Bohner, T.J. Brunner, N. Doebelin, R. Tang, W.J. Stark, Effect of thermal treatments on the reactivity of nanosized tricalcium phosphate powders, J. Mater. Chem. 18 (2008) 4460, https://doi.org/10.1039/b804314k.
[230] M. Espanol, J. Portillo, J.-M. Manero, M.-P. Ginebra, Investigation of the hydroxyapatite obtained as hydrolysis product of α-tricalcium phosphate by transmission electron microscopy, CrystEngComm. 12 (2010) 3318, https://doi.org/10.1039/C001754J.
[231] M. Bohner, T.J. Brunner, W.J. Stark, Controlling the reactivity of calcium phosphate cements, J. Mater. Chem. 18 (2008) 5669, https://doi.org/10.1039/B811953H.
[232] Ö. Demir, A. Pylostomou, D. Loca, Octacalcium phosphate phase forming cements as an injectable bone substitute materials: preparation and in vitro structural study, Biomater. Adv. 157 (2024) 213731, https://doi.org/10.1016/j.bioadv.2023.213731.
[233] S. Graham, P.W. Brown, The low temperature formation of octacalcium phosphate, J. Cryst. Growth 132 (1993) 215–225, https://doi.org/10.1016/0022-0248(93)90265-X.
[234] C. Durucan, P.W. Brown, Kinetic model for α–Tricalcium phosphate hydrolysis, J. Am. Ceram. Soc. 85 (2002) 2013–2018, https://doi.org/10.1111/j.1151-2916.2002.tb00397.x.
[235] H. Monma, T. Kanazawa, The hydration of a-tricalcium phosphate, Yogyo-Kyokai-Shi 84 (1976) 209–213, https://doi.org/10.2109/jcersj1950.84.968_209 [4].
[236] C. Huang, P. Cao, Tuning Ca:P ratio by NaOH from monocalcium phosphate monohydrate (MCPM), Mater. Chem. Phys. 181 (2016) 159–166, https://doi.org/10.1016/j.matchemphys.2016.06.045.
[237] A. Mortier, J. Lemaitre, L. Rodrique, P.G. Rouxhet, Synthesis and thermal behavior of well-crystallized calcium-deficient phosphate apatite, J. Solid State Chem. 78 (1989) 215–219, https://doi.org/10.1016/0022-4596(89)90099-6.
[238] D.G.A. Nelson, J.D. McLean, High-resolution electron microscopy of octacalcium phosphate and its hydrolysis products, Calcif. Tissue Int. 36 (1984) 219–232, https://doi.org/10.1007/BF02405321.
[239] C.C. Rey, C. Combes, C. Drouet, Synthesis and physical chemical characterizations of octacalcium phosphate–based biomaterials for hard-tissue regeneration. Octacalcium Phosphate Biomater, Elsevier, 2020, pp. 177–212, https://doi.org/10.1016/B978-0-08-102511-6.00008-X.
[240] O. Suzuki, S. Kamakura, T. Katagiri, M. Nakamura, B. Zhao, Y. Honda, R. Kamijo, Bone formation enhanced by implanted octacalcium phosphate involving conversion into Ca-deficient hydroxyapatite, Biomaterials 27 (2006) 2671–2681, https://doi.org/10.1016/j.biomaterials.2005.12.004.
[241] C. Rey, A. Hina, A. Tofighi, M.J. Glimcher, Maturation of poorly crystalline apatites: chemical and structural aspects in vivo and in vitro, Cells Mater 5 (1995) 345–356.
[242] T. Okuda, K. Ioku, I. Yonezawa, H. Minagi, Y. Gonda, G. Kawachi, M. Kamitakahara, Y. Shibata, H. Murayama, H. Kurosawa, T. Ikeda, The slow resorption with replacement by bone of a hydrothermally synthesized pure calcium-deficient hydroxyapatite, Biomaterials 29 (2008) 2719–2728, https://doi.org/10.1016/j.biomaterials.2008.03.028.
[243] Y. Gonda, K. Ioku, Y. Shibata, T. Okuda, G. Kawachi, M. Kamitakahara, H. Murayama, K. Hideshima, S. Kamihira, I. Yonezawa, H. Kurosawa, T. Ikeda, Stimulatory effect of hydrothermally synthesized biodegradable hydroxyapatite granules on osteogenesis and direct association with osteoclasts, Biomaterials 30 (2009) 4390–4400, https://doi.org/10.1016/j.biomaterials.2009.05.002.
[244] R.E. Munteanu, L. Stănică, M. Gheorghiu, S. Gáspár, Measurement of the extracellular pH of adherently growing mammalian cells with high spatial resolution using a voltammetric pH microsensor, Anal. Chem. 90 (2018) 6899–6905, https://doi.org/10.1021/acs.analchem.8b01124.
[245] M. Kamitakahara, Y. Enari, N. Watanabe, K. Ioku, Morphology and composition of hydroxyapatite particles synthesized hydrothermally from tricalcium phosphates, Trans. Mater. Res. Soc. Jpn 36 (2011) 405–408, https://doi.org/10.14723/tmrsj.36.405.
[246] T. Watanabe, G. Kawachi, M. Kamitakahara, K. Kikuta, C. Ohtsuki, Formation of needle-like hydroxyapatite by hydrothermal treatment of CaHPO4·2H2O combined with β-Ca3(PO4)2, J. Ceram. Soc. Jpn. 117 (2009) 759–764, https://doi.org/10.2109/jcersj2.117.759.
[247] S. Takagi, L. Chow, Formation of macropores in calcium phosphate cement implants, J. Mater. Sci. Mater. Med. 12 (2001) 135–139, https://doi.org/10.1023/A:1008917910468.
[248] J.E. Barralet, L. Grover, T. Gaunt, A.J. Wright, I.R. Gibson, Preparation of macroporous calcium phosphate cement tissue engineering scaffold, Biomaterials 23 (2002) 3063–3072, https://doi.org/10.1016/s0142-9612(01)00401-x.
[249] M. Bohner, Calcium phosphate emulsions: possible applications, Key Eng. Mater. 192-195 (2001) 765–768, https://doi.org/10.4028/www.scientific.net/KEM.192-195.765.
[250] J.T. Alexander, C.L. Branch, B.R. Subach, R.W. Haid, Applications of a resorbable interbody spacer via a posterior lumbar interbody fusion technique, Orthopedics 25 (2002) S1185–S1189.
[251] T. Steffen, T. Stoll, T. Arvinte, R.K. Schenk, Porous tricalcium phosphate and transforming growth factor used for anterior spine surgery, Eur. Spine J. 10 (2) (2001) S132–S140, https://doi.org/10.1007/s005860100325.
[252] A. Almirall, G. Larrecq, J.A. Delgado, S. Martinez, J.A. Planell, M.P. Ginebra, Fabrication of low temperature macroporous hydroxyapatite scaffolds by foaming and hydrolysis of an alpha-TCP paste, Biomaterials 25 (2004) 3671–3680, https://doi.org/10.1016/j.biomaterials.2003.10.066.

[253] S. Sarda, M. Nilsson, M. Balcells, E. Fernandez, Influence of surfactant molecules as air-entraining agent for bone cement macroporosity, J. Biomed. Mater. Res. Part A 65A (2003) 215–221, https://doi.org/10.1002/jbm.a.10458.
[254] M.P. Ginebra, J.A. Delgado, I. Harr, A. Almirall, S. Del Valle, J.A. Planell, Factors affecting the structure and properties of an injectable self-setting calcium phosphate foam, J. Biomed. Mater. Res. 80A (2007) 351–361, https://doi.org/10.1002/jbm.a.30886.
[255] W. Dai, S. Li, H. Jia, X. Zhao, C. Liu, C. Zhou, Y. Xiao, L. Guo, Y. Fan, X. Zhang, Indirect 3D printing CDHA scaffolds with hierarchical porous structure to promote osteoinductivity and bone regeneration, J. Mater. Sci. Technol. 207 (2025) 295–307, https://doi.org/10.1016/j.jmst.2024.04.032.
[256] A. Barba, A. Diez-Escudero, Y. Maazouz, K. Rappe, M. Espanol, E.B. Montufar, M. Bonany, J.M. Sadowska, J. Guillem-Marti, C. Öhman-Mägi, C. Persson, M.-C. Manzanares, J. Franch, M.-P. Ginebra, Osteoinduction by foamed and 3D-Printed calcium phosphate scaffolds: effect of nanostructure and pore architecture, ACS Appl. Mater. Interfaces 9 (2017) 41722–41736, https://doi.org/10.1021/acsami.7b14175.
[257] A. Barba, Y. Maazouz, A. Diez-Escudero, K. Rappe, M. Espanol, E.B. Montufar, C. Öhman-Mägi, C. Persson, P. Fontecha, M.C. Manzanares, J. Franch, M. P. Ginebra, Osteogenesis by foamed and 3D-printed nanostructured calcium phosphate scaffolds: effect of pore architecture, Acta Biomater. 79 (2018) 135–147, https://doi.org/10.1016/j.actbio.2018.09.003.
[258] Y. Raymond, E. Thorel, M. Liversain, A. Riveiro, J. Pou, M.P. Ginebra, 3D printing non-cylindrical strands: morphological and structural implications, Addit. Manuf. 46 (2021) 102129, https://doi.org/10.1016/j.addma.2021.102129.
[259] K. Ishikawa, T.I. Arifta, K. Hayashi, K. Tsuru, Fabrication and evaluation of interconnected porous carbonate apatite from alpha tricalcium phosphate spheres, J. Biomed. Mater. Res. - Part B Appl. Biomater. 107 (2019) 269–277, https://doi.org/10.1002/jbm.b.34117.
[260] S. Karashima, A. Takeuchi, S. Matsuya, K. Udoh, K. Koyano, K. Ishikawa, Fabrication of low-crystallinity hydroxyapatite foam based on the setting reaction of α-tricalcium phosphate foam, J. Biomed. Mater. Res. Part A 88A (2009) 628–633, https://doi.org/10.1002/jbm.a.31904.
[261] T.I. Arifta, M.L. Munar, K. Tsuru, K. Ishikawa, Fabrication of interconnected porous calcium-deficient hydroxyapatite using the setting reaction of α tricalcium phosphate spherical granules, Ceram. Int. 43 (2017) 11149–11155, https://doi.org/10.1016/j.ceramint.2017.05.162.
[262] O. Suzuki, M. Nakamura, Y. Miyasaka, M. Kagayama, M. Sakurai, Bone-Formation on synthetic precursors of hydroxyapatite, Tohoku J. Exp. Med. 164 (1991) 37–50, https://doi.org/10.1620/tjem.164.37.
[263] B. Bourgeois, O. Laboux, L. Obadia, O. Gauthier, E. Betti, E. Aguado, G. Daculsi, J. M. Bouler, Calcium-deficient apatite: a first in vivo study concerning bone ingrowth, J. Biomed. Mater. Res. 65A (2003) 402–408, https://doi.org/10.1002/jbm.a.10518.
[264] D. Grossin, S. Rollin-Martinet, C. Estournes, F. Rossignol, E. Champion, C. Combes, C. Rey, C. Geoffroy, C. Drouet, Biomimetic apatite sintered at very low temperature by spark plasma sintering: physico-chemistry and microstructure aspects, Acta Biomater. 6 (2010) 577–585, https://doi.org/10.1016/j.actbio.2009.08.021.
[265] M. Luginina, R. Orru, G. Cao, D. Grossin, F. Brouillet, G. Chevallier, C. Thouron, C. Drouet, First successful stabilization of consolidated amorphous calcium phosphate (ACP) by cold sintering: toward highly-resorbable reactive bioceramics, J. Mater. Chem. B 8 (2020) 629–635, https://doi.org/10.1039/C9TB02121C.
[266] K. Rubenis, S. Zemjane, J. Vecstaudza, K. Lazdovica, J. Bitenieks, P. Wiecinski, A. Indurkar, J. Locs, Sintering of amorphous calcium phosphate to near-full density by uniaxial compaction at room temperature, J. Eur. Ceram. Soc. 42 (2022) 6199–6205, https://doi.org/10.1016/j.jeurceramsoc.2022.06.041.
[267] M. Bohner, Bone substitute materials. Encycl. Biomed. Eng., Elsevier, RMS Foundation, Bettlach, Switzerland, 2018, pp. 513–529, https://doi.org/10.1016/B978-0-12-801238-3.00224-5.
[268] B.R. Constantz, I.C. Ison, M.T. Fulmer, R.D. Poser, S.T. Smith, M. VanWagoner, J. Ross, S.A. Goldstein, J.B. Jupiter, D.I. Rosenthal, Skeletal repair by in situ formation of the mineral phase of bone, Science (1979) 267 (1995) 1796–1799, https://doi.org/10.1126/science.7892603.
[269] F.S. Souza, M.J.S. Matos, B.R.L. Galvão, A.F.C. Arapiraca, S.N. Da Silva, I. P. Pinheiro, Adsorption of CO2 on biphasic and amorphous calcium phosphates: an experimental and theoretical analysis, Chem. Phys. Lett. 714 (2019) 143–148, https://doi.org/10.1016/j.cplett.2018.10.080.
[270] D.A. Nowicki, Utilisation of carbon dioxide in the synthesis of multifunctional AB-type carbonated hydroxyapatite compositions, J. Solid State Chem. 334 (2024) 124678, https://doi.org/10.1016/j.jssc.2024.124678.
[271] J. Gustavsson, M.P. Ginebra, E. Engel, J. Planell, Ion reactivity of calcium-deficient hydroxyapatite in standard cell culture media, Acta Biomater. 7 (2011) 4242–4252, https://doi.org/10.1016/j.actbio.2011.07.016.
[272] J. Gustavsson, M.P. Ginebra, J. Planell, E. Engel, Osteoblast-like cellular response to dynamic changes in the ionic extracellular environment produced by calcium-deficient hydroxyapatite, J. Mater. Sci. Mater. Med. 23 (2012) 2509–2520, https://doi.org/10.1007/s10856-012-4705-4.
[273] M. Karimi, S. Hesaraki, M. Alizadeh, A. Kazemzadeh, Time and temperature mediated evolution of CDHA from ACP nanoparticles in deep eutectic solvents: kinetic and thermodynamic considerations, Mater. Des. 122 (2017) 1–10, https://doi.org/10.1016/j.matdes.2017.02.076.
[274] E. Boanini, M. Gazzano, A. Bigi, Time course of zoledronate interaction with hydroxyapatite nanocrystals, J. Phys. Chem. C 116 (2012) 15812–15818, https://doi.org/10.1021/jp304472s.
[275] G. Hulsart-Billström, J. Dawson, S. Hofmann, R. Müller, M. Stoddart, M. Alini, R. Redl, A. El Haj, R. Brown, V. Salih, J. Hilborn, S. Larsson, R. Oreffo, A surprisingly poor correlation between in vitro and in vivo testing of biomaterials for bone regeneration: results of a multicentre analysis, Eur. Cell Mater. 31 (2016) 312–322, https://doi.org/10.22203/eCM.v031a20.
[276] K. Klimek, A. Belcarz, R. Pazik, P. Sobierajska, T. Han, R.J. Wiglusz, G. Ginalska, "false" cytotoxicity of ions-adsorbing hydroxyapatite - Corrected method of cytotoxicity evaluation for ceramics of high specific surface area, Mater. Sci. Eng. C 65 (2016) 70–79, https://doi.org/10.1016/j.msec.2016.03.105.
[277] D.P. Link, J. Van Den Dolder, J.G.C. Wolke, J.A. Jansen, The cytocompatibility and early osteogenic characteristics of an injectable calcium phosphate cement, Tissue Eng. 13 (2007) 493–500, https://doi.org/10.1089/ten.2006.0015.
[278] P. Kasten, R. Luginbuhl, M. van Griensven, T. Barkhausen, C. Krettek, M. Bohner, U. Bosch, Comparison of human bone marrow stromal cells seeded on calcium-deficient hydroxyapatite, beta-tricalcium phosphate and demineralized bone matrix, Biomaterials 24 (2003) 2593–2603, https://doi.org/10.1016/S0142-9612(03)00062-0.
[279] P. Kasten, J. Vogel, R. Luginbuhl, P. Niemeyer, M. Tonak, H. Lorenz, L. Helbig, S. Weiss, J. Fellenberg, A. Leo, H.G. Simank, W. Richter, Ectopic bone formation associated with mesenchymal stem cells in a resorbable calcium deficient hydroxyapatite carrier, Biomaterials 26 (2005) 5879–5889, https://doi.org/10.1016/j.biomaterials.2005.03.001.
[280] H. Guo, J. Su, J. Wei, H. Kong, C. Liu, Biocompatibility and osteogenicity of degradable Ca-deficient hydroxyapatite scaffolds from calcium phosphate cement for bone tissue engineering, Acta Biomater. 5 (2009) 268–278, https://doi.org/10.1016/j.actbio.2008.07.018.
[281] J. Hu, Y. Zhou, L. Huang, J. Liu, H. Lu, Effect of nano-hydroxyapatite coating on the osteoinductivity of porous biphasic calcium phosphate ceramics, BMC Musculoskelet. Disord. 15 (2014) 114, https://doi.org/10.1186/1471-2474-15-114.
[282] Y. Zhao, Y. Zhang, F. Ning, D. Guo, Z. Xu, Synthesis and cellular biocompatibility of two kinds of HAP with different nanocrystal morphology, J. Biomed. Mater. Res. B Appl. Biomater. 83B (2007) 121–126, https://doi.org/10.1002/jbm.b.30774.
[283] L. Wu, X. Pei, B. Zhang, Z. Su, X. Gui, C. Gao, L. Guo, H. Fan, Q. Jiang, L. Zhao, C. Zhou, Y. Fan, X. Zhang, 3D-printed HAp bone regeneration scaffolds enable nano-scale manipulation of cellular mechanotransduction signals, Chem. Eng. J. 455 (2023) 140699, https://doi.org/10.1016/j.cej.2022.140699.
[284] M. Mateu-Sanz, P. Varela, L. del-Mazo-Barbara, I. Lodoso-Torrecilla, E. Jiménez-Piqué, J. Franch, M. Alaminos, M. Ginebra, Mechanically tunable bone scaffolds: in vivo hardening of 3D-Printed calcium phosphate/polycaprolactone inks, Adv. Funct. Mater. 36 (2026) e09357, https://doi.org/10.1002/adfm.202509357.
[285] S.S.D. Carter, A.R. Atif, A. Diez-Escudero, M. Grape, M.P. Ginebra, M. Tenje, G. Mestres, A microfluidic-based approach to investigate the inflammatory response of macrophages to pristine and drug-loaded nanostructured hydroxyapatite, Mater. Today Bio 16 (2022) 100351, https://doi.org/10.1016/J.MTBIO.2022.100351.
[286] K. Matsuo, N. Irie, Osteoclast–osteoblast communication, Arch. Biochem. Biophys. 473 (2008) 201–209, https://doi.org/10.1016/j.abb.2008.03.027.
[287] G. Ciapetti, G. Di Pompo, S. Avnet, D. Martini, A. Diez-Escudero, E.B. Montufar, M.-P. Ginebra, N. Baldini, Osteoclast differentiation from human blood precursors on biomimetic calcium-phosphate substrates, Acta Biomater. 50 (2017) 102–113, https://doi.org/10.1016/j.actbio.2016.12.013.
[288] M.Á. Brennan, D.S. Monahan, B. Brulin, S. Gallinetti, P. Humbert, C. Tringides, C. Canal, M.P. Ginebra, P. Layrolle, Biomimetic versus sintered macroporous calcium phosphate scaffolds enhanced bone regeneration and human mesenchymal stromal cell engraftment in calvarial defects, Acta Biomater. 135 (2021) 689–704, https://doi.org/10.1016/j.actbio.2021.09.007.
[289] A. Diez-Escudero, M. Espanol, E.B. Montufar, G. Di Pompo, G. Ciapetti, N. Baldini, M.-P. Ginebra, Focus ion beam/scanning electron microscopy characterization of osteoclastic resorption of calcium phosphate substrates, Tissue Eng. - Part C Methods 23 (2017) 118–124, https://doi.org/10.1089/ten.tec.2016.0361.
[290] E.P. Frankenburg, S.A. Goldstein, T.W. Bauer, S.A. Harris, R.D. Poser, Biomechanical and histological evaluation of a calcium phosphate cement*, J. Bone Jt. Surg. 80 (1998) 1112–1124, https://doi.org/10.2106/00004623-199808000-00004.
[291] H. Yuan, Y. Li, J.D. de Bruijn, K. de Groot, X. Zhang, Tissue responses of calcium phosphate cement: a study in dogs, Biomaterials 21 (2000) 1283–1290, https://doi.org/10.1016/s0142-9612(00)00016-8.
[292] E.M. Ooms, E.A. Egglezos, J.G. Wolke, J.A. Jansen, Soft-tissue response to injectable calcium phosphate cements, Biomaterials 24 (2003) 749–757, https://doi.org/10.1016/s0142-9612(02)00408-8.
[293] R.P. Del Real, E. Ooms, J.G. Wolke, M. Vallet-Regi, J.A. Jansen, In vivo bone response to porous calcium phosphate cement, J. Biomed. Mater. Res. 65A 65A (2003) 30–36, https://doi.org/10.1002/jbm.a.10432.
[294] P. Kasten, J. Vogel, F. Geiger, P. Niemeyer, R. Luginbuehl, K. Szalay, The effect of platelet-rich plasma on healing in critical-size long-bone defects, Biomaterials 29 (2008) 3983–3992, https://doi.org/10.1016/j.biomaterials.2008.06.014.
[295] P. Šponer, M. Strnadová, K. Urban, In vivo behaviour of low-temperature calcium-deficient hydroxyapatite: comparison with deproteinised bovine bone, Int. Orthop. 35 (2011) 1553–1560, https://doi.org/10.1007/s00264-010-1113-6.
[296] M.W. Laschke, K. Witt, T. Pohlemann, M.D. Menger, Injectable nanocrystalline hydroxyapatite paste for bone substitution: in vivo analysis of biocompatibility and vascularization, J. Biomed. Mater. Res. B Appl. Biomater. 82B (2007) 494–505, https://doi.org/10.1002/jbm.b.30755.

[297] O. Kilian, S. Wenisch, S. Karnati, E. Baumgart-Vogt, A. Hild, R. Fuhrmann, T. Jonuleit, E. Dingeldein, R. Schnettler, R.P. Franke, Observations on the microvasculature of bone defects filled with biodegradable nanoparticulate hydroxyapatite, Biomaterials 29 (2008) 3429–3437, https://doi.org/10.1016/j.biomaterials.2008.05.003.

[298] V. Hruschka, S. Tangl, Y. Ryabenkova, P. Heimel, D. Barnewitz, G. Möbus, C. Keibl, J. Ferguson, P. Quadros, C. Miller, R. Goodchild, W. Austin, H. Redl, T. Nau, Comparison of nanoparticular hydroxyapatite pastes of different particle content and size in a novel scapula defect model, Sci. Rep. 7 (2017) 43425, https://doi.org/10.1038/srep43425.

[299] D. Busenlechner, S. Tangl, B. Mair, G. Fugger, R. Gruber, H. Redl, G. Watzek, Simultaneous in vivo comparison of bone substitutes in a guided bone regeneration model, Biomaterials 29 (2008) 3195–3200, https://doi.org/10.1016/j.biomaterials.2008.04.021.

[300] F.-X. Huber, N. McArthur, L. Heimann, E. Dingeldein, H. Cavey, X. Palazzi, G. Clermont, J.-P. Boutrand, Evaluation of a novel nanocrystalline hydroxyapatite paste OSTIM® in comparison to Alpha-BSM® - more bone ingrowth inside the implanted material with OSTIM® compared to Alpha BSM®, BMC Musculoskelet. Disord. 10 (2009) 164, https://doi.org/10.1186/1471-2474-10-164.

[301] C. Schwartz, Review of 15 years of use of synthetic bone substitutes in orthopaedic surgery and traumatology, E-Mém, Académie Natl. Chir. 9 (2010) 76–86.

[302] M.Y. Tarar, A. Khalid, M. Usman, K. Javed, N. Shah, M.W. Abbas, Wound leakage with the use of calcium sulphate beads in prosthetic joint surgeries: a systematic review, Cureus. (2021), https://doi.org/10.7759/cureus.19650.

[303] C.J. Damien, J.R. Parsons, J.J. Benedict, D.S. Weisman, Investigation of a hydroxyapatite and calcium sulfate composite supplemented with an osteoinductive factor, J. Biomed. Mater. Res. 24 (1990) 639–654, https://doi.org/10.1002/jbm.820240602.

[304] Scientific committee on consumer safety, opinion on hydroxyapatite (nano) submission iv, 2025.

[305] A.K. Gosain, L. Song, P. Riordan, M.T. Amarante, P.G. Nagy, C.R. Wilson, J. M. Toth, J.L. Ricci, A 1-year study of osteoinduction in hydroxyapatite-derived biomaterials in an adult sheep model: part I, Plast. Reconstr. Surg. 109 (2002) 619–630, https://doi.org/10.1097/00006534-200202000-00032.

[306] E.W.H. Bodde, C.T.R. Cammaert, J.G.C. Wolke, P.H.M. Spauwen, J.A. Jansen, Investigation as to the osteoinductivity of macroporous calcium phosphate cement in goats, J. Biomed. Mater. Res. - Part B Appl. Biomater. 83B (2007) 161–168, https://doi.org/10.1002/jbm.b.30780.

[307] U. Ripamonti, The morphogenesis of bone in replicas of porous hydroxyapatite obtained from conversion of calcium carbonate exoskeletons of coral, J. Bone. Joint Surg. Am. 73 (1991) 692–703.

[308] R. Duan, L.A. van Dijk, D. Barbieri, F. de Groot, H. Yuan, J.D. de Bruijn, Accelerated bone formation by biphasic calcium phosphate with a novel sub-micron surface topography, Eur. Cell Mater. 37 (2019) 60–73, https://doi.org/10.22203/ECM.V037A05.

[309] Z. Tang, X. Li, Y. Tan, H. Fan, X. Zhang, The material and biological characteristics of osteoinductive calcium phosphate ceramics, Regen. Biomater. 5 (2018) 43–59, https://doi.org/10.1093/rb/rbx024.

[310] M. Bohner, Y. Maazouz, M.P. Ginebra, P. Habibovic, J.G. Schoenecker, H. Seeherman, J.J.J.P. van den Beucken, F. Witte, Sustained local ionic homeostatic imbalance caused by calcification modulates inflammation to trigger heterotopic ossification, Acta Biomater. 145 (2022) 1–24, https://doi.org/10.1016/j.actbio.2022.03.057.

[311] T. Arnett, Regulation of bone cell function by acid-base balance, Proc. Nutr. Soc. 62 (2003) 511–520.

[312] Y. Maazouz, F. El Harouni, J. Piot, N. Warfing, R. De Miguel, N. Döbelin, M. Bohner, Acidic phosphate microenvironment within calcium phosphate bone graft substitutes drives ectopic bone formation in mice, Mater. Today Bio 37 (2026) 102918, https://doi.org/10.1016/j.mtbio.2026.102918.

[313] Y. Zhang, T. Yu, Q. Xiang, F. Van Den Tillaart, J. Ma, Z. Zhuang, T. Stessuk, H. Wang, J.J.J.P. Van Den Beucken, Osteoclasts drive bone formation in ectopic and orthotopic environments, Biomaterials 322 (2025) 123377, https://doi.org/10.1016/j.biomaterials.2025.123377.

[314] T. Yuasa, Y. Miyamoto, K. Ishikawa, M. Takechi, M. Nagayama, K. Suzuki, In vitro resorption of three apatite cements with osteoclasts, J. Biomed. Mater. Res. 54 (2001) 344–350, https://doi.org/10.1002/1097-4636(20010305)54:3%3C344::aid-jbm50%3E3.0.co;2-1.

[315] M. Otsuka, Y. Matsuda, D. Yu, J. Wong, J.L. Fox, W.I. Higuchi, A novel skeletal drug delivery system for anti-bacterial drugs using self-setting hydroxyapatite cement, Chem. Pharm. Bull. (Tokyo) 38 (1990) 3500–3502, https://doi.org/10.1248/cpb.38.3500.

[316] M. Otsuka, Y. Matsuda, Y. Suwa, J.L. Fox, W.I. Higuchi, A novel skeletal drug delivery system using self-setting calcium phosphate cement. 2. physicochemical properties and drug release rate of the cement-containing indomethacin, J. Pharm. Sci. 83 (1994) 611–615, https://doi.org/10.1002/jps.2600830502.

[317] M. Otsuka, Y. Matsuda, Y. Suwa, J.L. Fox, W.I. Higuchi, A novel skeletal drug-delivery system using self-setting calcium phosphate cement. 3. physicochemical properties and drug-release rate of bovine insulin and bovine albumin, J. Pharm. Sci. 83 (1994) 255–258, https://doi.org/10.1002/jps.2600830229.

[318] M. Otsuka, Y. Matsuda, Y. Suwa, J.L. Fox, W.I. Higuchi, A novel skeletal drug-delivery system using self-setting calcium phosphate cement. 4. effects of the mixing solution volume on the drug-release rate of heterogeneous aspirin-loaded cement, J. Pharm. Sci. 83 (1994) 259–263, https://doi.org/10.1002/jps.2600830230.

[319] M. Otsuka, Y. Matsuda, Y. Suwa, J.L. Fox, W.I. Higuchi, A novel skeletal drug delivery system using a self-setting calcium phosphate cement. 5. drug release behavior from a heterogeneous drug-loaded cement containing an anticancer drug, J. Pharm. Sci. 83 (1994) 1565–1568, https://doi.org/10.1002/jps.2600831109.

[320] A. Barroug, J. Lemaître, P.G. Rouxhet, Influence of crystallite size on the surface properties of calcium-deficient hydroxyapatites, J. Alloys Compd. 188 (1992) 152–156, https://doi.org/10.1016/0925-8388(92)90664-U.

[321] A. Ebrahimpour, M. Johnsson, C.F. Richardson, G.H. Nancollas, The characterization of hydroxyapatite preparations, J. Colloid Interface Sci. 159 (1993) 158–163, https://doi.org/10.1006/jcis.1993.1307.

[322] H. Seeherman, J. Wozney, R. Li, Bone morphogenetic protein delivery systems, Spine Phila Pa 1976 27 (2002) S16–S23, https://doi.org/10.1097/00007632-200208151-00005.

[323] E.J. Blom, J. Klein-Nulend, J.G. Wolke, M.A. van Waas, F.C. Driessens, E. H. Burger, Transforming growth factor-beta1 incorporation in a calcium phosphate bone cement: material properties and release characteristics, J. Biomed. Mater. Res. 59 (2002) 265–272, https://doi.org/10.1002/jbm.1241.

[324] P.Q. Ruhe, H.C. Kroese-Deutman, J.G. Wolke, P.H. Spauwen, J.A. Jansen, Bone inductive properties of rhBMP-2 loaded porous calcium phosphate cement implants in cranial defects in rabbits, Biomaterials 25 (2004) 2123–2132, https://doi.org/10.1016/j.biomaterials.2003.09.007.

[325] V. Sokolova, M. Epple, Inorganic nanoparticles as carriers of nucleic acids into cells, Angew. Chem. Int. Ed Engl. 47 (2008) 1382–1395, https://doi.org/10.1002/anie.200703039.

[326] V. Sokolova, M. Epple, Biological and medical applications of calcium phosphate nanoparticles, Chem. – Eur. J. 27 (2021) 7471–7488, https://doi.org/10.1002/chem.202005257.

[327] L. Wang, Z. Dai, J. Bi, Y. Chen, Z. Wang, Z. Sun, Z. Ji, H. Wang, Y. Zhang, L. Wang, J. Mao, J. Yang, Polydopamine-functionalized calcium-deficient hydroxyapatite 3D-printed scaffold with sustained doxorubicin release for synergistic chemo-photothermal therapy of osteosarcoma and accelerated bone regeneration, Mater. Today Bio 29 (2024) 101253, https://doi.org/10.1016/j.mtbio.2024.101253.

[328] B. Palazzo, M. Iafisco, M. Laforgia, N. Margiotta, G. Natile, C.L. Bianchi, D. Walsh, S. Mann, N. Roveri, Biomimetic hydroxyapatite–drug nanocrystals as potential bone substitutes with antitumor drug delivery properties, Adv. Funct. Mater. 17 (2007) 2180–2188, https://doi.org/10.1002/adfm.200600361.

[329] H. Limeback, J. Enax, F. Meyer, Clinical evidence of biomimetic hydroxyapatite in oral care products for reducing dentin hypersensitivity: an updated systematic review and meta-analysis, Biomimetics. 8 (2023) 23, https://doi.org/10.3390/biomimetics8010023.

[330] P. Bodier-Houlle, P. Steuer, J.C. Voegel, F.J. Cuisinier, First experimental evidence for human dentine crystal formation involving conversion of octacalcium phosphate to hydroxyapatite, Acta Crystallogr Biol Crystallogr 54 (1998) 1377–1381, https://doi.org/10.1107/S0907444998005769.

[331] M. Iijima, D.G.A. Nelson, Y. Pan, A.T. Kreinbrink, M. Adachi, T. Goto, Y. Moriwaki, Fluoride analysis of apatite crystals with a central planar OCP inclusion: concerning the role of F− ions on apatite/OCP/apatite structure formation, Calcif. Tissue Int. 59 (1996) 377–384, https://doi.org/10.1007/s002239900143.

[332] M. Aizawa, A.E. Porter, S.M. Best, W. Bonfield, Ultrastructural observation of single-crystal apatite fibres, Biomaterials 26 (2005) 3427–3433, https://doi.org/10.1016/j.biomaterials.2004.09.044.

[333] S. Amrah-Bouali, C. Rey, A. Lebugle, D. Bernache, Surface modifications of hydroxyapatite ceramics in aqueous media, Biomaterials 15 (1994) 269–272, https://doi.org/10.1016/0142-9612(94)90050-7.

[334] V. Bolis, C. Busco, G. Martra, L. Bertinetti, Y. Sakhno, P. Ugliengo, F. Chiatti, M. Corno, N. Roveri, Coordination chemistry of Ca sites at the surface of nanosized hydroxyapatite: interaction with H2O and CO, Philos. Trans. Math. Phys. Eng. Sci. 370 (2012) 1313–1336, https://doi.org/10.1098/rsta.2011.0273.

[335] D. Proudfoot, Calcium signaling and tissue calcification, Cold Spring Harb. Perspect. Biol. 11 (2019) a035303, https://doi.org/10.1101/cshperspect.a035303.

[336] A. Barba, A. Diez-Escudero, M. Espanol, M. Bonany, J.M. Sadowska, J. Guillem-Marti, C. Öhman-Mägi, C. Persson, M.-C. Manzanares, J. Franch, M.-P. Ginebra, Impact of biomimicry in the design of osteoinductive bone substitutes: nanoscale matters, ACS Appl. Mater. Interfaces 11 (2019) 8818–8830, https://doi.org/10.1021/acsami.8b20749.

[337] I.A. Grafe, M. Baier, G. Noldge, C. Weiss, K.Da Fonseca, J. Hillmeier, M. Libicher, G. Rudofsky, C. Metzner, P. Nawroth, P.J. Meeder, C. Kasperk, Calcium-phosphate and polymethylmethacrylate cement in long-term outcome after kyphoplasty of painful osteoporotic vertebral fractures, Spine (Phila Pa 1976) 33 (2008) 1284–1290, https://doi.org/10.1097/BRS.0b013e3181714a84.

[338] I. Khairoun, F.C. Driessens, M.G. Boltong, J.A. Planell, R. Wenz, Addition of cohesion promotors to calcium phosphate cements, Biomaterials 20 (1999) 393–398, https://doi.org/10.1016/s0142-9612(98)00202-6.

[339] R.P. del Real, J.G. Wolke, M. Vallet-Regi, J.A. Jansen, A new method to produce macropores in calcium phosphate cements, Biomaterials 23 (2002) 3673–3680, https://doi.org/10.1016/s0142-9612(02)00101-1.

[340] A. Tofighi, S. Mounic, P. Chakravarthy, C. Rey, D. Lee, Setting reactions involved in injectable cements based on amorphous calcium phosphate, Key Eng. Mater. 192-195 (2001) 769–772, https://doi.org/10.4028/www.scientific.net/KEM.192-195.769.

[341] D.D. Lee, A. Tofighi, M. Aiolova, P. Chakravarthy, A. Catalano, A. Majahad, D. Knaack, alpha-BSM: a biomimetic bone substitute and drug delivery vehicle,

Clin. Orthop. 367 (1999) S396–S405, https://doi.org/10.1097/00003086-199910001-00038.
[342] P. Habibovic, F. Barrere, C.A. van Blitterswijk, K. de Groot, P. Layrolle, Biomimetic hydroxyapatite coating on metal implants, J. Am. Ceram. Soc. 85 (2002) 517–522, https://doi.org/10.1111/j.1151-2916.2002.tb00126.x.
[343] R.L. Hammonds, M.S. Harrison, T.C. Cravanas, W.H. Gazzola, C.P. Stephens, R. S. Benson, Biomimetic hydroxyapatite powder from a bacterial cellulose scaffold, Cellulose 19 (2012) 1923–1932, https://doi.org/10.1007/s10570-012-9767-4.
[344] J. Barralet, S. Best, W. Bonfield, Carbonate substitution in precipitated hydroxyapatite: an investigation into the effects of reaction temperature and bicarbonate ion concentration, J. Biomed. Mater. Res. 41 (1998) 79–86, https://doi.org/10.1002/(sici)1097-4636(199807)41:1%3C79::aid-jbm10%3E3.0.co;2-c.
[345] A.S. Posner, N.C. Blumenthal, F. Betts, Formation and structure of chemically precipitated hydroxyapatites. Phosphate Miner., Springer, 1984, pp. 330–350.
[346] S. Al-Maawi, M. Barbeck, C.H. Vizcaíno, R. Egli, R. Sader, C.J. Kirkpatrick, M. Bohner, S. Ghanaati, Thermal treatment at 500 °C significantly reduces the reaction to irregular tricalcium phosphate granules as foreign bodies: an in vivo study, Acta Biomater. 121 (2021) 621–636, https://doi.org/10.1016/j.actbio.2020.11.034.
[347] J.C. Elliott, Structure and chemistry of the apatites and other calcium orthophosphates. , 1994, https://doi.org/10.1016/B978-0-444-81582-8.50006-7.
[348] G. Kühl, W.H. Nebergall, Hydrogenphosphat- und Carbonatapatite, Z. Für Anorg. Allg. Chem. 324 (1963) 313–320, https://doi.org/10.1002/zaac.19633240513.
[349] S.J. Joris, C.H. Amberg, The nature of deficiency in nonstoichiometric hydroxyapatites. II. spectroscopic studies of calcium and strontium hydroxyapatites, J. Phys. Chem. 75 (1971) 3172–3178, https://doi.org/10.1021/j100689a025.
[350] E.E. Berry, The structure and composition of some calcium-deficient apatites—II, J. Inorg. Nucl. Chem. 29 (1967) 1585–1590, https://doi.org/10.1016/0022-1902(67)80200-8.
[351] A. Delay, Comportement thermique et composition des phosphates calciques de Ca/P molaire supérieur à 3/2, Bull. Soc. Chim. Fr. (1974).
[352] J.C. Labarthe, Contribution à L'étude De La Structure Et Des Propriétés Des Apatites Carbonatées De Type B phospho-Calcique, Université Paul Sabatier, 1972.
[353] J. Weichhold, M. Pfeiffle, J.C. Kade, K. Hurle, U. Gbureck, Aqueous calcium phosphate cement inks for 3D printing, Adv. Eng. Mater. 25 (2023) 2300789, https://doi.org/10.1002/adem.202300789.
[354] J.K. Konrad, J. Rudnik, A.-C. Pöppler, K. Hurle, U. Gbureck, Interaction mechanisms between antibiotics and calcium phosphate cements as pharmacologically active bone graft substitutes, Acta Biomater. 205 (2025) 687–704, https://doi.org/10.1016/j.actbio.2025.08.051.
[355] ISO Standard, Implants for surgery - Hydroxyapatite - part 3: chemical analysis and characterization of crystallinity and phase purity, second ed. 2018 (2018).
[356] J.L. Miquel, L. Facchini, A.P. Legrand, C. Rey, J. Lemaitre, Solid state NMR to study calcium phosphate ceramics, Colloids Surf. 45 (1990) 427–433, https://doi.org/10.1016/0166-6622(90)80041-2.
[357] J.D. Termine, A.S. Posner, Infra-red determination of the percentage of crystallinity in apatitic calcium phosphates, Nature 211 (1966) 268–270, https://doi.org/10.1038/211268a0.
[358] D. Lee, C. Leroy, C. Crevant, L. Bonhomme-Coury, F. Babonneau, D. Laurencin, C. Bonhomme, G. De Paëpe, Interfacial Ca2+ environments in nanocrystalline apatites revealed by dynamic nuclear polarization enhanced 43Ca NMR spectroscopy, Nat. Commun. 8 (2017) 14104, https://doi.org/10.1038/ncomms14104.
[359] ISO Standard, Biological evaluation of medical devices - Part 1: evaluation and testing within a risk management process, (2018).
[360] N.C. Blumenthal, A.S. Posner, J.M. Holmes, Effect of preparation conditions on the properties and transformation of amorphous calcium phosphate, Mater. Res. Bull. 7 (1972) 1181–1189, https://doi.org/10.1016/0025-5408(72)90097-9.
[361] J.D. Termine, R.A. Peckauskas, A.S. Posner, Calcium phosphate formation in vitro. II. effects of environment on amorphous-crystalline transformation, Arch. Biochem. Biophys. 140 (1970) 318–325, https://doi.org/10.1016/0003-9861(70)90072-x.
[362] J.D. Termine, A.S. Posner, Calcium phosphate formation in vitro. I. factors affecting initial phase separation, Arch. Biochem. Biophys. 140 (1970) 307–317, https://doi.org/10.1016/0003-9861(70)90071-8.
[363] S.J. Gadaleta, E.P. Paschalis, F. Betts, R. Mendelsohn, A.L. Boskey, Fourier transform infrared spectroscopy of the solution-mediated conversion of amorphous calcium phosphate to hydroxyapatite: new correlations between X-Ray diffraction and infrared data, Calcif. Tissue Int. 58 (1996) 9–16, https://doi.org/10.1007/BF02509540.
[364] C.G. Wang, J.W. Liao, B.D. Gou, J. Huang, R.K. Tang, J.H. Tao, T.L. Zhang, K. Wang, Crystallization at multiple sites inside particles of amorphous calcium phosphate, Cryst. Growth Des. 9 (2009) 2620–2626, https://doi.org/10.1021/cg801069t.
[365] S. Somrani, C. Rey, M. Jemal, Thermal evolution of amorphous tricalcium phosphate, J. Mater. Chem. 13 (2003) 888–892, https://doi.org/10.1039/B210900J.
[366] T. Kanazawa, T. Umegaki, N. Uchiyama, Thermal crystallisation of amorphous calcium phosphate to α-tricalcium phosphate, J. Chem. Technol. Biotechnol. 32 (1982) 399–406, https://doi.org/10.1002/jctb.5030320206.
[367] T. Aoba, E.C. Moreno, Preparation of hydroxyapatite crystals and their behavior as seeds for crystal growth, J. Dent. Res. 63 (1984) 874–880, https://doi.org/10.1177/00220345840630061201.
[368] A. Lebugle, E. Zahidi, G. Bonel, Effect of structure and composition on the thermal decomposition of calcium phosphates (Ca/P = 1.33), React. Solids 2 (1986) 151–161, https://doi.org/10.1016/0168-7336(86)80071-7.
[369] H.C. Margolis, E.C. Moreno, Kinetics of hydroxyapatite dissolution in acetic, lactic, and phosphoric acid solutions, Calcif. Tissue Int. 50 (1992) 137–143, https://doi.org/10.1007/BF00298791.
[370] C. Liu, Y. Huang, W. Shen, J. Cui, Kinetics of hydroxyapatite precipitation at pH 10 to 11, Biomaterials 22 (2001) 301–306, https://doi.org/10.1016/s0142-9612(00)00166-6.
[371] J. Zhao, J. Chen, X. Wang, Z. Han, Y. Li, Rietveld refinement of hydroxyapatite, tricalcium phosphate and biphasic materials prepared by solution combustion method, Ceram. Int. 40 (2014) 3379–3388, https://doi.org/10.1016/j.ceramint.2013.09.094.
[372] S. Beaufils, T. Rouillon, P. Millet, J.Le Bideau, P. Weiss, J.-P. Chopart, A.-L. Daltin, Synthesis of calcium-deficient hydroxyapatite nanowires and nanotubes performed by template-assisted electrodeposition, Mater. Sci. Eng. C 98 (2019) 333–346, https://doi.org/10.1016/j.msec.2018.12.071.
[373] A. Prihanto, S. Muryanto, R. Ismail, J. Jamari, A.P. Bayuseno, Batch hydrothermal synthesis of nanocrystalline, thermostable hydroxyapatite at various pH and temperature levels, Inorg. Chem. Commun. 157 (2023) 111301, https://doi.org/10.1016/j.inoche.2023.111301.
[374] G.M.L. Dalmônico, E.O. López, M.M. Longuinho, N.R. Checca, M. Farina, O. Ersen, A.M. Rossi, A.L. Rossi, Insight by cryo-tem into the growth and crystallization processes of calcium phosphate nanoparticles in aqueous medium, Mater. Chem. Phys. 237 (2019) 121862, https://doi.org/10.1016/j.matchemphys.2019.121862.
[375] G. Gecim, S. Dönmez, E. Erkoc, Calcium deficient hydroxyapatite by precipitation: continuous process by vortex reactor and semi-batch synthesis, Ceram. Int. 47 (2021) 1917–1928, https://doi.org/10.1016/j.ceramint.2020.09.020.
[376] Y. Sakhno, I. Miletto, G. Paul, D.P. Jaisi, A novel route to enhance the dissolution of apatite: structural incorporation of hydrogen phosphate, NanoImpact. 28 (2022) 100422, https://doi.org/10.1016/j.impact.2022.100422.
[377] L.C. Bell, H. Mika, B.J. Kruger, Synthetic hydroxyapatite-solubility product and stoichiometry of dissolution, Arch. Oral. Biol. 23 (1978) 329–336, https://doi.org/10.1016/0003-9969(78)90089-4.
[378] T.Y. Liu, S.Y. Chen, D.M. Liu, S.C. Liou, On the study of BSA-loaded calcium-deficient hydroxyapatite nano-carriers for controlled drug delivery, J. Controlled Release 107 (2005) 112–121, https://doi.org/10.1016/j.jconrel.2005.05.025.
[379] A. Tiselius, S. Hjertén, Ö. Levin, Protein chromatography on calcium phosphate columns, Arch. Biochem. Biophys. 65 (1956) 132–155, https://doi.org/10.1016/0003-9861(56)90183-7.
[380] M.T. Fulmer, P.W. Brown, Hydrolysis of dicalcium phosphate dihydrate to hydroxyapatite, J. Mater. Sci.-Mater. Med. 9 (1998) 197–202, https://doi.org/10.1023/A:1008832006277.
[381] K. Kobayashi, T. Anada, T. Handa, N. Kanda, M. Yoshinari, T. Takahashi, O. Suzuki, Osteoconductive property of a mechanical mixture of octacalcium phosphate and amorphous calcium phosphate, ACS Appl. Mater. Interfaces 6 (2014) 22602–22611, https://doi.org/10.1021/am5067139.
[382] S. Saito, R. Hamai, Y. Shiwaku, T. Hasegawa, S. Sakai, K. Tsuchiya, Y. Sai, R. Iwama, N. Amizuka, T. Takahashi, O. Suzuki, Involvement of distant octacalcium phosphate scaffolds in enhancing early differentiation of osteocytes during bone regeneration, Acta Biomater. 129 (2021) 309–322, https://doi.org/10.1016/j.actbio.2021.05.017.
[383] K. Okuyama, Y. Shiwaku, R. Hamai, T. Mizoguchi, K. Tsuchiya, T. Takahashi, O. Suzuki, Differentiation of committed osteoblast progenitors by octacalcium phosphate compared to calcium-deficient hydroxyapatite in LEPR-CRE/tomato mouse tibia, Acta Biomater. 142 (2022) 332–344, https://doi.org/10.1016/j.actbio.2022.02.016.
[384] N.C. Blumenthal, F. Betts, A.S. Posner, Formation and structure of Ca-deficient hydroxyapatite, Calcif. Tissue Int. 33 (1981) 111–117, https://doi.org/10.1007/BF02409422.
[385] J. Yun, B. Holmes, A. Fok, Y. Wang, A kinetic model for hydroxyapatite precipitation in mineralizing solutions, Cryst. Growth Des. 18 (2018) 2717–2725, https://doi.org/10.1021/acs.cgd.7b01330.
[386] T. Goto, I.Y. Kim, K. Kikuta, C. Ohtsuki, Comparative study of hydroxyapatite formation from α- and β-tricalcium phosphates under hydrothermal conditions, J. Ceram. Soc. Jpn. 120 (2012) 131–137, https://doi.org/10.2109/jcersj2.120.131.
[387] H. Monma, Wet-process formation of non-stoichiometric hydroxyapatite from tricalcium phosphate, Yogyo-Kyokai-Shi 86 (1978) 72–76, https://doi.org/10.2109/jcersj1950.86.990_72.
[388] H. Monma, M. Goto, T. Kohmura, Effects of additives on hydration and hardening of tricalcium phosphate, Gypsum Lime 188 (1984) 11–16, https://doi.org/10.11451/mukimate1953.1984.11.
[389] K.S. TenHuisen, P.W. Brown, Hydrolysis of alpha-tricalcium phosphate in NAF solutions, Biomaterials 20 (1999) 427–434, https://doi.org/10.1016/s0142-9612(98)00186-0.
[390] C. Durucan, P.W. Brown, α-Tricalcium phosphate hydrolysis to hydroxyapatite at and near physiological temperature, J. Mater. Sci. Mater. Med. 11 (2000) 365–371, https://doi.org/10.1023/A:1008934024440.
[391] C. Durucan, P.W. Brown, Reactivity of alpha-tricalcium phosphate, J. Mater. Sci. 37 (2002) 963–969, https://doi.org/10.1023/A:1014347814241.
[392] L. Vecbiskena, K.A. Gross, U. Riekstina, T.C.K. Yang, Crystallized nano-sized alpha-tricalcium phosphate from amorphous calcium phosphate: microstructure,

cementation and cell response, Biomed. Mater. Bristol 10 (2015) 025009, https://doi.org/10.1088/1748-6041/10/2/025009.
[393] M. Fulmer, R.I. Martin, P.W. Brown, Formation of calcium deficient hydroxyapatite at near-physiological temperature, J. Mater. Sci. Mater. Med. 3 (1992) 299–305, https://doi.org/10.1007/BF00705297.
[394] Y.E. Greish, P.W. Brown, Phase evolution during the formation of stoichiometric hydroxyapatite at 37.4 degrees C, J. Biomed. Mater. Res. 67B (2003) 632–637, https://doi.org/10.1002/jbm.b.10056.
[395] Y. Fukase, E.D. Eanes, S. Takagi, L.C. Chow, W.E. Brown, Setting reactions and compressive strengths of calcium phosphate cements, J. Dent. Res. 69 (1990) 1852–1856, https://doi.org/10.1177/00220345900690121201.
[396] M. Fulmer, P.W. Brown, The effects of particle size and solution chemistry on the formation of hydroxyapatite, Mat. Res. Soc. Symp. Proc. 3 (1992) 299–305, https://doi.org/10.1007/BF00705297.
[397] P.W. Brown, D. Sample, N. Hocker, The low temperature formation of synthetic bone, Mat. Res. Soc. Symp. Proc. 179 (1989) 41–48, https://doi.org/10.1557/PROC-179-41.
[398] P.W. Brown, N. Hocker, S. Hoyle, Variations in solution chemistry during the low-temperature formation of hydroxyapatite, J. Am. Ceram. Soc. 74 (1991) 1848–1854, https://doi.org/10.1111/j.1151-2916.1991.tb07798.x.
[399] P.W. Brown, M. Fulmer, The effects of electrolytes on the rates of hydroxyapatite formation at 25 and 38 degrees C, J. Biomed. Mater. Res. 31 (1996) 395–400, https://doi.org/10.1002/(SICI)1097-4636(199607)31:3%3C395::AID-JBM14%3E3.0.CO;2-I.
[400] E.A. De Maeyer, R.M. Verbeeck, C.W. Vercruysse, Conversion of octacalcium phosphate in calcium phosphate cements, J. Biomed. Mater. Res. 52 (2000) 95–106, https://doi.org/10.1002/1097-4636(200010)52:1%3C95::aid-jbm12%3E3.0.co;2-x.
[401] S. Heinemann, S. Rössler, M. Lemm, M. Ruhnow, B. Nies, Properties of injectable ready-to-use calcium phosphate cement based on water-immiscible liquid, Acta Biomater. 9 (2013) 6199–6207, https://doi.org/10.1016/j.actbio.2012.12.017.
[402] S. Tanaka, T. Kishi, R. Shimogoryo, S. Matsuya, K. Ishikawa, Biopex acquires anti-washout properties by adding sodium alginate into its liquid phase, Dent. Mater. J. 22 (2003) 301–312, https://doi.org/10.4012/dmj.22.301.
[403] G. Hannink, J.G.C. Wolke, B.W. Schreurs, P. Buma, In vivo behavior of a novel injectable calcium phosphate cement compared with two other commercially available calcium phosphate cements, J. Biomed. Mater. Res. - Part B Appl. Biomater. 85 (2008) 478–488, https://doi.org/10.1002/jbm.b.30969Digital%20Object%20Identifier.
[404] N. Döbelin, O. Suzuki, C. Drouet, J. Ločs, G. Insley, P. Procter, Workshop on the latest advances in biomedical applications of octacalcium phosphate, J. Biomed. Mater. Res. B Appl. Biomater. 113 (2025) e35500, https://doi.org/10.1002/jbm.b.35500.
[405] R. Karalkeviciene, E. Raudonyte-Svirbutaviciene, J. Gaidukevic, A. Zarkov, A. Kareiva, Solvothermal synthesis of calcium-deficient hydroxyapatite via hydrolysis of α-Tricalcium phosphate in different aqueous-organic media, Crystals 12 (2022) 253, https://doi.org/10.3390/cryst12020253.
[406] R. Karalkeviciene, E. Raudonyte-Svirbutaviciene, A. Zarkov, J.-C. Yang, A. I. Popov, A. Kareiva, Solvothermal synthesis of calcium hydroxyapatite via hydrolysis of alpha-tricalcium phosphate in the presence of different organic additives, Crystals 13 (2023) 265, https://doi.org/10.3390/cryst13020265.
[407] M. Andrés-Vergés, C. Fernández-González, M. Martínez-Gallego, Hydrothermal synthesis of calcium deficient hydroxyapatites with controlled size and homogeneous morphology, J. Eur. Ceram. Soc. 18 (1998) 1245–1250, https://doi.org/10.1016/S0955-2219(98)00049-1.
[408] A. Destainville, Etude du phosphate tricalcique. application à l'élaboration de biomatériaux céramiques macroporeux en phosphates de calcium. PhD Thesis, Université de Limoges, 2005.
[409] S. Chernousova, J. Klesing, N. Soklakova, M. Epple, A genetically active nano-calcium phosphate paste for bone substitution, encoding the formation of BMP-7 and vegf-a, RSC Adv. 3 (2013) 11155, https://doi.org/10.1039/c3ra23450a.
[410] W. Habraken, P. Habibovic, M. Epple, M. Bohner, Calcium phosphates in biomedical applications: materials for the future? Mater. Today 19 (2016) 69–87, https://doi.org/10.1016/J.MATTOD.2015.10.008.
[411] L. Galea, D. Alexeev, M. Bohner, N. Doebelin, A.R. Studart, C.G. Aneziris, T. Graule, Textured and hierarchically structured calcium phosphate ceramic blocks through hydrothermal treatment, Biomaterials 67 (2015) 93–103, https://doi.org/10.1016/j.biomaterials.2015.07.026.